



Technische Universität München
Lehrstuhl für Technische Chemie II

Solvent effects on Pd catalyzed hydrodeoxygenation reactions

Guanhua Cheng

Vollständiger Abdruck der von der Fakultät für Chemie der Technischen Universität
München zur Erlangung des akademischen Grades eines

Doktors der Naturwissenschaften (Dr. rer. nat.)
genehmigten Dissertation.

Vorsitzende(r): Prof. Dr. Dr. h.c. Bernhard Rieger

Prüfer der Dissertation:

1. Prof. Dr. Johannes A. Lercher
2. Prof. Dr. Klaus Köhler

Die Dissertation wurde am 30.06.2021 bei der Technischen Universität München
eingereicht und durch die Fakultät für Chemie am 10.08.2021 angenommen.

Wir müssen wissen, wir werden wissen.

—*David Hilbert*

Acknowledgements

Though so many ups and downs during the past five years, my doctoral study comes to an end. There is no doubt that I could not have made it without the help and support from my friends and colleagues in TC II.

Foremost, I would like to thank Prof. Johannes A. Lercher for providing me the opportunity to work in his group, and also the patient guidance throughout my doctoral study. I do have gained a lot from the invaluable and dense scientific group meeting and inspired by his constantly seeking attitude.

I also would like to show my sincere appreciation to my supervisors Dr. Oliver Y. Gutiérrez, Dr. Erika Ember, Prof. Dr. Andreas Jentys and especially Dr. Yue Liu. Oliver, even we only worked together for few months in Munich, your encouragement helped me a lot to go through my adaptation part to PhD study. Erika, I am really grateful for your kindness and patience. Thank you so much for your efforts on coordination for the project activity and the discussion about the science, culture, cat and your daughter are unforgettable. Andy, I am appreciated for your patience and suggestion on my research work. The conversation about travelling and culture diversity with you are delightful. I learned from you to balance the life and the work and enjoy my holidays. Then I would like to show my sincere gratitude to Yue for the fruitful and invaluable discussions we had and amazing suggestion you gave me. You always have uncountable smart ideas and your unique view always amazes me.

Next, I would like to thank Prof. Ya-Huei (Cathy) Chin. I deeply treasured the collaboration and your rigorous scientific research attitude and profound knowledge in kinetics taught me a lot.

I would like to thank all former and current senior scientists in TCII at TUM, Dr. Hui Shi, Dr. Maricruz Sanchez- Sanchez and Dr. Ricardo Bermejo-Deval. Thank all of you for your input in science as well as in consultation.

I would like to thank my former and current colleagues in our group, Dr. Yuanshuai Liu, Dr. Yang Song, Dr. Wei Zhang, Dr. Kaming Yu, Dr. Yong Wang, Dr. Rachit Khare, Ruixue Zhao, Xi Chen, Ling li Ni, Lei Tao, Fuli Deng, Insu Lee, Martina Aigner, Phillip Fischer, Simon Krebs and Niklas Pfriem for their suggestion and help in both study and life.

Moreover, I would like to thank all following colleagues in TCII, Dr. Madita Einemann, Dr. Karen Resende, Martin Baumgärtl, Verena Höpfl, Laura Löbbert, Lara Milakovic, Jakub Pazdera, Teresa Schachtl, Aimen Shahpal, Ferdinand Vogelgsang, Mirjam Wenig, Roland Weindl, Alexander Wellmann and Lennart Wahl for their support and help in the past years.

Furthermore, I would like to thank Franz-Xaver Hecht, Martin Neukamm, Andreas Marx and Iqbal Muhammad are acknowledged for their technical supports. Stefanie Seibold, Kateryna Kryvko, Bettina Federmann, and Ulrike Sanwald are acknowledged for their administrative helps.

Last but not least, I am deeply indebted to my family, relatives and friends from whom I've been receiving endless support and unconditional understanding.

Guanhua Cheng

May 2021

Abstract

The impact of the solvent on the catalytic activity and selectivity in hydrodeoxygenation has been explored on Pd supported on activated carbon. The reaction pathways for benzaldehyde and cinnamaldehyde hydrogenation in different solvents were clarified. The reaction rate varied sympathetically with weaker adsorption of hydrogen. The activity of benzyl alcohol hydrogenolysis is highly dependent on the electric double layer formed on Pd in water influencing surface charge and ion concentration.

Kurzzusammenfassung

Die Rolle des Lösungsmittels auf die katalytische Aktivität und Selektivität bei der Hydrodeoxygenierung wurde an Pd/C erforscht. Die Mechanismen für die Hydrierung von Benzaldehyd und Zimtaldehyd wurden aufgeklärt. Die Reaktionsrate variierte sympathisch mit der schwächeren Adsorption von Wasserstoff. Die Aktivität der Benzylalkohol-Hydrogenolyse ist stark abhängig von der auf Pd gebildeten elektrischen Doppelschicht in Wasser, die die Oberflächenladung und Ionenkonzentration beeinflusst.

Table of Contents

Acknowledgements	i
Abstract	iii
Chapter 1 Introduction	1
1.1 General background.....	2
1.2 Heterogeneous catalysis	4
1.3 Hydrodeoxygenation	5
1.3.1 Hydrogenation.....	6
1.3.2 C-O bond cleavage of alcohols	7
1.4 Factors to affect the heterogeneous catalytic process.....	8
1.4.1 Catalyst	8
1.4.2 Solvent	9
1.4.2.1 Transport phenomena.....	10
1.4.2.2 Competitive adsorption.....	10
1.4.2.3 Solvation effect	11
1.4.2.4 Involvement in catalytic reaction.....	12
1.4.2.5 pH effect.....	13
1.5 Chemical kinetics	14
1.6 Scope of this thesis	16
1.7 References	18
Chapter 2 Towards a quantitative understanding of solvent effects on Pd catalyzed benzaldehyde hydrogenation	25
2.1 Introduction	26
2.2 Experimental method.....	27
2.2.1 Chemicals and Catalysts	27
2.2.2 Catalyst Characterizations.....	27

2.2.3 Catalytic hydrogenation of benzaldehyde.....	28
2.2.4 Transient response method	29
2.2.5 Isotopic labeling experiments	30
2.2.6 Vapor pressure of benzaldehyde in solution	30
2.2.7 Determination of equilibrium constant of H ₂ and benzaldehyde in gas phase	30
2.3 Results and discussions	30
2.3.1 Effects of solvent on turnover rates and reaction orders for benzaldehyde hydrogenation on Pd/C	30
2.3.2 Mechanism of benzaldehyde hydrogenation on Pd—elementary steps, their reversibility, and kinetic relevance of H addition steps to the carbonyl C and O of benzaldehyde.....	32
2.3.3 Thermodynamic and kinetic contributions determining the rate of benzaldehyde hydrogenation in different solvents	34
2.3.4 Effects of solvents on the catalytic paths of benzaldehyde hydrogenation.....	39
2.3.5 Difference in solvation extent of reacting substrates and transition states	43
2.4 Conclusions	48
2.5 Appendix	50
2.6 Reference	63
Chapter 3 Role of solvents on the selectivity hydrogenation of cinnamaldehyde	68
3.1 Introduction	69
3.2 Experimental method.....	70
3.2.1 Chemicals.....	70
3.2.2 Catalyst Characterization	71
3.2.3 Thermal catalytic hydrogenation	71
3.2.4 ATR-IR measurement.....	72
3.2.5 Isotope-labeling experiments	72
3.2.6 Measurement of equilibrium constant of H ₂ adsorption	72
3.3 Results and Discussion	72

3.3.1 Catalytic pathways, rates, and chemical selectivity of cinnamaldehyde hydrogenation	72
3.3.2 Solvent effects on the C=C and C=O hydrogenation over Pd/C	74
3.3.3 Correlation of solvation effects on cinnamaldehyde molecular and hydrogenation rates	75
3.3.4 Comparison of reaction orders in EtOH and dioxane	76
3.3.5 Effects of solvents on catalytic pathway of cinnamaldehyde hydrogenation	77
3.4 Conclusions	82
3.5 Appendix	83
3.6 Reference	87
Chapter 4 Understanding of the rate-enhancement with hydronium ions on the reaction of benzyl alcohol hydrogenolysis over Pd/C	90
4.1 Introduction	91
4.2 Experimental method.....	92
4.2.1 Chemicals and Catalyst.....	92
4.2.2 Catalyst characterization	92
4.2.3 Catalytic reaction measurements under OCV (open circuit potential)	93
4.2.4 Electrocatalytic reaction.....	94
4.2.5 Cyclic Voltammetry	94
4.3 Results and discussion	94
4.3.1 pH effect on TOF and reaction orders for Pd/C catalyzed benzyl alcohol hydrogenolysis in buffer solution	94
4.3.2 Reaction pathways	98
4.3.3 The role of acid in benzyl alcohol hydrogenolysis	99
4.4 Conclusions	104
4.5 Appendix	105
4.6 References	112
Chapter 5 Summary	116

Curriculum vitae.....	119
List of publications.....	120
List of presentations	122

Chapter 1

Introduction

1.1 General background

Taking the advantage of industrial evolution, human civilization and global economy have been rapidly developing. However, global energy consumption has also increased dramatically since industrial evolution ¹, as shown in the **Figure 1-1**. In the last hundred years (from 1919 to 2019) the energy consumption increased by one order of magnitude and fossil fuels (gas, oil and coal), which are not renewable on human timescale, always dominate. The good news is that the usage of renewable energy, such as solar, wind and hydropower, keeps increasing during the past 50 years.

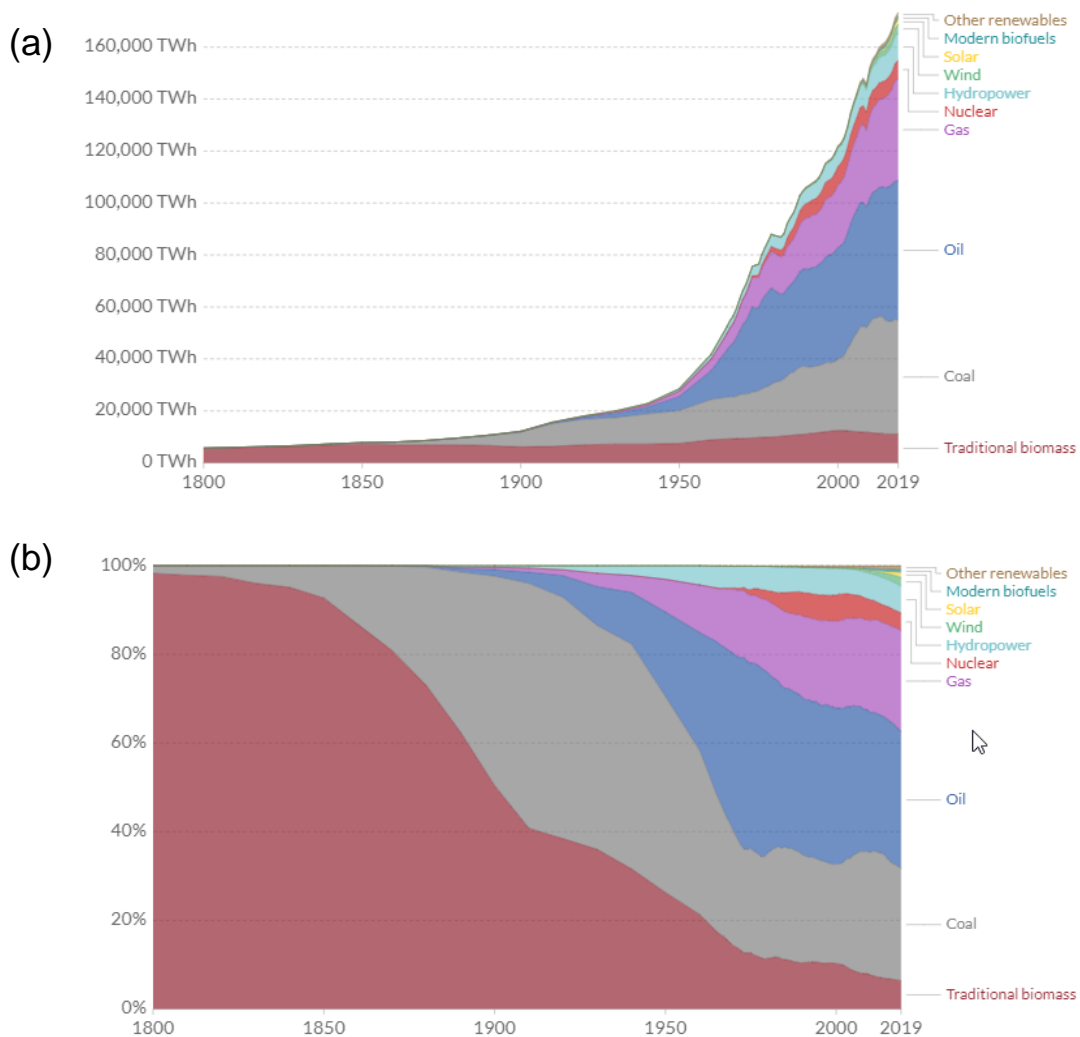


Figure 1-1. (a) Global primary energy consumption (1919-2019). (b) Percentage of various energy sources ¹. Primary energy denotes the energy which is from nature and has not been subjected to any human engineered conversion process.

Biomass, the only sustainable organic carbon resource in nature, is a promising alternative as sustainable, renewable and carbon-neutral source, which can release the world's energy problems. The energy in biomass can be directly used in combustion, which is less efficient but

takes the largest quantity a century ago. The other way is to upgrade biomass into a more valuable and usable liquid fuel or higher value products for the chemical industry. Therefore, utilization of biomass resources has become an alternative to fossil resources for the production of fuels and chemicals ^{2,3}.

A broad range of conversion technologies, including enzymatic ⁴, catalytic ⁵⁻⁸ and thermochemical process (gasification, pyrolysis, liquefaction) ^{9,10} have been employed in the conversion of crude biomass feedstocks ¹¹. Enzymes are industrially expensive because they must be produced by living systems and are thermally unstable. Another challenge is to obtain the highly pure enzymes ¹². In comparison, catalytic technology is considered as an adaptable, efficient and economic strategy and has been widely used in biomass conversion and even been used in thermochemical process ^{6,8,13,14}. Moreover, catalysts play an important role in upgrading of biomass derived biofuels ¹⁵⁻¹⁹. The production of chemicals from catalytic processes accounts for 85% of industrial energy use as shown in **Figure 1-2a** ²⁰.

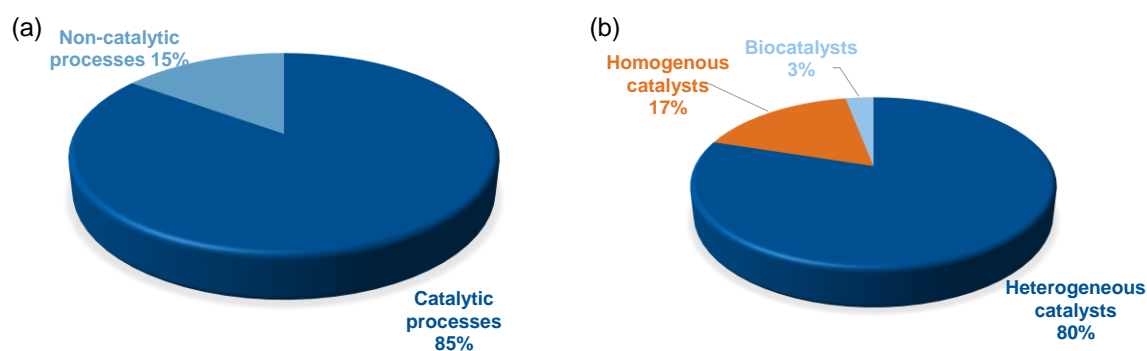


Figure 1-2. Pie charts showing (a) the percentage of catalytic process in all chemical industries and (b) the contributions of heterogeneous, homogeneous and bio-catalysis in the catalytic process ²⁰. (Reprinted with permission from reference 20. Copyright © 2016, Royal Society of Chemistry.)

Catalysis is a chemical process in presence of catalyst, a substance that can largely increase the reaction rate without consumption during the reaction process. In general, catalysts increase the reaction rate by providing an alternative reaction pathway with a lower activation barrier on the catalytically active sites and enable a higher concentration of reacting molecules in a local volume/area. Therefore, catalysts allow a reaction to perform at a relative mild reaction condition, lower temperature and pressure. It should be noted that the catalyst can equally decrease the activation barrier for both forward and reverse reaction, thus to accelerate both directions and permit the whole system arriving at an equilibrium in a shorter time, while the equilibrium position won't be affected. Generally, catalysts can be divided into two categories: homogeneous and heterogeneous catalyst based on the differences of catalysts and reactants in phase (solid, liquid and gas). Homogeneous catalyst is also called molecular catalyst

which is dispersed in the reactant, which makes the separation of catalysts from products and catalysts recycling challengeable. In comparison, heterogeneous catalysts can be easily separated from products and recycled, and more intensively used in the catalytic process (> 80%, **Figure 1-2b**)^{21,22}.

1.2 Heterogeneous catalysis

The catalytic process involves breaking and forming chemical bonds, and the energy required determines the activation barrier, which is directly related to the reaction rate. It is well accepted that only chemisorbed species can proceed for further surface reaction in heterogeneous catalysis. Two main mechanisms are proposed for surface reactions: Langmuir-Hinshelwood mechanism and Eley-Rideal mechanism. The difference for the two mechanisms is that both reactants need to be first adsorbed on the catalyst surface for reactions described by Langmuir-Hinshelwood mechanism; while in Eley-Rideal mechanism, one reactant is adsorbed, the other reactant can directly react with the adsorbed species from the gas phase without adsorption. It needs to be noticed that the adsorption site can be different to the active site, for example, although H_{ad} can adsorb on supports like activated carbon and Al_2O_3 , hydrogen can only be activated on active sites of transition metals²³. In this case, adsorbed molecule/atom needs to migrate from support to active sites for further hydrogenation reaction by following a more energetically favored reaction route.

The energy profile for a typical catalytic reaction is as shown in **Figure 1-3**. The reaction begins with gaseous reactants, in presence of catalyst, the reactants are adsorbed on the catalysts surface as ground states with a lower free energy level (a solvation process will also be included if in presence of solvents), followed by a transition state (active complex) formation before the final products. The adsorption process is spontaneous and decreases the energy to a lower level. The energy difference between the ground state and the transition state gives the energy barrier, which is related to the reaction rate. Either individually or simultaneously changing the energy of ground state and transition state will change the energy barrier and thus the rate constant, which can be achieved by either tuning the components and morphology of catalysts or controlling the reaction conditions.

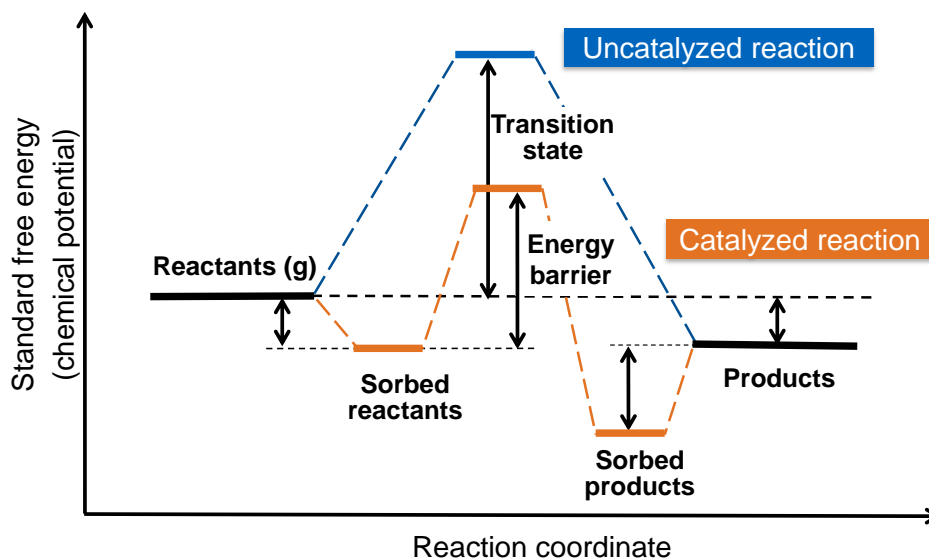


Figure 1-3. Energy profile showing the reactive states during heterogeneous catalysis reaction.

1.3 Hydrodeoxygenation

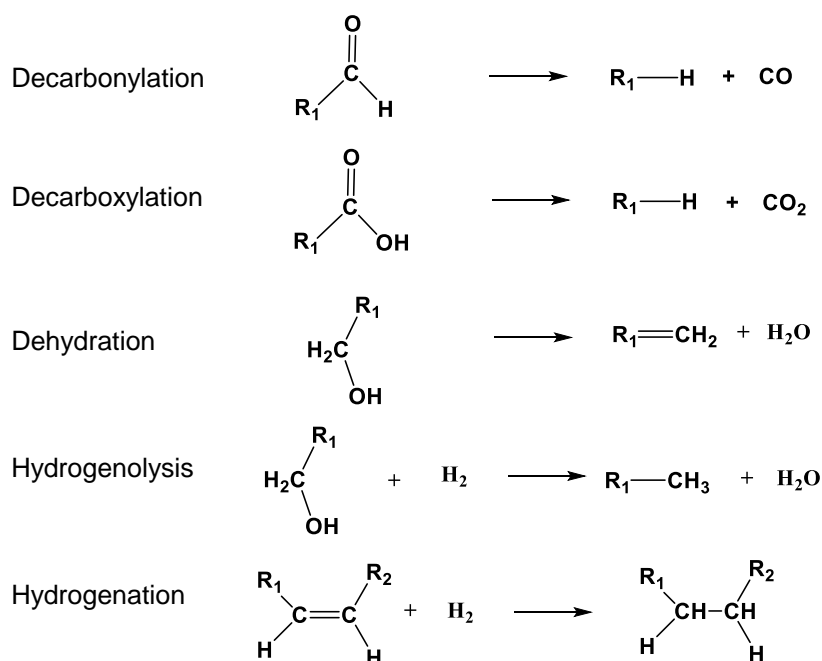


Figure 1-4. Typical reaction pathways for bio-oil upgrading ¹⁶. (Reprinted with permission from reference 16. Copyright © 2017, Elsevier.)

The rising interest to utilize biomass resources for the production of fuels and chemicals replacing fossil hydrocarbon feedstocks has made it important to better understand the catalyzed transformations of oxygenated compounds ^{3,24,25}. Before upgrading, biomass has a low density and contains a significant fraction of unsaturated bonds ²⁶. Therefore, the transformation to biofuel requires hydrodeoxygenation reactions to lower the oxygen content and increase heat values. The main aim of the transformation is to saturate C=C and C=O bonds (hydrogenation)

and remove oxygen from the oxygen-containing compounds as shown in **Figure 1-4**¹⁶.

1.3.1 Hydrogenation

Hydrogen addition to unsaturated groups, e.g. C=O and C=C, allows its conversion into alcohols, and alkanes. The reduction process can be achieved by (i) addition of electrons followed by protons, the proton donors include water, acids, alcohols, alkalis, and amines and the frequently used catalysts are metals such as Li, Na, K, Mg, Ca, Fe and Zn and corresponding metal salts when the metals possess two or more valence states; (ii) addition of a hydride followed by protons, the hydride derived from hydride reagents like lithium tetrahydroaluminate, alcohol or amine; and (iii) hydrogen atoms addition, which is from either molecular hydrogen or hydrogen donors like alcohols^{27,28}. Catalytic hydrogenation of the unsaturated compounds requires the formation of active hydrogen species and the subsequent bimolecular reaction. Taking C=O hydrogenation as an example for a Langmuir-Hinshelwood based mechanism, the heterogeneous catalytic reaction starts with the dissociative adsorption of molecular hydrogen, which forms two H*, while the substrate molecularly adsorbs on the catalyst surface. The hydrogenation of the C=O bond needs two sequential H addition steps. As a result of the asymmetric structure of the aldehyde/ketone molecular, the H addition sequence can proceed via two plausible pathways as shown in **Figure 1-5**: the alkoxy pathway, in which a reactive hydrogen adatom, H* first attacks the carbonyl carbon, forming an alkoxy intermediate, followed by a second H* attack to the carbonyl oxygen and the formation of an alcohol and hydroxyl pathway, by adding H* to the carbonyl oxygen forming hydroxyl intermediate before adding to the carbonyl carbon. In protic solvents like water, H* can dissociate to a proton and electron, which can result in a proton-electron transfer instead of H* added to the carbonyl group.

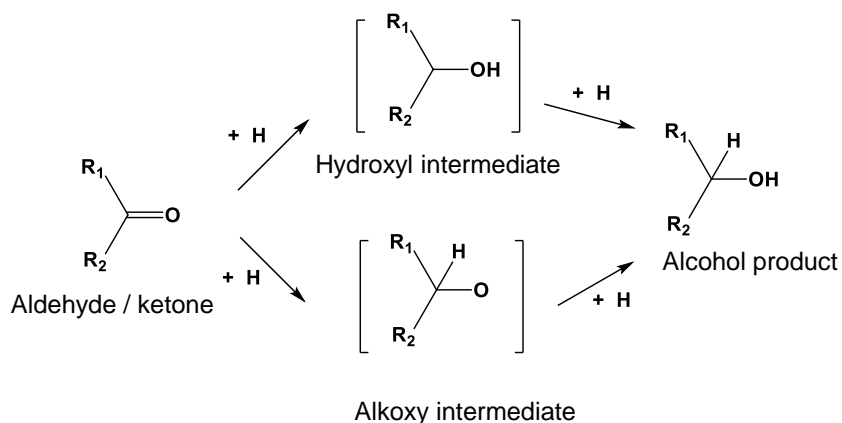


Figure 1-5. Plausible reaction pathways for the hydrogenation of aldehydes and ketones based on Langmuir-Hinshelwood mechanism²⁹. (Reprinted with permission from reference 29. Copyright © 2012, Elsevier.)

The reaction pathway of carbonyl hydrogenation has been intensively studied. Density functional theory (DFT) calculations suggested that in vapor phase, the alkoxy pathway prevails because the formation of alkoxy intermediate is thermodynamically favored^{29,30}. Zhen et al. reported that according to isotope studies, butanal-H₂ reactions proceed via the alkoxy pathway at the vapor-Ru interfaces on Ru/SiO₂ at 323 K³¹. In comparison, the hydroxyl pathway is apparently favored over alkoxy route in presence of solvents, due to the lower barrier to form the O-H bond over the C-H bond and the increased stability of the hydroxyl intermediate over the alkoxy intermediate over Ru³⁰. The proton-electron transfer pathway prevails in water during guaiacol hydrogenation³² and especially in presence of negative potential^{33,34}.

1.3.2 C-O bond cleavage of alcohols

C-O bond cleavage is a necessary procedure to decrease the oxygen content in the organic compounds, which can be achieved by dehydration and hydrogenolysis reactions. Acid-catalyzed alcohol dehydration leads to the formation of olefins (via intramolecular dehydration) or ethers (via intermolecular dehydration)^{35,36}. Generally, the dehydration reactions are performed at relatively high temperatures (≥ 100 °C) due to the large activation energy (~ 150 kJ mol⁻¹)³⁷⁻³⁹. Hydrogenolysis reactions require transition metals for hydrogen activation as well as for the sorption of the reactant, while acid sites are not necessary. The reaction can proceed via a S_N2 reaction mechanism, in which a surface hydrogen directly replaces the carbonyl group from its attachment to the carbon atom in one step^{23,40}. Alternatively, the reaction can follow a stepwise route starting with the dissociation of the C-O bond, leading to a temporary bonding of OH and corresponding residue, and finish with a hydrogen adatom addition in the absence of acid sites²³. In presence of protons, the carbonyl group can be protonated leading to a better leaving group (H₂O⁺) and the C-O bond cleavage yields a carbenium ion. The reaction completes with hydride transfer or deprotonation^{23,40,41}.

Deuterium labeling study is an effective way to distinguish the reaction mechanisms mentioned above. Taking 1-(4-isobutylphenyl) ethanol (4-IBPE) hydrogenolysis as an example, the potential reaction pathways in presence of H₂/D₂ are shown in **Figure 1-6**. The C-O bond scission of 1-(4-isobutylphenyl) ethanol (4-IBPE) leads to the formation of 4-isobutylethylbenzene (4-IBEB) via dehydration-hydrogenation pathway catalyzed by the acidic functional groups on the activated carbon supported Pd²³ or hydrogenolysis route on Pd. The reaction pathways can be distinguished by using isotopic-labeled reactants. The presence of one D can be detected in position 6 (**Figure 1-6**) if the reaction follows dehydration-hydrogenation pathway, while it is not this case with a direct hydrogenolysis route. It was reported over

Pd/SiO₂ and Pd black, the C–O bond scission of 4-IBPE occurred exclusively by direct hydrogenolysis, whereas over Pd/C, both hydrogenolysis and the dehydration–hydrogenation route were observed due to the acidic functional groups on the carbon support. This indicates that the functional groups on the support will change the reaction pathways.

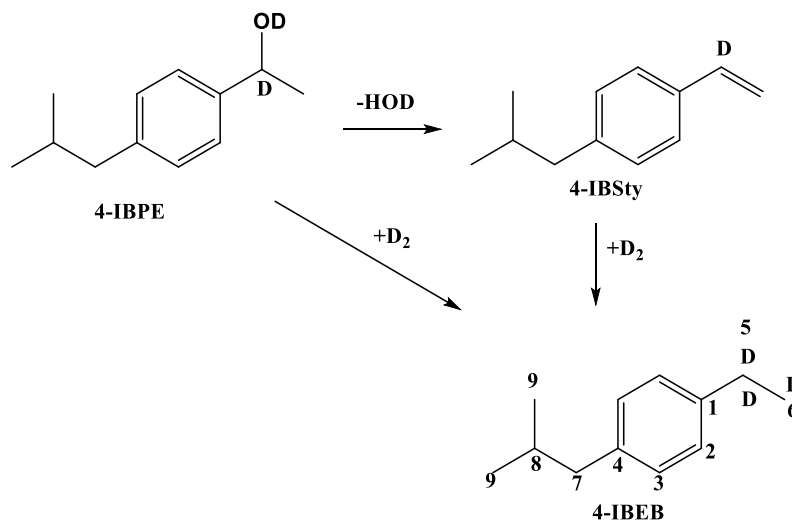


Figure 1-6. Reaction pathways to C–O bond cleavage of 1-(4-isobutylphenyl) ethanol ²³. 4-IBPE, 4-IBSty and 4-IBEB are 1-(4-isobutylphenyl) ethanol, 4-isobutylstyrene and 4-isobutylethylbenzene, respectively. (Reprinted with permission from reference 23. Copyright © 2007, Elsevier.)

1.4 Factors to affect the heterogeneous catalytic process

1.4.1 Catalyst

Common heterogeneous catalysts consist of solid acid catalysts (for acid catalytic reaction, e.g. dehydration, cracking), transition metals (for hydrogenation and dehydrogenation reaction) and transition metal oxides (mainly for oxidation reaction) ^{42–44}. The catalytic activity and product selectivity can be highly affected by catalyst properties, such as particle size, pore size, morphology, catalyst composition, catalyst-support interaction and so on.

Transition metals act as good catalysts because they can donate electrons or withdraw electrons from the reagent, and form chemical bond with reactants. It should be noted that the interaction between catalyst and substrate should be neither too strong nor too weak, so that it can achieve highest activity. If the interaction is too strong, the energy barrier from sorbed state to transition state will be too large for the reaction to happen or the active sites will be blocked by the products. In addition, for a bimolecular reaction, this will lead to a low local concentration for the other reactant due to the competitive adsorption. While if the interaction is too weak, the substrate will fail to bind to the active site and no reaction takes place. This is called Sabatier principle, which has been verified by tons of investigations and used as a

descriptor in heterogeneous catalysis^{45,46}. Pd shows high activity for hydrogenation reactions due to its electronic properties and was chosen for investigation.

1.4.2 Solvent

Solvents are widely used in the heterogeneous catalytic reactions to dissolve and dilute the reactant as well as to increase the contact between the reactant and the catalyst for solid substrates. Thus, to develop the fundamental understanding of reactivity at solid–liquid interfaces is of significant importance^{47,48}. The properties of solvents, such as polarity, acidity, density, hydrogen-bond donating ability and hydrogen-bond accepting ability, are critical in catalysis⁴⁹⁻⁵².

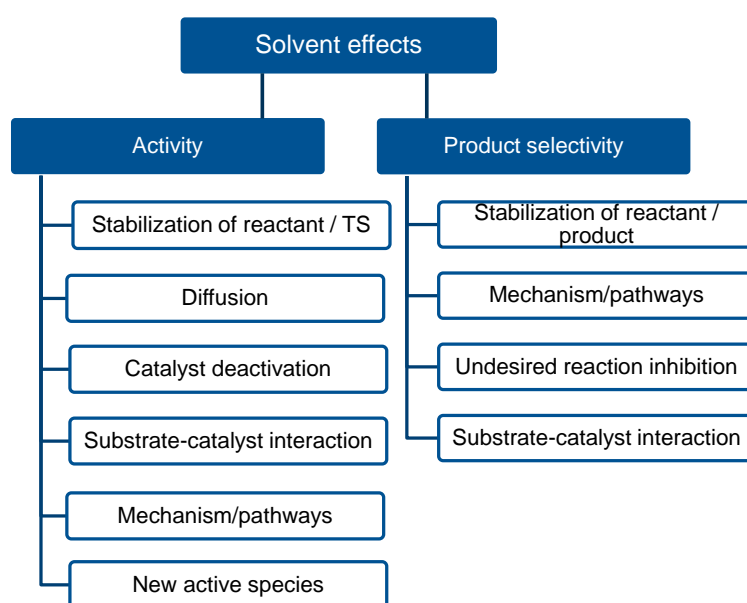


Figure 1-7. Plausible solvent effects in catalysis, which result in differences in reactivity/performance of catalytic reactions and product selectivity/distribution⁵³. (Reprinted with permission from reference 53. Copyright © 2019, Royal Society of Chemistry.)

Compared to the gas-solid interface reaction, the presence of a dense surrounding medium have multiple effects on the catalytic reaction with respect to the 1) reaction rate⁴⁷, 2) product selectivity⁵², 3) reaction pathway⁵⁴, 4) reaction mechanism⁵⁵ and 5) stability of catalysts. The potential reasons that solvent can affect reaction rates are due to the effect on mass transfer⁵⁶, dissolution, kinetics of the reaction by the interaction of the solvent with reactant, intermediate, transition complex and products⁵⁷⁻⁶¹, and also the effect on the catalyst electronic⁶² and geometric structures⁶³ as well as the substrate coverage on catalytic sites via competitive adsorption. Moreover, the solvent can directly involve in the catalytic reaction^{64,65}. **Figure 1-7** categorized the effects as the intrinsic factors responsible for the change in catalytic activity as well as those which influence product selectivity⁵³. Several chosen points will be discussed in

detail as following.

1.4.2.1 Transport phenomena

The viscosity of a solvent can directly affect the mass transfer of the agents⁶⁶, for example, the effective diffusivity for H₂ changes from $1.69 \times 10^{-5} \text{ cm}^2 \text{ s}^{-1}$ in cyclohexanol to $14.9 \times 10^{-5} \text{ cm}^2 \text{ s}^{-1}$ in n-hexane⁶⁷. Kinetic study is meaningless in presence of mass transport limitation. Therefore, it is important to eliminate transport diffusion. A higher stirring speed can help to reduce the external diffusion limitation (film diffusion, from bulk phase to particle surface). In comparison, the internal transport phenomenon (pore diffusion) is more complicated⁶⁸. The most widely used experimental method to examine mass transport limitations is Madon–Boudart (MB) test in catalysis⁶⁹. The test requires a series of rate measurements on catalysts with various number of active sites. The reaction rate will be proportional to the number of active sites, or we can say turn over frequency that the reaction rate is normalized to the number of active sites keeps constant if in the absence of mass transport limitations (both internal and external diffusion).

1.4.2.2 Competitive adsorption

The major difference between liquid phase reaction and gaseous reaction is that the active sites on liquid-solid interface is always saturated with reactants, intermediates, transition states, products and also, the solvent. Thus, the competitive adsorption exists between not only the reactive species but also with the solvent in liquid phase reactions. Apparently, preferential adsorption of the solvent molecules on the active site will inhibit the reactant molecules accessibility and lead to a decrease in reaction rate. In some cases, coadsorbed species might change the adsorption strength of specific adsorbates. For example, the hydroxyl group of sorbed methanol can interact with the π electrons of sorbed cyclohexene, leading to a weaker adsorption strength on Ru⁶⁹. Consequently, an increased selectivity in the hydrogenation of benzene to cyclohexene, rather than the completely hydrogenated cyclohexane, was observed.

Moreover, the sorbed solvent might change the configuration of the substrate and then affect the product selectivity. As shown in **Figure 1-8**, the adsorption of polar solvents on Pd surface decreases the reactivity of the reactants⁷⁰. Besides, the competitive adsorption by the polar solvent molecules makes the benzene ring impossible to be planar adsorption and the hydroxy group of phenol inaccessible to the acid sites, which effectively intercepts the process of cyclohexanol dehydration.

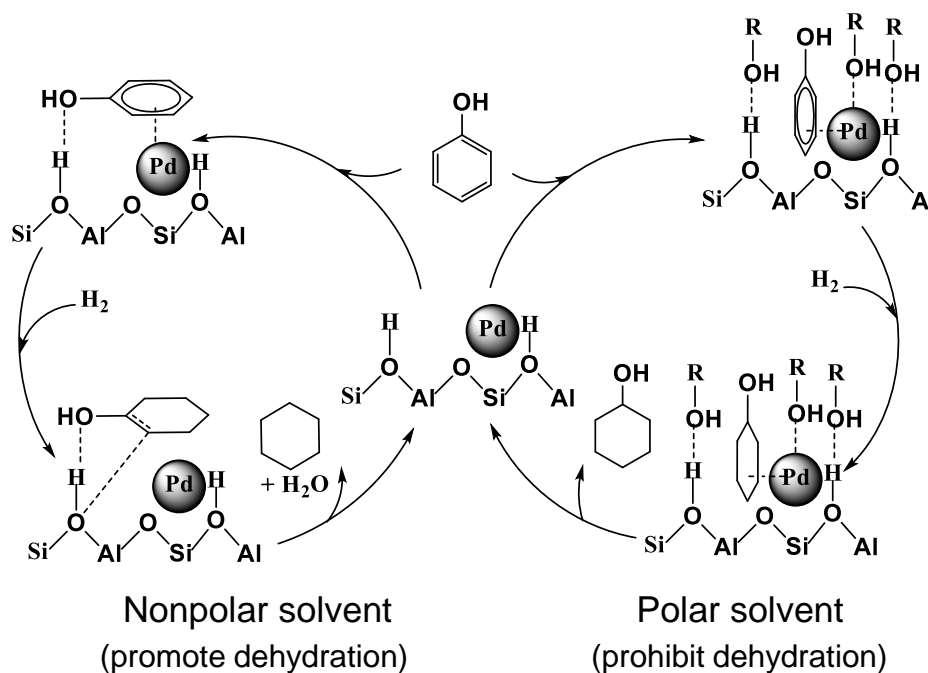


Figure 1-8. Schematic illustration of the solvent effect on product selectivity for the phenol conversion over the bifunctional Pd/NaY catalyst in nonpolar solvent and polar solvent ⁷⁰. (Reprinted with permission from reference 70. Copyright © 2021, Royal Society of Chemistry.)

1.4.2.3 Solvation effect

The solvation, during the catalytic process, including the interaction between the solvent and all reactive species (reactant, intermediate, transition complex and even the products) is of great importance for both activity and selectivity. The intermolecular interactions include hydrogen bonding, ion-dipole interactions, and van der Waals forces. Before the surface reaction starts, the reactant needs to be dissolved in the selected solvent. In this process, a lower coverage of reactant on the active sites will be obtained in a solvent that the reactant can be solvated better compared to a solvent with a weaker interaction under the same reaction condition. It is reported that polar solvents can enhance the adsorption of nonpolar reactants ⁷¹. The adsorption of reactant on catalyst surface can lower the free energy of the reactant in bulk phase, thus a worse solvated reactant (with a higher free energy) will prefer to adsorb on the active sites to lower the system free energy. This is why the equilibrium adsorption constant is generally larger for an agent with a lower solubility. The driving force for surface adsorption includes not only the free energy change for adsorption of substrate (A) onto a surface site ($\Delta G_{\text{ads,A}}$), but also free energy changes associated with the desorption of previously adsorbed solvent (B) ($\Delta G_{\text{ads,B}}$) and interactions of A and B with bulk solvent, both in solution and on the surface ($\Delta G_{\text{solv,solution}}$ and $\Delta G_{\text{solv,surface}}$) ⁶⁸. The interaction between adsorbed species are not considered. Therefore, the driving force expression is,

$$\Delta G = \Delta G_{\text{ads,A}} - \Delta G_{\text{solv,solution,A}} - \Delta G_{\text{solv,surface,A}} - (\Delta G_{\text{ads,B}} + \Delta G_{\text{solv,solution,B}} + \Delta G_{\text{solv,surface,B}})$$

Actually, a better solvated reactant indicates a strong interaction between reactant and solvent (larger $\Delta G_{\text{solv,solution,A}}$), and will lead to a small driving force for substrate adsorption.

On one hand, the reactant solvation will decrease its coverage on the catalytic surface; on the other hand, the activation barrier can also be affected. The free energy difference between transition state and ground state (adsorbed reactants) decides the intrinsic reaction rate, thus the destabilization of the ground state will reduce the energy barrier and then accelerate the reaction rate. Similarly, the stabilization of transition state can also decrease the activation energy.

A significant higher reaction rate in γ -valerolactone (GVL) is obtained compared to water on acid-catalyzed conversion of xylose into furfural, which is attributed to the stabilization of the acidic proton relative to the protonated transition state⁷². Combined the reaction kinetics studies as well as classical and ab initio molecular dynamics simulations, Max et al. reported that altering the relative stabilities of initial states and transition states can achieve a higher rate and selectivity by the use of organic solvents and inorganic additives (water) in acid-catalyzed dehydration of fructose, tert-butanol, 1,2-propanediol and hydroxymethyl furfural⁶¹.

Except for the solvation of ground state and transition state, stabilization of the key intermediate by solvents also significantly affect the reaction activity. Heyden et al. found that the polar solvents such as n-butanol and water increased the turnover frequency by a factor of up to 30 from the gas-phase, via stabilization of key surface intermediates in hydrodeoxygenation of propionic acid on Pd (111)⁷³. In addition, the decarboxylation rate was increased by two orders of magnitude in water making the decarbonylation and decarboxylation pathways become essentially competitive.

1.4.2.4 Involvement in catalytic reaction

It is well known that some side reactions occur due to the reaction of reactant and solvent which are not expected, e.g. aldol condensation in aldehyde hydrogenation in alcohol solvent^{50,74}. Moreover, solvents can be involved in the elementary steps of the expected catalytic reaction and thus change the reaction pathway or reaction mechanism. For example, in hydrogenation reactions, the adsorbed H (H^*) can transform into a solvated proton and an electron at the solvent-metal interface in presence of protic solvents on transition metals^{75,76}. Therefore, the reaction mechanism of the saturation reaction could be either Langmuir-Hinshelwood mechanism with a direct H atom (from the dissociation of hydrogen adsorption) addition^{77,78} or Eley-Rideal mechanism with a proton coupled electron transfer^{31,32,54}. In

addition, it was reported that the H atom from water molecular can directly add to the unsaturated bonds of cinnamaldehyde as shown in **Figure 1-9**, based on isotopic labeling studies and theoretic calculation in Pt₃Fe/CNT catalyzed hydrogenation⁵⁵.

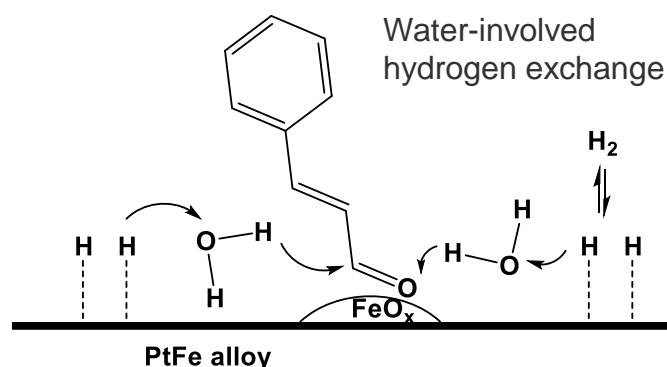


Figure 1-9. The schematic diagram of the reaction pathway of water-involved hydrogen exchange in the Pt₃Fe/CNT-catalyzed CALD hydrogenation⁵⁵. (Reprinted with permission from reference 55. Copyright © 2018, Elsevier.)

1.4.2.5 pH effect

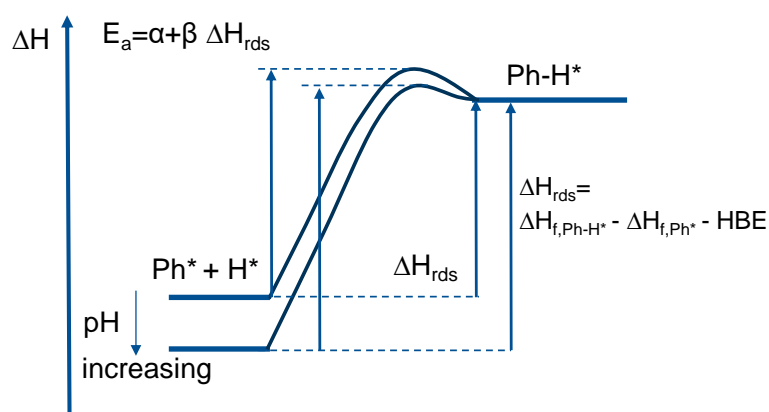


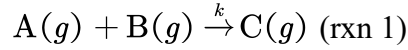
Figure 1-10. Enthalpy diagram of a hydrogenation step at different pH values⁸⁵. (Reprinted with permission from reference 85. Copyright © 2019, American Chemical Society.)

The concentration of hydronium ions is an important parameter of catalysis that can be utilized to control catalytic reaction, such as hydrogenation and dehydration reaction. It is clear that the hydronium ions directly affects the reaction conversion in acid-catalyzed reaction^{39,79}. In addition, increasing concentrations of hydronium ions has been found to enhance the reactivity of Pt-group metals for hydrogenation of aromatic rings and carbonyl groups in oxygenates^{80,81}. This beneficial effect of raising hydronium ion concentrations has been quantitatively related with the weakening of the H-metal bond, and this argument is put forward to explain the orders of magnitude faster electrochemical H₂ evolution and oxidation on Pt-group metals in acid than in base media⁸²⁻⁸⁴. On basis of Brønsted-Evans-Polanyi relationship, the activation energy is proportional to the reaction enthalpy. Therefore, a lower hydrogen

binding energy results in a decreasing hydrogenation barriers (as shown in **Figure 1-10**)⁸⁵.

1.5 Chemical kinetics

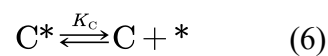
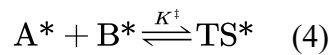
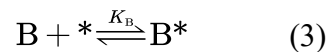
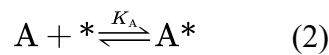
Chemical kinetics is about the reaction rate of a chemical reaction. For a di-molecular heterogeneous reaction in gas phase (rxn 1), the rate equation can be expressed as Equation 1.



$$r = \frac{dP_C}{dt} = kP_A^\alpha P_B^\beta \quad (1)$$

Where P_A and P_B express the concentration (usually used unit of bar) of the species A and B. k is the reaction rate constant which is related to the reactant nature and reaction conditions, e.g. temperature. The exponents α and β are the partial orders with respect to species A and B, stating how the reactant pressure affects the reaction rate. The reaction orders can be positive, zero and negative.

A chemical reaction is composed with one or more elementary steps, in which the chemical species directly form the product in a single step without the formation of transition state and intermediate. Based on Langmuir-Hinshelwood mechanism, the elementary steps of rxn 1 consist of adsorption-surface reaction-desorption. Adsorption/desorption steps are generally considered as quasi-equilibrated and surface reaction as the slower step (rate determining step or kinetic relevant step).



Where $*$ is the empty site, A^* and B^* denote as sorbed A and sorbed B. K_A and K_B are equilibrium constant of A and B adsorption, K^\ddagger is the equilibrium constant of transition state

formation, and k^\ddagger is the rate constant for the product formation. The reaction rate of every elementary step follows law of mass-fraction that the reaction orders equal to the stoichiometric coefficients for each reactant. Therefore the reaction rate for each elementary step is

$$\theta_A = K_A P_A / P^\circ \theta^* \quad (7)$$

$$\theta_B = K_B P_B / P^\circ \theta^* \quad (8)$$

$$\theta_{TS} = K^\ddagger \theta_A \theta_B \quad (9)$$

$$r = k^\ddagger \theta_{TS} \quad (10)$$

Where θ^* , θ_A , θ_B and θ_{TS} are coverage of empty site, reactant A, reactant B and transition state. P° is at standard state pressure (1 bar). The number of active sites is constant, therefore, the sum of θ^* , θ_A , θ_B and θ_{TS} is one. Considering the coverage of transition state is low, this term is not involved in the site balance equation.

$$\theta_A + \theta_B + \theta^* = 1 \quad (11)$$

$$K_A P_A / P^\circ \theta^* + K_B P_B / P^\circ \theta^* + \theta^* = 1 \quad (12)$$

$$\theta^* = (1 + K_A P_A / P^\circ + K_B P_B / P^\circ)^{-1} \quad (13)$$

Combing K^\ddagger and k^\ddagger , the rate constant of the rate determining step is k . The formation rate of product C is

$$r = k^\ddagger \theta_{TS} = k^\ddagger K^\ddagger \theta_A \theta_B = k \theta_A \theta_B = \frac{k K_A P_A / P^\circ K_B P_B / P^\circ}{(1 + K_A P_A / P^\circ + K_B P_B / P^\circ)^2} \quad (14)$$

It should be note in liquid phase reaction in presence of solvent, the empty sites are occupied by solvent. Based on the elementary steps, the relations of chemical potential can be obtained as follows,

$$\mu_{A(g)} = \mu_{A(ad)} \quad (15)$$

$$\mu_{B(g)} = \mu_{B(ad)} \quad (16)$$

$$\mu_{B(ad)} + \mu_{B(ad)} = \mu_{TS} \quad (17)$$

$\mu_{A(g)}$, $\mu_{B(g)}$ are chemical potentials of A and B in gas phase, $\mu_{A(ad)}$, $\mu_{B(ad)}$ are chemical potentials of sorbed A and B. The chemical potential expression of each species are

$$\mu_{A(g)} = \mu_{A(g)}^{\circ} + RT \ln P_A / P^{\circ} + RT \ln \varphi_A \quad (18)$$

$$\mu_{B(g)} = \mu_{B(g)}^{\circ} + RT \ln P_B / P^{\circ} + RT \ln \varphi_B \quad (19)$$

$$\mu_{A(ad)} = \mu_{A(ad)}^{\circ} + RT \ln \theta_A / \theta^* + RT \ln \gamma_A \quad (20)$$

$$\mu_{B(ad)} = \mu_{B(ad)}^{\circ} + RT \ln \theta_B / \theta^* + RT \ln \gamma_B \quad (21)$$

$\mu_{A(g)}^{\circ}$, $\mu_{B(g)}^{\circ}$, $\mu_{A(ad)}^{\circ}$, $\mu_{B(ad)}^{\circ}$ are chemical potential at standard state. φ and γ are activity coefficient, to express the ideality. Under ideal condition, the activity approaches to 1.

1.6 Scope of this thesis

The object of this research is to develop a deeper understanding of the significance of solvents in heterogeneous catalytic reactions. We chose hydrodeoxygenation of biofuels, including the hydrogenation of saturated and unsaturated aldehydes as well as the hydrogenolysis of alcohols as model reactions. All reactions present involve the activation of hydrogen as well as substrate on metal surface before further reaction. Pd nanoparticles supported on activated carbon were used as the catalyst due to the high activity on hydrogen activation. Reaction rate and reaction orders were measured in different solvents. The reaction mechanisms were confirmed based on kinetic isotope effect and deuterium labelling analysis. Kinetic study gives the intrinsic reason for the solvent effect.

In Chapter 2, benzaldehyde was used as a model carbonyl reactant for probing the mechanistic influence of the solvent on aldehyde reduction over Pd/C. The kinetics of the reaction were studied in MeOH, water, dioxane, and THF. The specific hydrogen addition sequence was explored via isotopic labeling of product and reactant in water and dioxane. For both solvents, the hydroxy pathway, which occurs via an initial H attack to the carbonyl oxygen followed by a second H attack to the carbonyl carbon, prevails. With kinetic modeling analysis, we confirmed that the second H addition step is the rate determining step and obtained the equilibrium constants and rate constant of each catalytic step, including those for hydrogen and

substrate adsorption and for the two consecutive hydrogen addition events. The solvent interacts differently with the various reactive precursors and their transition states, and destabilizes them to a different extent. Sorbed substrate and transition state are dissolved to the similar extent and the solvation energy of adsorbed hydrogen decides the reactivity differences in various solvents.

In Chapter 3, the activity and selectivity of the C=O and C=C bond hydrogenation of cinnamaldehyde were explored in both protic and aprotic solvents over activated carbon supported Pd. The hydrogenation rate of both C=C and C=O bond in protic solvents are higher than that in aprotic solvents. Different from sole H_{ad} addition mechanism in aprotic solvent, We suggest protic solvents can act as H transfer shuttle to accelerate the hydrogenation rate, which was supported by the isotope labeling results.

In Chapter 4, hydrogenolysis of benzyl alcohol is catalyzed by activated carbon supported Pd in buffer solutions. In presence of acidic sites, the reaction rate of benzyl alcohol conversion is accelerated by 2-3 orders of magnitude. We proposed a mechanism in which both metal sites and protons, contribute to the benzyl alcohol conversion. The rate determining step is protonated benzyl alcohol losing the hydroxyl group as a water molecule and forming benzyl carbenium ion. Due to the presence of positive charged species, e.g. protonated benzyl alcohol and transition state, electric potential on Pd surface can affect the conversion by changing the chemical potentials of these species. Both hydrogen pressure and hydronium ion concentration can change the electric potential, which is equivalent to an external electric potential. Moreover, hydronium ions can also affect the concentration of transition state.

At the end, summary, conclusions and outlook are given in Chapter 5.

1.7 References

1. Ritchie, H. Energy Production and Consumption. *Our World in Data* <https://ourworldindata.org/energy-production-consumption>.
2. Gallezot, P. Conversion of biomass to selected chemical products. *Chem. Soc. Rev.* **41**, 1538–1558 (2012).
3. Corma, A., Iborra, S. & Velty, A. Chemical routes for the transformation of biomass into chemicals. *Chem. Rev.* **107**, 2411–2502 (2007).
4. Yang, B., Dai, Z., Ding, S. Y. & Wyman, C. E. Enzymatic hydrolysis of cellulosic biomass. *Biofuels* **2**, 421–449 (2011).
5. Samolada, M. C., Papafotica, A. & Vasalos, I. A. Catalyst evaluation for catalytic biomass pyrolysis. *Energy and Fuels* **14**, 1161–1167 (2000).
6. French, R. & Czernik, S. Catalytic pyrolysis of biomass for biofuels production. *Fuel Process. Technol.* **91**, 25–32 (2010).
7. Gallezot, P. Catalytic conversion of biomass: Challenges and issues. *ChemSusChem* **1**, 734–737 (2008).
8. Alonso, D. M., Bond, J. Q. & Dumesic, J. A. Catalytic conversion of biomass to biofuels. *Green Chem.* **12**, 1493–1513 (2010).
9. Goyal, H. B., Seal, D. & Saxena, R. C. Bio-fuels from thermochemical conversion of renewable resources: A review. *Renew. Sustain. Energy Rev.* **12**, 504–517 (2008).
10. Zhang, L., Xu, C. (Charles) & Champagne, P. Overview of recent advances in thermochemical conversion of biomass. *Energy Convers. Manag.* **51**, 969–982 (2010).
11. Alonso, D. M., Bond, J. Q. & Dumesic, J. A. Catalytic conversion of biomass to biofuels. *Green Chem.* **9**, 1493–1513 (2010) doi:10.1039/c004654j.
12. Banerjee, G., Scott-Craig, J. S. & Walton, J. D. Improving enzymes for biomass conversion: A basic research perspective. *Bioenergy Res.* **3**, 82–92 (2010).
13. Mukundan, S., Sriganesh, G. & Kumar, P. Upgrading prosopis juliflora to biofuels via a two-step pyrolysis – Catalytic hydrodeoxygenation approach. *Fuel* **267**, 117320 (2020).
14. Ren, J., Liu, Y. L., Zhao, X. Y. & Cao, J. P. Biomass thermochemical conversion: A review on tar elimination from biomass catalytic gasification. *J. Energy Inst.* **93**, 1083–1098 (2020).

15. Bu, Q. *et al.* A review of catalytic hydrodeoxygenation of lignin-derived phenols from biomass pyrolysis. *Bioresour. Technol.* **124**, 470–477 (2012).
16. Li, X. *et al.* Hydrodeoxygenation of lignin-derived bio-oil using molecular sieves supported metal catalysts: A critical review. *Renew. Sustain. Energy Rev.* **71**, 296–308 (2017).
17. Tran, N., Uemura, Y., Chowdhury, S. & Ramli, A. A review of bio-oil upgrading by catalytic hydrodeoxygenation. *Appl. Mech. Mater.* **625**, 255–258 (2014).
18. Shu, R. *et al.* A review on the catalytic hydrodeoxygenation of lignin-derived phenolic compounds and the conversion of raw lignin to hydrocarbon liquid fuels. *Biomass and Bioenergy* **132**, 105432 (2020).
19. Balaraju, M. *et al.* Influence of solid acids as co-catalysts on glycerol hydrogenolysis to propylene glycol over Ru/C catalysts. *Appl. Catal. A Gen.* **354**, 82–87 (2009).
20. Thomas, J. M. & Harris, K. D. M. Some of tomorrow's catalysts for processing renewable and non-renewable feedstocks, diminishing anthropogenic carbon dioxide and increasing the production of energy. *Energy Environ. Sci.* **9**, 687–708 (2016).
21. Zecchina, A., Califano, S. *The Development of Catalysis*. Published by JohnWiley & Sons, Inc., Hoboken, New Jersey.
22. Ertl, G., Knozinger, H. & Weitkamp, J. *Handbook of Heterogeneous Catalysis*.
23. Thakar, N. *et al.* Deuteration study to elucidate hydrogenolysis of benzylic alcohols over supported palladium catalysts. *J. Catal.* **246**, 344–350 (2007).
24. Venderbosch, R. H., Ardiyanti, A. R., Wildschut, J., Oasmaa, A. & Heeres, H. J. Stabilization of biomass-derived pyrolysis oils. *J. Chem. Technol. Biotechnol.* **85**, 674–686 (2010).
25. Gallezot, P. Conversion of biomass to selected chemical products. *Chem. Soc. Rev.* **41**, 1538–1558 (2012).
26. Ramirez, J. A., Brown, R. J. & Rainey, T. J. A review of hydrothermal liquefaction bio-crude properties and prospects for upgrading to transportation fuels. *Energies* **8**, 6765–6794 (2015).
27. Johnstone, R. A. W., Wilby, A. H. & Entwistle, I. D. Heterogeneous catalytic transfer hydrogenation and its relation to other methods for reduction of organic compounds.

- Chem. Rev.* **85**, 129–170 (1985).
28. Brieger, G. & Nestrick, T. J. Catalytic transfer hydrogenation. *Chem. Rev.* **74**, 567–580 (1974).
 29. Sinha, N. K. & Neurock, M. A first principles analysis of the hydrogenation of C₁C₄ aldehydes and ketones over Ru(0 0 0 1). *J. Catal.* **295**, 31–44 (2012).
 30. Akpa, B. S. *et al.* Solvent effects in the hydrogenation of 2-butanone. *J. Catal.* **289**, 30–41 (2012).
 31. Wu, Z. & Chin, Y.-H. C. Catalytic pathways and mechanistic consequences of water during vapor phase hydrogenation of butanal on Ru/SiO₂. *J. Catal.* **394**, 429–443 (2020) doi:10.1016/j.jcat.2020.10.022.
 32. Shangguan, J. *et al.* The role of protons and hydrides in the catalytic hydrogenolysis of guaiacol at the ruthenium nanoparticle-water interface. *ACS Catal.* **10**, 12310–12332 (2020).
 33. Sanyal, U. *et al.* Hydrogen bonding enhances the electrochemical hydrogenation of benzaldehyde in the aqueous phase. *Angew. Chemie* **133**, 294–300 (2021).
 34. Akhade, S. A. *et al.* Electrocatalytic hydrogenation of biomass-derived organics: A Review. *Chem. Rev.* **120**, 11370–11419 (2020) doi:10.1021/acs.chemrev.0c00158.
 35. Zhang, W., Cheng, G., Haller, G. L., Liu, Y. & Lercher, J. A. Rate enhancement of acid-catalyzed alcohol dehydration by supramolecular organic capsules. *ACS Catal.* **10**, 13371–13376 (2020).
 36. Zhi, Y. *et al.* Dehydration pathways of 1-Propanol on HZSM-5 in the presence and absence of water. *J. Am. Chem. Soc.* **137**, 15781–15794 (2015).
 37. Roy, S. *et al.* Mechanistic study of alcohol dehydration on γ -Al₂O₃. *ACS Catal.* **2**, 1846–1853 (2012).
 38. Kang, M., Dewilde, J. F. & Bhan, A. Kinetics and mechanism of alcohol dehydration on γ -Al₂O₃: Effects of carbon chain length and substitution. *ACS Catal.* **5**, 602–612 (2015).
 39. Liu, Y. *et al.* Enhancing the catalytic activity of hydronium ions through constrained environments. *Nat. Commun.* **8**, 2–9 (2017).
 40. Kieboom, A. P. G., Kreuk, J. F. D. E. & Bekkum, H. V. A. N. Substituent effects in the hydrogenolysis of benzyl alcohol over palladium. *J. Catal.* **66**, 58–66 (1971).

41. Sawadjoon, S., Lundstedt, A. & Samec, J. S. M. Pd-catalyzed transfer hydrogenolysis of primary, secondary, and tertiary benzylic alcohols by formic acid: a mechanistic study. *ACS Catal.* **3**, 635–642 (2013) doi:10.1021/cs300785r.
42. Shimizu, K. I. & Satsuma, A. Toward a rational control of solid acid catalysis for green synthesis and biomass conversion. *Energy Environ. Sci.* **4**, 3140–3153 (2011).
43. Ngaosuwan, K., Lotero, E., Suwannakarn, K., Goodwin, J. G. & Praserthdam, P. Hydrolysis of triglycerides using solid acid catalysts. *Ind. Eng. Chem. Res.* **48**, 4757–4767 (2009).
44. Barton, D. G., Soled, S. L. & Iglesia, E. Solid acid catalysts based on supported tungsten oxides. *Top. Catal.* **6**, 87–99 (1998).
45. Medford, A. J. *et al.* From the Sabatier principle to a predictive theory of transition-metal heterogeneous catalysis. *J. Catal.* **328**, 36–42 (2015).
46. Nørskov, J. K. *et al.* Origin of the overpotential for oxygen reduction at a fuel-cell cathode. *J. Phys. Chem. B* **108**, 17886–17892 (2004).
47. Wang, H. *et al.* Dramatically different kinetics and mechanism at solid/liquid and solid/gas interfaces for catalytic isopropanol oxidation over size-controlled platinum nanoparticles. *J. Am. Chem. Soc.* **136**, 10515–10520 (2014).
48. Gilbert, L. & Mercier, C. Solvent effects in heterogeneous catalysis : Application to the synthesis of fine chemicals. *Stud. Surf. Sci. Catal.* **78**, 51–66 (1993).
49. Murzin, D. Y. Solvent effects in catalysis: Implementation for modelling of kinetics. *Catal. Sci. Technol.* **6**, 5700–5713 (2016).
50. Lashdaf, M., Nieminen, V., Tiitta, M., Ven, T. & Osterholm, H. Role of acidity in hydrogenation of cinnamaldehyde on platinum beta zeolite. **75**, 149–158 (2004).
51. Li, Y. *et al.* Solvent effects on heterogeneous catalysis in the selective hydrogenation of cinnamaldehyde over a conventional Pd/C catalyst. *Catal. Sci. Technol.* **8**, 3580–3589 (2018).
52. Yoshida, H., Onodera, Y., Fujita, S. I., Kawamori, H. & Arai, M. Solvent effects in heterogeneous selective hydrogenation of acetophenone: Differences between Rh/C and Rh/Al₂O₃ catalysts and the superiority of water as a functional solvent. *Green Chem.* **17**, 1877–1883 (2015).
53. Varghese, J. J. & Mushrif, S. H. Origins of complex solvent effects on chemical reactivity

- and computational tools to investigate them: A review. *React. Chem. Eng.* **4**, 165–206 (2019).
54. Hensley, A. J. R., Bray, J., Shangguan, J., Chin, Y.-H. C. & McEwen, J.-S. Catalytic consequences of hydrogen addition events and solvent-adsorbate interactions during guaiacol-H₂ reactions at the H₂O-Ru (0001) interface. *J. Catal.* **395**, 467–482 (2020) doi:10.1016/j.jcat.2020.09.034.
 55. Dai, Y. *et al.* On the role of water in selective hydrogenation of cinnamaldehyde to cinnamyl alcohol on PtFe catalysts. *J. Catal.* **364**, 192–203 (2018).
 56. Klaewkla, R., Arend, M. & F., W. A Review of mass transfer controlling the reaction rate in heterogeneous catalytic systems. *Mass Transfer-Advanced Aspects* doi:10.5772/22962 (2011).
 57. Madon, R. J. & Iglesia, E. Catalytic reaction rates in thermodynamically non-ideal systems. *J. Mol. Catal. A Chem.* **163**, 189–204 (2000).
 58. Sun, Q. *et al.* Creating solvation environments in heterogeneous catalysts for efficient biomass conversion. *Nat. Commun.* **9**, (2018).
 59. Ahmad, E., Khan, T. S., Alam, M. I., Pant, K. K. & Ali Haider, M. Understanding reaction kinetics, deprotonation and solvation of brønsted acidic protons in heteropolyacid catalyzed synthesis of biorenewable alkyl levulinates. *Chem. Eng. J.* **400**, 125916 (2020).
 60. Li, H. & Smith, R. L. Solvents take control. *Nat. Catal.* **1**, 176–177 (2018).
 61. Mellmer, M. A. *et al.* Solvent-enabled control of reactivity for liquid-phase reactions of biomass-derived compounds. *Nat. Catal.* **1**, 199–207 (2018).
 62. Yoon, Y., Rousseau, R., Weber, R. S., Mei, D. & Lercher, J. A. First-principles study of phenol hydrogenation on Pt and Ni catalysts in aqueous phase. *J. Am. Chem. Soc.* **136**, 10287–10298 (2014).
 63. Gould, N. S. *et al.* Understanding solvent effects on adsorption and protonation in porous catalysts. *Nat. Commun.* **11**, 1–13 (2020).
 64. Shangguan, J. & Chin, Y. H. C. Kinetic significance of proton-electron transfer during condensed phase reduction of carbonyls on transition metal clusters. *ACS Catal.* **9**, 1763–1778 (2019).
 65. Mayer, J. M., Hrovat, D. A., Thomas, J. L. & Borden, W. T. Proton-coupled electron transfer versus hydrogen atom transfer in benzyl/toluene, methoxyl/methanol, and

- phenoxy/phenol self-exchange reactions. *J. Am. Chem. Soc.* **124**, 11142–11147 (2002).
66. King, C. J., Hsueh, L. & Mao, K. W. Liquid phase diffusion of nonelectrolytes at high dilution. *J. Chem. Eng. Data* **10**, 348–350 (1965).
67. Mukherjee, S. & Vannice, M. A. Solvent effects in liquid-phase reactions I. Activity and selectivity during citral hydrogenation on Pt / SiO₂ and evaluation of mass transfer effects. **243**, 108–130 (2006).
68. Sievers, C. *et al.* Phenomena affecting catalytic reactions at solid–liquid interfaces. *ACS Catal.* **6**, (2016).
69. Madon, R. J. & Boudart, M. Experimental criterion for the absence of artifacts in the measurement of rates of heterogeneous catalytic reactions. *Ind. Eng. Chem. Fundam.* **21**, 438–447 (1982).
70. Xia, H. *et al.* Tunable selectivity of phenol hydrogenation to cyclohexane or cyclohexanol by solvent-driven effect over bifunctional Pd/NaY catalyst. *Catal. Sci. Technol.* **11**, 1881–1887 (2021) doi:10.1039/d0cy02188a.
71. Singh, U. K. & Vannice, M. A. Kinetics of liquid-phase hydrogenation reactions over supported metal catalysts — a review. **213**, 1–24 (2001).
72. Mellmer, M. A. *et al.* Solvent effects in acid-catalyzed biomass conversion reactions. *Angew. Chemie - Int. Ed.* **53**, 11872–11875 (2014).
73. Behtash, S., Lu, J., Faheem, M. & Heyden, A. Solvent effects on the hydrodeoxygenation of propanoic acid over Pd(111) model surfaces. *Green Chem.* **16**, 605–616 (2014).
74. Yamada, H. & Goto, S. The effect of solvents polarity on selective hydrogenation of unsaturated aldehyde in gas-liquid-solid three phase reactor. *J. Chem. Eng. Japan* **36**, 586–589 (2003).
75. Kizhakevariam, N. & Stuve, E. M. Coadsorption of water and hydrogen on Pt(100): formation of adsorbed hydronium ions. *Surf. Sci.* **275**, 223–236 (1992).
76. Dubouis, N. & Grimaud, A. The hydrogen evolution reaction: From material to interfacial descriptors. *Chem. Sci.* **10**, 9165–9181 (2019).
77. Song, Y. *et al.* Hydrogenation of benzaldehyde via electrocatalysis and thermal catalysis on carbon-supported metals. *J. Catal.* **359**, 68–75 (2018).
78. Singh, N. *et al.* Carbon-supported Pt during aqueous phenol hydrogenation with and

- without applied electrical potential: X-ray absorption and theoretical studies of structure and adsorbates. *J. Catal.* **368**, 8–19 (2018).
79. Liu, Y. *et al.* Solvent-determined mechanistic pathways in zeolite-H-BEA-catalysed phenol alkylation. *Nat. Catal.* **1**, 141–147 (2018).
 80. Hiyoshi, N., Sato, O., Yamaguchi, A. & Shirai, M. Acetophenone hydrogenation over a Pd catalyst in the presence of H₂O and CO₂. *Chem. Commun.* **47**, 11546–11548 (2011).
 81. Lin, H. W., Yen, C. H. & Tan, C. S. Aromatic hydrogenation of benzyl alcohol and its derivatives using compressed CO₂/water as the solvent. *Green Chem.* **14**, 682–687 (2012).
 82. Cheng, T., Wang, L., Merinov, B. V. & Goddard, W. A. Explanation of dramatic pH-dependence of hydrogen binding on noble metal electrode: Greatly weakened water adsorption at high pH. *J. Am. Chem. Soc.* **140**, 7787–7790 (2018).
 83. Sheng, W. *et al.* Correlating hydrogen oxidation and evolution activity on platinum at different pH with measured hydrogen binding energy. *Nat. Commun.* **6**, 6–11 (2015).
 84. Roger, B. Y. The rate of electric hydrogen evolution and the heat of adsorption of hydrogen. *Transactions of the faraday society*, **54**, 1053–1063 (1958).
 85. Singh, N. *et al.* Impact of pH on aqueous-phase phenol hydrogenation catalyzed by carbon-supported Pt and Rh. *ACS Catal.* **9**, 1120–1128 (2019).

Chapter 2

Towards a quantitative understanding of solvent effects on Pd catalyzed benzaldehyde hydrogenation

The nature of the solvent induces variations in the rate of the metal catalyzed hydrogenation of benzaldehyde on Pd (dioxane < tetrahydrofuran < water < methanol). Despite these large differences, the reaction pathway does not change; the majority of turnovers occurs via the adsorption of H₂ and benzaldehyde, followed by stepwise addition of H, first to the carbonyl oxygen, forming an adsorbed hydroxyl intermediate, followed by the kinetically relevant H addition to the C atom of the formyl group (forming benzyl alcohol) and the desorption. The alternative pathways involving the H addition first to C, forming an alkoxy intermediate, occurs to a significantly lesser extent. A pathway in which a proton is added in the first step followed by an electron transfer is excluded on the basis of kinetic isotope effects of H₂O/D₂O and H₂/D₂. An analysis of the solvation energy using excess chemical potentials shows that ground and transition states are destabilized by the solvents compared to those under solvent-free (gas phase) reaction environment. Despite marked differences of the solvent in destabilizing reacting organic substrates in ground and transition states, their nearly identical shifts render the rate differences inconsequential. Instead, the marked reactivity differences arise solely from the differences in the solvation energy of adsorbed hydrogen. The approach provides fundamental insight into the impact of solvents and solvent mixtures for catalyzed hydrogenation.

This chapter is based on the article: Guanhua Cheng et al. Towards a quantitative understanding of solvent effects on Pd catalyzed benzaldehyde hydrogenation (submitted to Nature Catalysis). Guanhua Cheng performed the experiments, did the data analysis and wrote the manuscript.

2.1 Introduction

Catalytic reduction of organic molecules on transition metals is highly relevant in petroleum and petrochemical processes ¹. The reaction typically uses stepwise hydrogen addition to chemically unsaturated bonds with both hydrogen and the reacting substrate chemisorption to the metal surface, i.e., via a Langmuir-Hinshelwood mechanism ^{2,3}. Thus, rates depend on the activities and the adsorption equilibrium constants for H₂ and the organic substrates, which reflect their excess chemical potentials in the sorbed state, as well as the rate parameters prior to the rate determining step.

Such hydrogenation of organic molecules at gas-solid interfaces has been excellently studied and is well understood ^{4,5}. For aldehydes, it is generally accepted that the stronger adsorption reduces the rate of hydrogenation by reducing the coverage of adsorbed hydrogen ⁶. The presence of a liquid phase, particularly a solvent, significantly complicates the quantitative understanding of these rates and thermodynamic parameters in the rate expression. Attempts have been made to interpret the weaker adsorption of organic reactants and hydrogen on transition metal surfaces ⁷⁻⁹. The most prominent factor is the stabilization of the reaction partners in the solvent and the impact of the solvent on binding of reacting fragments to the metal ¹⁰⁻¹². For example, higher catalytic activity for acetophenone hydrogenation in aliphatic C₁-C₅ alcohols ¹³ has been attributed to better stabilization by solvents of higher polarity that reduce the strength of reactant adsorption ¹⁴.

The interaction of solvent molecules with catalyst surfaces and with reactants, transition states, and products has made it very challenging to analyze quantitatively, why the specific solvents influence catalytic reaction rates and selectivities. In a more general way, the marked impact of solvents is hypothesized to be caused by the solvent (i) via altering the adsorption configurations of the reductive groups on the transition metal surfaces ¹⁵, (ii) via altering the potential energy landscape caused by the hydrogen bonding between the protic solvent and organic substrates ¹⁶⁻¹⁸, and (iii) by promoting the adsorption of adsorbates with opposite polarity ¹⁹. These effects of solvents on the standard free energies of reaction precursors, together with similar effects on the transition states of the catalytic steps, influence the free energy landscape of hydrogenation catalysis and in turn rates.

The Langmuir-Hinshelwood type mechanism for hydrogenation has, however, also not been found under all conditions. Especially in water, additional electrochemical effects will influence the surface states of the metal itself ²⁰. In the presence of water adsorbed hydrogen atoms (H*) will be equilibrated with solvated protons and the associated electrons at the metal

interface²¹⁻²³. This may lead to the possibility that hydrogenation occurs via a proton coupled electron transfer^{24,25}. Such reaction paths have been invoked to explain, for example, the promotional effects of water for aliphatic carbonyl reduction on Ru/C catalysts²⁵ and the dependence of benzaldehyde hydrogenation on acid concentrations²⁶.

Hydrogenation of benzaldehyde to benzyl alcohol is a frequently studied model reaction for organic molecules with multiple unsaturated bonds, providing both the aromatic ring and the carbonyl group. Such combination of functional groups mimic frequent chemical motives found in biomass-derived oxygenates, and the product benzyl alcohol is widely used as specialty chemical²⁷. Studies have reported that the rates and selectivities of benzaldehyde hydrogenation depend strongly on the identity of solvent²⁸⁻³⁰³¹, but also on the nature and particle size of the transition metal catalyst^{32,33}, and the acid-base properties of the support³⁴⁻³⁷.

We investigate in this study the impact of four solvents, i.e., methanol (MeOH), water, dioxane, and tetrahydrofuran (THF) on the reduction of benzaldehyde on activated carbon supported Pd (Pd/C) using kinetic methods including isotope labelling and kinetic effects. Reaction pathways are elucidated and the solvation energies as well as their impact on elementary steps are quantified. Detailed kinetic modeling was used to quantify the reversibility and kinetic relevance of the reaction steps. The results underline the importance of the stabilization of sorbed hydrogen, while the substrate is less influential on the reaction rates.

2.2 Experimental method

2.2.1 Chemicals and Catalysts

Pd/C catalyst with a metal content of 5 wt. % and Pd black were purchased from Sigma Aldrich (catalog No. 75992). Benzaldehyde ($\geq 99.0\%$, CAS No. 100-52-7), benzyl alcohol ($\geq 99.0\%$, CAS No. 100-51-6), ethyl acetate ($\geq 99.9\%$, CAS No. 141-78-6), 1,4-dioxane ($\geq 99.0\%$, CAS No. 123-91-1), tetrahydrofuran (THF, $\geq 99.0\%$, CAS No. 109-99-9), methanol (MeOH, $\geq 99.0\%$, CAS No. 67-56-1) and NaCl ($\geq 99.9\%$, CAS No. 7647-14-5) were obtained from Sigma Aldrich and used as received. Doubly deionized water was prepared from purification of deionized water with a Milli-Q water purification system to a resistivity of 18.2 M Ω ·cm. H₂ (Air Liquide, $>99.99\%$) was used for hydrogenation.

2.2.2 Catalyst Characterizations

The specific surface area and pore diameter distributions of the Pd/C catalyst were determined by N₂ physisorption isotherms, measured at 77 K on a PMI automated BET sorptometer with

BET and BJH models. Pd dispersion was determined with H₂ chemisorption at 298 K. Prior to the measurement, the materials were pre-reduced in hydrogen at 573 K for 1 h, treated in vacuum at 573 K for 1h and then cooled to 298 K. The first adsorption isotherm was measured from 1 to 40 kPa H₂, which gives the total H₂ uptakes. Afterwards, the sample was outgassed at 298 K for 1h and the second isotherm was measured, which gives the amount of physisorbed H₂. The amount of chemisorbed H₂ was determined by the difference in the adsorbed amounts between the two isotherms, extrapolated to zero H₂ pressure. The Pd dispersion was determined from the amount of chemisorbed H₂ at zero pressure, by assuming a stoichiometry of 1 H:1 Pd surface atom. Additionally, the average particle size of Pd was measured by transmission electron microscopy (TEM). The catalyst sample was grounded and ultrasonically dispersed in ethanol. Drops of the catalyst suspensions were applied on a copper-carbon grid and the measurements were carried out in a JEOL JEM-2011 electron microscope with an accelerating voltage of 120 keV. Statistical treatment of the metal particle size was carried out by counting at least 300 particles from representative TEM micrographs. The characterization of Pd/C is shown in SI, Section S1.

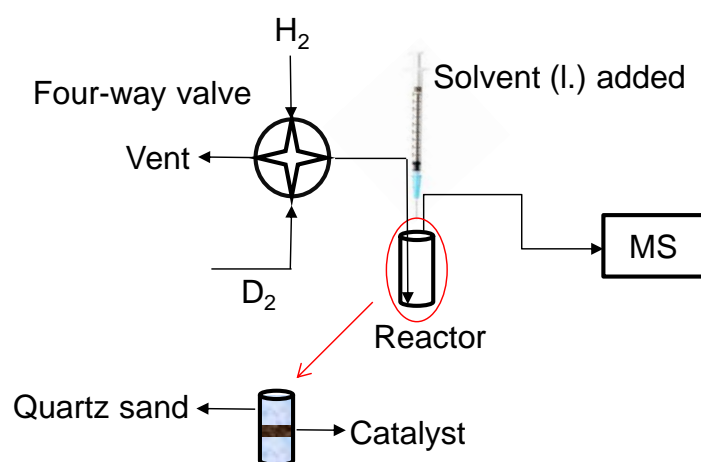
2.2.3 Catalytic hydrogenation of benzaldehyde

Benzaldehyde hydrogenation in different solvents was carried out in a 300 mL Hastelloy PARR reactor. Rate and selectivity measurements were performed in the batch reaction mode at 298 K. In a typical reaction, an aliquote of benzaldehyde (225-7000 μ L) was dissolved in 100-150 cm³ of solvent (H₂O, dioxane, THF, and MeOH). 5-80 mg Pd/C was added to this reaction mixture. The reactor was purged three times with 20 bar H₂ to ensure the complete removal of air from the reactor before the subsequent introduction of 0.5-10 bar H₂ (at atmospheric temperature). After H₂ introduction, the reactor was heated to the reaction temperature (298 K) under vigorous stirring (> 750 rpm). The reaction time is defined by the time in which the reactor has reached the desired reaction temperature and maintained at that temperature. During the reaction in batch mode, \sim 1 cm³ sample was withdrawn from the reactor periodically at specific time intervals; the concentrations of reactants and products in these samples obtained at different reaction times were quantified using a gas chromatograph (GC) equipped with a wax capillary column (30 m \times 250 μ m) and a flame ionization detector (FID). The reaction order in H₂ was determined at 298 K by systematically varying the H₂ pressure from 0.2 to 5 bar; the reaction orders in benzaldehyde with water MeOH, THF, and dioxane solvents were measured by varying the benzaldehyde concentration when keeping the H₂ pressure at 1 and 5 bar, respectively, at 298 K.

Benzaldehyde hydrogenation in gas phase was performed in a continuous stirred tank reactor (CSTR) with 1mg Pd/C at 298K and ambient pressure. Before the reaction, the catalyst was reduced in H₂ (10 mL min⁻¹) for 1 h, then a reactant fed of H₂ with gaseous benzaldehyde was introduced to the reactor. The gaseous benzaldehyde was introduced by N₂ flowing through a bottle of liquid benzaldehyde at room temperature, carrying out the gaseous benzaldehyde with saturated vapor pressure. By changing the flow of H₂ and N₂, the partial pressure of H₂ and benzaldehyde were varied. Typically, the total flow rate was 40 mL min⁻¹ with a hydrogen partial pressure from 20 mbar to 50 mbar. The benzaldehyde partial pressure in the CSTR was detected in-situ using an infrared spectroscopy with a Thermo Fischer Nicolet 6700 spectrometer at a resolution of 1 cm⁻¹ accumulating 32 scans.

2.2.4 Transient response method

A transient response method was used to measure the H coverage on Pd black at room temperature and 1 bar pressure in presence of solvent. The approach is to replace pre-adsorbed H on Pd with D from D₂, producing quantitatively HD and D₂. Then the H coverage on Pd is calculated by quantifying the amount of H in the desorbed HD and H₂. The schematic diagram of the setup is as shown in Scheme S1, gas line of H₂/D₂ connecting with a transparent microreactor tube and followed by a mass spectrometer. 50-100 mg Pd black was placed in the center of two layers of quartz sand (particle size of 200-300 μm) in a microreactor (~1.5 mL). The catalyst was first reduced by H₂ flow and then 0.6 ml liquid solvent was added to immerse the Pd. After that, H₂ and D₂ was alternatively flowing through the catalyst, and the gas components was detected using a mass spectrometer (MS, Omni Star GSD 320). Solvent was added in liquid phase by a syringe.



Schematic diagram of the transient response analysis system.

2.2.5 Isotopic labeling experiments

The isotopic experiments were carried out in a 300 mL Hastelloy PARR reactor. For the reaction in water solvent, 14.8 mM benzaldehyde, 150 mL H₂O/D₂O solvent, 1 bar H₂/D₂, and 5 mg Pd/C were used. For reaction with dioxane solvent, 115 mM benzaldehyde, 100 mL dioxane solvent, 5 bar D₂, and 80 mg Pd/C were used. Before the reaction, air was removed from the reactor by introducing 20 bar H₂/D₂, followed by depressurizing the reactor for three times. For reactions in the aqueous phase, ethyl acetate was used to extract the chemical species and then were quantified using GC-MS equipped with a HP-5 capillary column. Selected samples obtained in H₂/D₂O were also analyzed with ¹H nuclear magnetic resonance (NMR) spectroscopy (500 MHz).

2.2.6 Vapor pressure of benzaldehyde in solution

The gas composition of 1M benzaldehyde solution in dioxane, THF and MeOH, saturated aqueous benzaldehyde solution as well as condensed benzaldehyde was analyzed by mass spectrometer (MS, Omni Star GSD 320) at 298K. With the calibration of condensed benzaldehyde which is respect to saturated benzaldehyde vapor pressure, benzaldehyde vapor pressure in the respective solution was obtained and further equilibrated constant of benzaldehyde dissolution.

2.2.7 Determination of equilibrium constant of H₂ and benzaldehyde in gas phase

The adsorption of H₂ was obtained by hydrogen chemisorption as described in 2.2. The adsorption of benzaldehyde from gas phase onto Pd black was performed using a Seteram microbalance connected to a vacuum system and a pressure controlled liquid vaporizing system. In the experiment, 20 mg Pd black was loaded on the microbalance and activated in H₂ (~1mbar) at 313 K for 20 min, then vacuum, this step was repeated until the catalyst weight was constant to make sure the catalyst was reduced thoroughly. After that, the catalyst was kept in vacuum state overnight for H₂ desorption. The benzaldehyde vapor was introduced stepwise onto the catalyst through a dosing valve under a delicate control of the pressure. When the mass keep constant even benzaldehyde pressure increase indicates the Pd surface is fully covered. After equilibration under a certain pressure, the adsorbed amount was quantified by the mass increase.

2.3 Results and discussions

2.3.1 Effects of solvent on turnover rates and reaction orders for benzaldehyde hydrogenation on Pd/C

Condensed phase benzaldehyde hydrogenation on Pd/C leads to selective C=O bond

saturation, forming benzyl alcohol as the sole product without hydrogenating the arene ring. Such high selectivity was found also for Rh/C, Ni/C, and Pt/C³⁸. The turnover number (TON) and turnover frequency (TOF) for benzyl alcohol formation in different solvents (water, methanol (MeOH), tetrahydrofuran (THF), and dioxane) are compared in **Table 2-1** and **Figure A2-2**. The TONs and TOFs for benzyl alcohol formation were considerably higher in water and MeOH than in THF and dioxane. Most strikingly, the reaction orders for benzaldehyde and H₂ differ among the solvents (**Table 2-1** and **Figure A2-2b** and **A2-2c**).

Table 2-1. Summary of reaction rates and reaction orders for the reduction of benzaldehyde on Pd/C.

Solvent	TOF (mol mol _{Pd} ⁻¹ s ⁻¹) at 298 K ^a	Reaction order in benzaldehyde (α_s)	Reaction order in H ₂ (β_s)
MeOH	0.99	0.01±0.08	0.81±0.01
Water	0.47	0.05±0.13	1.02±0.05
THF	0.11	0.47±0	0.26±0.02
Dioxane	0.033	0.31±0.02	0.17±0.02

^a Initial TOF at 1 bar H₂ and 14.8 mM initial benzaldehyde concentration.

Figure A2-2b shows the TOF as a function of benzaldehyde concentration. As the benzaldehyde concentration increases, TOFs increase in THF and dioxane, but remain unchanged in water and MeOH. Therefore, the apparent rate equation for the hydrogenation ($r_{\text{BZH},s}$, where subscript BZH denotes benzaldehyde and s denotes solvent, $s = \text{H}_2\text{O}$, MeOH, dioxane, THF) is:

$$r_{\text{BZH},s} = - \frac{dn_{\text{BZH}}}{dt} = k_{\text{eff},s} n_{\text{Pd}} C_{\text{BZH}}^{\alpha_s} P_{\text{H}_2}^{\beta_s} \quad (1)$$

$k_{\text{eff},s}$ is the lumped rate constant in solvent s , which contains the Henry constant of H₂ dissolution, equilibrium constants of dissolved H₂ and benzaldehyde adsorption as well as rate constant of the kinetically relevant H addition step; n_{Pd} is amount of surface Pd sites; α_s and β_s are the apparent reaction orders with respect to benzaldehyde and H₂ in solvent s , respectively. Under constant P_{H_2} , TOFs decreased in the order of MeOH > water > THF > dioxane. The reaction orders with respect to benzaldehyde in these solvents, α_s , vary from 0 (MeOH, water), 0.31 (dioxane), to 0.47 (THF). The 0th order in water and MeOH suggests that in these solvents, Pd surfaces are fully saturated and covered with adsorbed benzaldehyde or benzaldehyde derived intermediates before the rate determining step. A positive, fractional order in THF and dioxane suggests the metal surfaces to be only partly covered with adsorbed benzaldehyde and/or the

quasi-equilibrated intermediates. **Figure A2-2c** shows the initial TOF values as a function of the H₂ pressure (1-5 bar). The reaction orders with respect to H₂, β_s , vary from 0.81 (MeOH), 1.02 (water), 0.26 (THF), to 0.17 (dioxane) (**Table 2-1**). The variation in rates and reaction orders demonstrates the strong impact of the solvents on the adsorption and, hence, coverage of benzaldehyde and hydrogen.

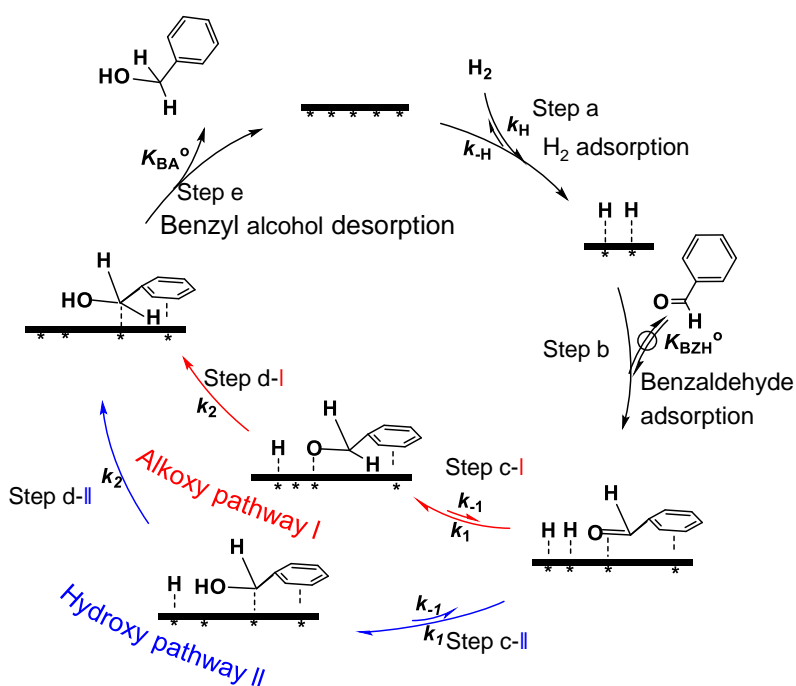
It should be emphasized, however, that solvents may also alter the nature and free energy of the transition states for catalytic steps and in turn influence the rates and the kinetic relevance of the elementary steps along the reaction coordinate. These effects may alter the catalytic pathways, observed kinetic dependencies, and net rates. Additionally, protic solvents such as water and MeOH can coordinate and solvate the hydrogen adatoms on Pd surfaces, converting them to interfacial protons, which have been shown to promote C=O bond hydrogenation of carbonyl groups²⁵. In contrast, the aprotic solvents, such as THF and dioxane neither assist with interfacial proton formation nor form strong hydrogen bonds with the reactants, intermediates, and transition states.

2.3.2 Mechanism of benzaldehyde hydrogenation on Pd—elementary steps, their reversibility, and kinetic relevance of H addition steps to the carbonyl C and O of benzaldehyde.

To interpret the marked variation in kinetic dependencies among the different solvents, we first interrogate the general mechanism of the individual hydrogen addition events, without assigning their kinetic relevance and equilibrium position, and then probe, how solvents may influence the free energies of the adsorbates, the intermediates, and transition states within the catalytic cycle and in turn the identity of the kinetically relevant step.

Scheme 2-1 describes the catalytic sequences and their elementary steps in condensed phase benzaldehyde hydrogenation. The catalytic cycle begins with H₂ dissociative adsorption on a Pd site pair (*-*), forming two adsorbed H adatoms (H*) (Step a). Meanwhile, benzaldehyde adsorbs on an ensemble of vacant Pd (*) as chemisorbed benzaldehyde (BZH*) (Step b). The C=O bond hydrogenation reaction requires two successive hydrogen addition steps, i.e., Step c and Step d. Two pathways for hydrogen addition exist, i.e., the alkoxy pathway and the hydroxy pathway, depending on H addition sequence³⁹. The latter pathway resembles the proton-electron coupled transfer pathway (PECT), but adds a hydrogen atom instead of a proton in the initial step. Addition of a proton coupled to an electron transfer has been ruled out (see below).

For the alkoxy pathway (labeled Alkoxy pathway I and indicated by the red arrows), a reactive hydrogen adatom, H^* , first attacks the carbonyl carbon, forming an alkoxy intermediate ($BZH-H^*$, Step c-I), followed by a second hydrogen attack to the carbonyl oxygen, which forms the benzyl alcohol (BA^* , Step d-I). For the alternate hydroxy pathway (labeled Hydroxy pathway II and indicated by blue arrows), the reactive H^* first attacks the oxygen, forming an O-H bond ($BZH-H^*$, Step c-II), followed by the second attack to the carbonyl carbon, which forms the C-H bond (BA^* , Step d-II). The catalytic cycle completes with the quasi-equilibrated desorption of benzyl alcohol from Pd (Step e).



Scheme 2-1 Schematic illustration of benzaldehyde hydrogenation pathways: alkoxy (red) and hydroxy (blue).

In general, the adsorption-desorption steps (Steps a-b and e) occur much faster than the surface reaction. Thus, they are considered to be quasi-equilibrated. However, the H_2 adsorption step does not reach chemical equilibrium, because its desorption rate is comparable with that of benzaldehyde hydrogenation in water⁴⁰. For this reason, H_2 adsorption was considered here to be reversible, but not quasi-equilibrated in the kinetic treatment.

Irrespective of the pathways, the rate expressions have an identical form. Considering the first H addition to be reversible (which could be Steps c-I and c-II) and the second H addition step (Steps d-I and d-II) to be irreversible, the complete rate expression is (see derivation in Appendix 2-6, Section A2-3):

$$r_d = -\frac{dn_{\text{BZH}}}{dt} = \frac{n_{\text{Pd}} k_2 K_1^\circ \eta_1 K_{\text{BZH}}^\circ C_{\text{BZH}} K_{\text{H}_2}^\circ P_{\text{H}_2} \frac{k_{-\text{H}}}{k_{-\text{H}} + k_2 K_1^\circ \eta_1 K_{\text{BZH}}^\circ C_{\text{BZH}}}}{\left(1 + \sqrt{K_{\text{H}_2}^\circ P_{\text{H}_2} \frac{k_{-\text{H}}}{k_{-\text{H}} + k_2 K_1^\circ \eta_1 K_{\text{BZH}}^\circ C_{\text{BZH}}}} + K_{\text{BZH}}^\circ C_{\text{BZH}} + K_1^\circ \eta_1 \sqrt{K_{\text{H}_2}^\circ P_{\text{H}_2} \frac{k_{-\text{H}}}{k_{-\text{H}} + k_2 K_1^\circ \eta_1 K_{\text{BZH}}^\circ C_{\text{BZH}}}} K_{\text{BZH}}^\circ C_{\text{BZH}}\right)^2} \quad (2)$$

Despite the identical formalism, the individual thermodynamic and rate constants contained within the rate expressions differ in their values and chemical meaning for the two pathways. In Equation 2, n_{Pd} is amount of surface active sites; C_{BZH} and P_{H_2} denote the benzaldehyde concentration and hydrogen pressure, respectively; k_2 is the rate constant of the 2nd H addition step; K_{BZH}° is the equilibrium constant of benzaldehyde adsorption step; k_{H} and $k_{-\text{H}}$ are the forward and reverse rate constants of hydrogen adatom adsorption step (from $\text{H}_2(\text{g})$), respectively, and their ratio ($k_{\text{H}}/k_{-\text{H}}$) equals $K_{\text{H}_2}^\circ$, the adsorption constant of H_2 dissociative adsorption; K_1° is the thermodynamic equilibrium constant of step c, which equals the ratio of the forward rate constant to the reverse rate constant of the 1st H addition (k_1/k_{-1}); η_{H} and η_1 denote the approaches-to-equilibrium for hydrogen adsorption (Step a) and the 1st H addition (Step c), respectively; each approach-to-equilibrium is defined by the ratio of its reverse rate to its forward rate of the reaction, which also equals the ratio of the reaction quotient to equilibrium constant of the respective reaction step. It should be noted that the $K_{\text{H}_2}^\circ$ is the product of the Henry constant of H_2 dissolution (K_{Henry}) and the adsorption constant of dissolved H_2 on Pd ($K_{\text{H}_2, \text{solv}}^\circ$), $K_{\text{H}_2}^\circ = K_{\text{Henry}} K_{\text{H}_2, \text{solv}}^\circ$.

2.3.3 Thermodynamic and kinetic contributions determining the rate of benzaldehyde hydrogenation in different solvents

Figure 2-1 shows the change of benzaldehyde concentration during its hydrogenation on Pd/C in dioxane and water at constant H_2 pressure. The slopes along these profiles reflect the instantaneous rate at a particular benzaldehyde concentration. For reactions with different initial benzaldehyde concentrations in dioxane (**Figure 2-1a**), the concentration decrease appears to be largely linear, but such consumption becomes less pronounced as a large portion of benzaldehyde is consumed. The dependencies confirm that the reaction order with respect to benzaldehyde, α_{dioxane} (Equation 1), is positive, but significantly smaller than unity and consistent with that derived from the initial rates (**Table 2-1**, 0.26). **Figure 2-1b** shows the nearly overlapping time-dependent benzaldehyde concentration profiles, irrespectively of the H_2 pressure. A close examination shows that the benzaldehyde concentration decay appears to be slightly higher for reactions conducted at higher H_2 pressures, thus, the effective reaction

order with respect to H_2 , β_{dioxane} , is a modestly positive (**Table 2-1**, 0.17). Similar benzaldehyde concentration decays and the associated kinetic interpretations were also found with THF (**Figure A2-3**).

For dioxane, incorporating 59 mM of benzyl alcohol (the product) into the reaction mixture alters neither the benzaldehyde concentration profiles nor rates (**Figure A2-4**, **Appendix, Section A2-4**), indicating the competitive adsorption of benzyl alcohol alters neither the fractional coverages of the various intermediates nor the turnover rates. This finding is consistent with those of DFT calculations on uncovered Pd (111) that showed a weaker adsorption of benzyl alcohol than that of benzaldehyde (109 kJ mol^{-1} ⁴¹ vs. 156 kJ mol^{-1} ⁴²).

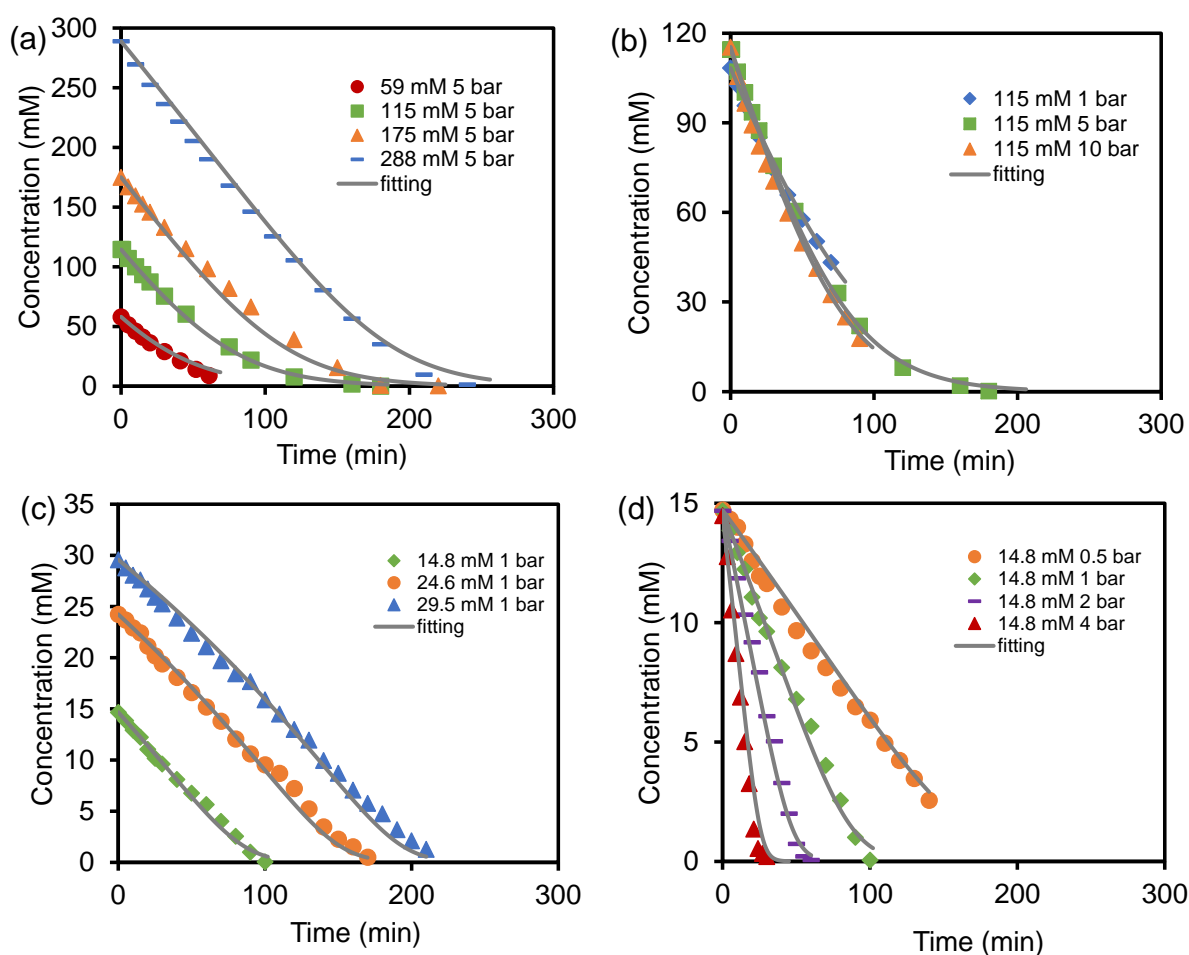


Figure 2-1. Hydrogenation of benzaldehyde on Pd/C under different starting benzaldehyde concentration and H_2 pressure. (a) Changes of benzaldehyde concentration with time for different starting benzaldehyde concentrations in dioxane (80 mg Pd/C) at 298 K and 5 bar H_2 . (b) Changes of benzaldehyde concentration with time at different hydrogen pressures in dioxane (115 mM, 80 mg Pd/C) at 298 K. (c) Changes of benzaldehyde concentration with time for different starting benzaldehyde concentrations in H_2O (5 mg Pd/C) at 298 K and 1 bar H_2 . (d) Changes of benzaldehyde concentration with time under different hydrogen pressures in H_2O (14.8 mM, 5 mg Pd/C) at 298 K. The grey lines refer to the regression curves based on Equation 2.

For the contrasting case with water (**Figures 2-1c and 2-1d**), benzaldehyde concentrations decrease nearly linearly over the entire conversion range (0-100%), as also verified with separate kinetic studies by varying the initial benzaldehyde concentration (15-30 mM). Taken together this linear benzaldehyde concentration decrease and the variation of the initial benzaldehyde concentrations, we conclude that TOFs are insensitive to benzaldehyde concentrations. In contrast, the rates increase proportionally to the H₂ pressure (0.5-4 bar, **Figure 2-1d**). Similar rate dependencies were observed for MeOH as solvent (**Figure A2-3**), suggesting that the effective reaction orders in protic solvents are distinctly different from those in aprotic solvent.

An integral analysis, carried out on regression of these time-dependent decays of benzaldehyde concentration in **Figure 2-1** and **Figure A2-3** against the generalized rate expression in Equation 2, results in the kinetic parameters, which consist of the rate and equilibrium constant values. Prior to the regression, we first determined $K_{H_2}^\circ$, the equilibrium constant for dissociative H₂ adsorption on Pd using a thermodynamic approach. In principle, $K_{H_2}^\circ$ can be obtained, by measuring the H coverage (θ_H) on Pd under a certain pressure of H₂ and using Equation 3:

$$K_{H_2}^\circ = \frac{\theta_H^2}{P_{H_2} (1 - \theta_H)^2} \quad (3)$$

Under solvent-free conditions, this measurement was easily done using a gaseous H₂-chemisorption approach (see Section S5 in Supporting Information for details). However, this approach is not adaptable to the condition with liquid solvent, because a minimum pressure is required to maintain the solvent as liquid. Therefore, we designed a transient response method to determine the coverage of H (θ_H) in the presence of solvent under flowing H₂ (~1 bar), in which the sorbed H on Pd was replaced and purged out into an on-line mass spectrometer after switching from H₂ flow to D₂ flow. Detail are reported in the experimental section.

Figure 2-2 shows the time dependent partial pressures of H₂, HD and D₂ in the transient H₂-D₂ experiments for dioxane, THF, water and methanol respectively. The grey curve is the H₂ partial pressure in the control experiments without Pd, which showed a gradual decreasing tail caused by backmixing in the empty volume of the reactor tube after switching to D₂ flow. The blue curve is the H₂ partial pressure in experiments with Pd, and its decreasing tail was caused by both the backmixing in the dead volume and desorption of the pre-adsorbed H. The difference between the blue curve and grey curve describes the desorbed H₂ from pre-adsorbed H. The black curve corresponds to D₂ and the orange curve to the formed HD by the transient

common presence of sorbed H and D on Pd. The HD shows a peak as it is formed and desorbs from the Pd surface. In dioxane (**Figure 2-2a**) and THF (**Figure 2-2b**), the H₂ tail was pronounced, indicating high coverages of H (θ_H). In contrast, in water and MeOH solvent, the tail of H₂ (blue) dropped and disappeared faster than that of the blank experiment. This is hypothesized to be caused by the low coverage of H and in parallel a fast consumption of back-mixed H₂ via reacting with D₂ into HD. The total H amount in desorbed HD and H₂ allows for the calculation of H adsorbed and the H* coverage (θ_H), by normalizing the cumulative amount of H desorbed (as HD and H₂) to the surface Pd atoms (the metal dispersion of Pd black used here is ~8 %). The measured θ_H and calculated $K_{H_2}^0$ are compiled in **Table 2-2**. It is worthwhile to note here that within the time scale of this transient experiment after switching gas (< 20 s), D₂ mainly reacts with the surface pre-adsorbed H during the transient reaction. The reaction and desorption of hydride (palladium hydride, PdH_x) in the bulk solid phase is very slow that takes hours of time span, and in particular the main desorption occurs, when the solvent is completely evaporated (see **Appendix, Section A2-6** for details).

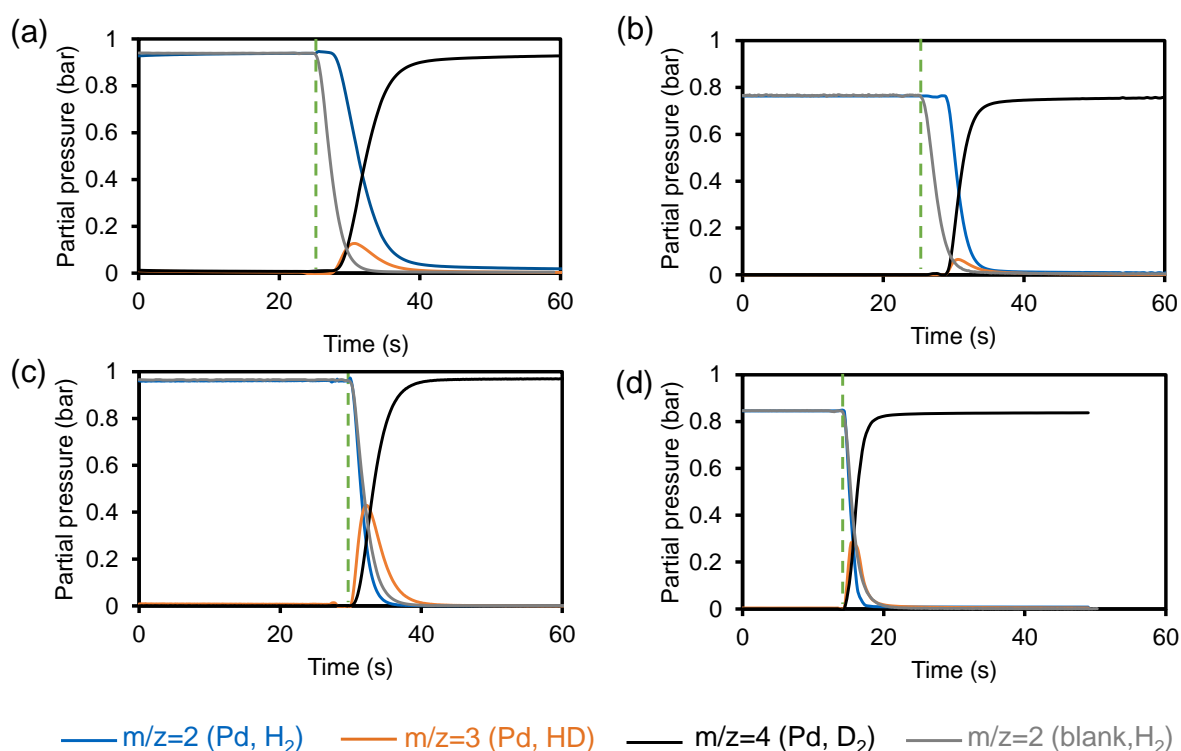


Figure 2-2. Transient response of HD and H₂ following the switch from H₂ to D₂. In (a) dioxane on 100 mg Pd black*, (b) THF on 100 mg Pd black, (c) water on 50 mg Pd black, and (d) methanol on 50 mg Pd black at 298 K and 1 bar pressure. Blank in the figures is signal of H₂ in control experiments without Pd black. The dash line in Figures shows the switch point from H₂ to D₂. (*Pd black instead of Pd/C was used here to avoid the sorption of H₂ on activated carbon support.)

Table 2-2. H coverage on Pd in the corresponding solvent and the equilibrium constant of H₂ adsorption at 298 K.

Solvent	H ₂ pressure ^a [bar]	H coverage [mol _H mol _{Pd-surf} ⁻¹]	K _{H₂} ^{o b}
Dioxane	0.95	0.89 ± 0.03	77
THF	0.77	0.44 ± 0.10	0.83
Water	0.97	0.31 ± 0.05	0.20
MeOH	0.85	0.02 ± 0.03	4.0×10 ⁻⁴

^a H₂ pressure and vapor pressure of the solvent add up to 1 bar. ^b The equilibrium constant of H₂ adsorption has been referred to 1 bar.

Using the $K_{H_2}^o$ reported in **Table 2-2**, the regression of the time dependent concentration profiles of benzaldehyde during its hydrogenation catalysis in **Figure 2-1** (dioxane and water) and **Figure A2-3** (THF and methanol) with Equation 2 yields the rate and equilibrium constants at 298 K compiled in **Table 2-3**. For comparison, the adsorption of H₂ and benzaldehyde on Pd as well as the hydrogenation reaction were also carried out in gas phase, representing the solvent-free condition (see **Appendix, Section A2-5** for details). The results demonstrate the strong effects of solvent on the individual kinetic and thermodynamic parameters.

We first compare the two solvent groups of polar protic (water and MeOH) vs. aprotic solvents (dioxane and THF). Although all solvents largely weaken the adsorption of H₂ and benzaldehyde compared to solvent-free condition, the equilibrium constant $K_{H_2}^o$ is larger in aprotic solvents than in protic solvents, ranging from 77 for dioxane to 4×10⁻⁴ for methanol and 4×10² for the gas phase (**Table 2-3**). In contrast, the difference in the equilibrium constants for benzaldehyde adsorption (K_{BZH}^o) is comparatively less pronounced between protic and aprotic solvents, ranging from 1.3 (THF) < 4.0 (methanol) < 11.3 (water) < 20 (dioxane). In dioxane and THF, the term η_H , which describes the approach-to-equilibrium for H₂ adsorption, is essentially near unity, indicating that this step is quasi-equilibrated. In contrast, it decreases to 0.90 in MeOH and to 0.02 in water, indicating deviation from the quasi-thermodynamic equilibrium. Since η_H reflects the ratio of the reverse and the forward rate for the H₂ dissociative adsorption (r_{-H}/r_H), the very small η_H of 0.02 in water suggests that the vast majority of surface bound hydrogen reacts with benzaldehyde, while only a small fraction recombines and desorbs as H₂. This is in accordance with the very high Faradaic efficiency (~99%) in electrocatalytic hydrogenation of benzaldehyde on Pd ³⁸.

Table 2-3. Summary of kinetic parameters of benzaldehyde hydrogenation in different solvents at 298 K.

Solvent	$K_{H_2}^{\circ a}$	$K_{BZH}^{\circ b}$	K_1°	k_2 (mol mol _{Pd} ⁻¹ s ⁻¹)	η_H	η_1	RMSE ^c
Dioxane	77	20	0.2	1.1	0.99	0.99	19.5
THF	0.83	1.3	7.0	2.5	0.99	0.99	10.6
Water	0.20	11.3	1.0×10^{-2}	4.1×10^4	0.02	0.99	4.2
MeOH	4.0×10^{-4}	4.0	1.2×10^2	2.5×10^2	0.90	0.99	3.3
Gas phase ^d (solvent-free)	4.0×10^2	9.4×10^2	$K_1^{\circ} \cdot k_2 = 4.5$		~1	~1	-

^a Equilibrium constant of dissociative hydrogen adsorption was determined from H coverage on Pd black in corresponding solvents at ~1 bar H₂, measured with transient response method with H_{ad}/D₂ reaction. ^b The equilibrium constant of benzaldehyde adsorption has been referred to 1 M. ^c RMSE is the root mean square error obtained from the difference between experimental results and simulated results, and the sensitivity analyses of all estimated rate and equilibrium constants are showing in the **Section A2-7 Appendix**. ^d The $K_{H_2}^{\circ}$ in gas was measured by H₂ chemisorption at 298 K on Pd/C, K_{BZH}° in gas was measured by gaseous benzaldehyde adsorption on Pd black at 298 K (gaseous benzaldehyde at saturated vapor pressure and H₂ at 1 bar are denoted as standard state). Both measurements are shown in Supporting Information Section S5. Rate constant ($K_1^{\circ} \cdot k_2$) in the gas phase was obtained based on benzaldehyde hydrogenation rate in gas phase (more details shown in **Section A2-5 Appendix**).

To further assess the reversibility of the first H addition step, we varied η_1 , which describes the approach-to-equilibrium for this step, over the entire range from 0.1 to 1.0 and probed the resulting RMSE, as shown in **Figure A2-5**. For all solvents, the RMSE becomes significantly smaller as η_1 value approaches unity. Thus, the optimum kinetic fitting would require η_1 to equal unity, in the kinetic scenario in which the initial H addition step is quasi-equilibrated and the second H addition step is kinetically relevant. The predicted time-dependent concentration profiles are also included in **Figure 2-1** and **Figure A2-3**, together with the measured profiles. As summarized in **Table 2-3**, the RMSEs are small for each of the four cases, indicating that the proposed rate equation (Equation 2) captures the kinetic behavior of benzaldehyde hydrogenation at liquid-Pd interface in all the solvents studied here, as confirmed in the parity plot comparing the measured and predicted concentrations in **Figure A2-6**.

2.3.4 Effects of solvents on the catalytic paths of benzaldehyde hydrogenation

Kinetic analysis alone is insufficient in to distinguish between the alkoxy and hydroxy pathways thus isotope labeling has to be used. **Figure 2-3a** shows the elementary steps and products during benzaldehyde and D₂ reaction. For the alkoxy pathway, addition of D to sorbed

benzaldehyde ($C_6H_5CHO^*$) leads to $C_6H_5CHDO^*$ and in its reverse step a certain fraction of the D-labeled benzaldehyde ($C_6H_5CDO^*$) in addition to $C_6H_5CHO^*$. For hydroxy pathway, the reaction of sorbed benzaldehyde ($C_6H_5CHO^*$) leads to $C_6H_5CHOD^*$, and the reverse reaction to $C_6H_5CHO^*$. Thus, we conclude that the presence of C_6H_5CDO is unequivocal of the alkoxy pathway.

The benzaldehyde- D_2 isotopic tracing experiments were carried out in dioxane and D_2O as representative aprotic and protic solvents (58 mM benzaldehyde and 5 bar D_2 in dioxane and 15 mM and 1 bar D_2 in D_2O , 298 K). The time-dependent 1D-benzaldehyde (C_6H_5CDO), 2D-benzyl alcohol (C_6H_5CHDOD) and 3D-benzyl alcohol ($C_6H_5CD_2OD$) concentrations in dioxane are shown in **Figure 2-3b**, and the formation rates of these compounds in dioxane and D_2O are shown in **Figure 2-3c**. In dioxane, the rate of D-benzaldehyde (C_6H_5CDO) formation was four times smaller than that of benzyl alcohol (60 vs. 308 mol mol $_{Pd}^{-1}$ h $^{-1}$). The detection of D-benzaldehyde establishes, however, the presence of the alkoxy pathway. The low rate of D-benzaldehyde formation allows the conclusion that this pathway is not the dominating pathway. The quasi-equilibrium of the first H (D) addition ($\eta_1 = 0.99$) suggests that C_6H_5CHO hydrogenates to C_6H_5CHDO and then forms C_6H_5CDO in the reverse step at a much higher rate than it undergoes 2nd H(D) addition to form the $C_6H_5CHDOD^*$ and desorb as benzyl alcohol. The observed significantly higher rate of benzyl alcohol formation excludes the alkoxy pathway as the predominant catalytic path. Thus, we conclude that the hydroxy pathway dominates the overall hydrogenation.

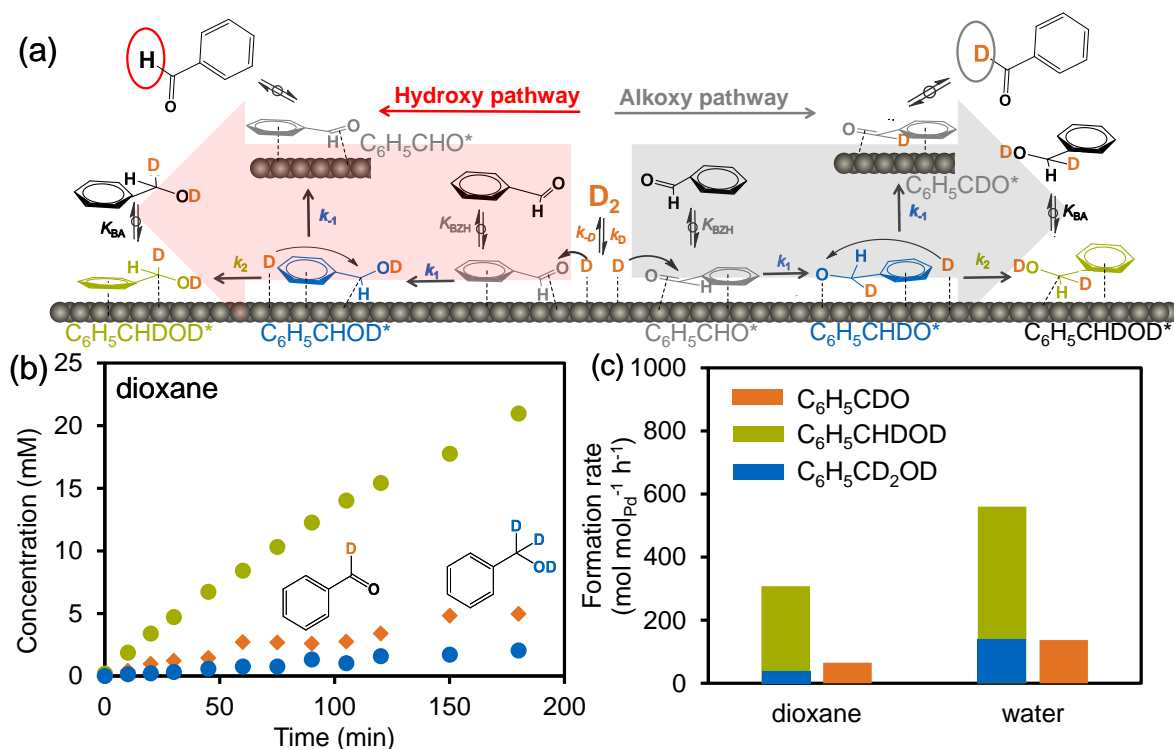


Figure 2-3. Deuterated products in the hydrogenation of benzaldehyde in the presence of D_2 and deuterated solvents. (a) The reaction pathway leading to the formation of D-benzaldehyde in the presence of D_2 on Pd/C at 298 K. (b) Product formation in the reaction of benzaldehyde in dioxane and D_2 . (c) Formation rate of D-benzaldehyde and D-benzyl alcohol in dioxane and D_2O under D_2 . (58 mM benzaldehyde and 5 bar D_2 in dioxane; 15 mM benzaldehyde and 1 bar D_2 in D_2O . Both performed at 298 K)

Similarly, D-benzaldehyde is also formed during benzaldehyde hydrogenation in D_2O , but at a much lower rate than benzyl alcohol formation (**Figure 2-3c**). Taken together, we conclude that the hydroxy pathway dominates in both water and dioxane. Since water and dioxane are the two extreme solvents within the four, we hypothesize the hydroxy pathway to be also the dominant path in THF and MeOH solvent. This establishes firmly that the solvent identity does not alter the reaction pathways, i.e., the solvent must influence kinetic and thermodynamic parameters of the hydroxy pathway.

The unequivocal mechanistic conclusion reached is in direct contrast to other catalytic pathways found for aliphatic aldehyde hydrogenation at slightly higher temperatures than in the current work (323 K vs. 298 K). At the gas-Ru interface, i.e., without a solvent, the alkoxy pathway has been concluded to dominate³⁹ and at Ru interfaces with protic solvents, the proton-electron coupled transfer pathway was concluded to dominate²⁵. There are several plausible explanations on the distinctly different hydrogenation mechanisms for aldehydes found on transition metal surfaces of (i) the aromatic ring of benzaldehyde used in the current study prefers to adsorb on transition metal surfaces via π -interactions⁴². If the reaction follows alkoxy pathway, after the C of C=O bond saturated and untouching to the metal surface, the alkoxy

intermediate will be less stable for further H addition. (ii) Interactions of the benzylic ring with transition metal are known to alter the work function of the metal and the d-band structure. Density functional theory calculations for Ru (0001) surfaces²², suggest that the reaction enthalpy for ionizing H* increases by 0.5 eV (making the formation of protons energetically difficult). Thus, hydrogenation of aliphatic aldehydes, not inducing such effects, could follow drastically different²⁵.

Next, we interrogate the potential formation of interfacial protons at the interface of protic solvents and Pd and, if formed, their potential involvement in hydrogenation catalysis. In the presence of protic solvents (e.g., water), solvation could promote the formation of hydronium ions from adsorbed hydrogen adatoms on transition metals^{21,43}. While it has been established at this point that the hydroxy pathway dominates kinetically, it is not firmly established whether the reaction occurs through proton coupled electron transfer mechanism (PCET) or via H* addition. This pathway has been proposed for the hydrogenation of the carbonyl group in furfural by the presence of H₂O⁴⁴. In the PCET mechanism, the reaction involves a proton addition event, during which a proton attacks the electronegative O of the formyl group. If hydrogenation follows PCET, both H* and the solvent must be involved in the elementary steps and we use this criterion to establish whether or not the PCET mechanism is operative (**Table A2-4**).

Figure 2-4 compares the conversion rate of benzaldehyde in H₂O-H₂, H₂O-D₂, D₂O-H₂ and D₂O-D₂ at 298 K and 1 bar pressure. If the solvent were involved in the elementary step, one would observe a strong kinetic isotope effect, as the solvent is switched from H₂O to D₂O. **Figure 2-4** shows that benzaldehyde conversion rates remained nearly unchanged when switching from H₂O to D₂O for benzaldehyde-H₂ reactions (1695 vs. 1460 mol mol_{Pd}⁻¹ h⁻¹ in experiments I vs. II), and also found for benzaldehyde-D₂ reaction (544 vs. 522 mol mol_{Pd}⁻¹ h⁻¹ in experiments III vs. IV). When comparing between the two groups of experiments, the rates were three times as high in H₂ than that in D₂ (experiments I-II vs. III-IV). This further suggests a strong kinetic isotope effect ($r_H/r_D = \sim 3$) with respect to the co-reactant H₂ (or D₂), but not to changing the solvent from H₂O to D₂O. We conclude from these observations that the benzaldehyde hydrogenation follows Langmuir-Hinshelwood mechanism, involving strictly H* but not the proton from hydronium ions (formed from water). Thus, we also conclude that water (the solvent) is not involved in the actual catalytic step, but affects the standard free energies of reactant and transition states via solvating the reacting species. This scenario might be due to the low concentration of generated proton in water, which could be kinetically insufficient for PCET.

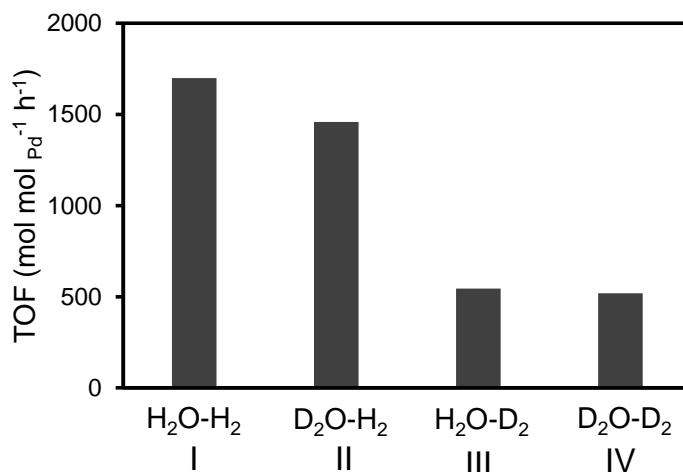


Figure 2-4. Kinetic isotope effect of H₂O/D₂O and H₂/D₂ on TOF of benzaldehyde hydrogenation. Turnover rates of benzaldehyde hydrogenation in H₂O-H₂, H₂O-D₂, D₂O-H₂ and D₂O-D₂ at 298 K and atmospheric pressure with a benzaldehyde concentration of 14.8 mM on Pd/C.

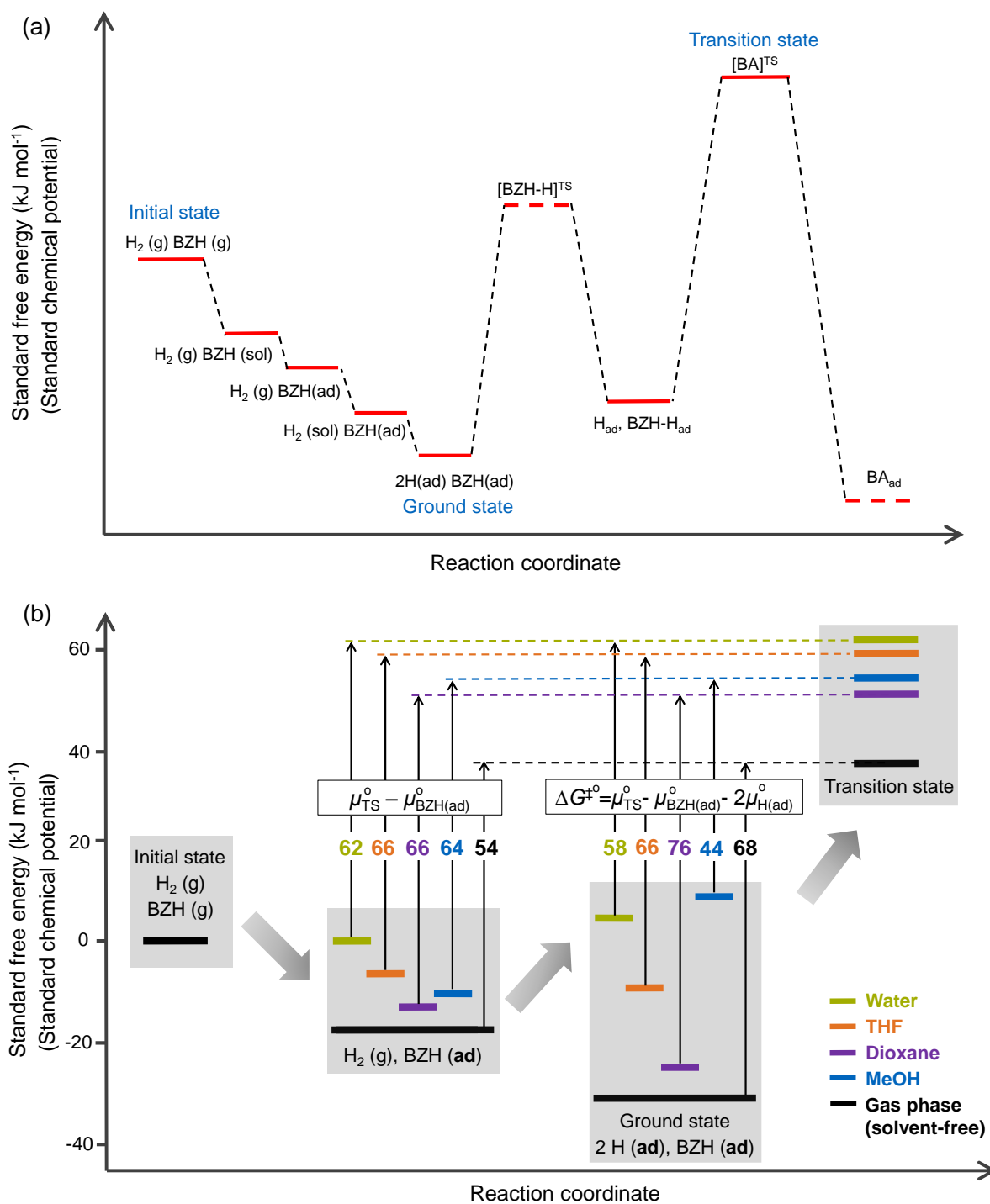
2.3.5 Difference in solvation extent of reacting substrates and transition states

Scheme 2-2a schematically shows the reaction free energy and chemical potential profiles for all elementary steps, including the solvation of reactants, reactant adsorption, and sequential H addition, during benzaldehyde hydrogenation on Pd/C. Since the 2nd H addition step is kinetically relevant, the specifics of the energy barrier for the 1st H addition step are kinetically inconsequential. Scheme 2b only focuses on the kinetic relevant steps, i.e., the sorbed benzaldehyde, the ground state and transition state for the 2nd H addition. Fixing the chemical potential of gaseous benzaldehyde ($\mu^{\circ}_{\text{BZH}(\text{g})}$) at saturated vapor pressure (1.3 mbar at 298 K) and H₂ ($\mu^{\circ}_{\text{H}_2(\text{g})}$) at 1 bar as 0 kJ mol⁻¹, the standard chemical potentials of each state (species) in different solvents are calculated from their corresponding equilibrium constant or rate constant shown in **Table 2-3**, and are summarized in **Table 2-4**. Although these reactions start with the same benzaldehyde concentration, the standard chemical potentials of benzaldehyde ($\mu^{\circ}_{\text{BZH}(\text{solv})}$) are different and depend on solvent identity. The value of $\mu^{\circ}_{\text{BZH}(\text{solv})}$ at 1 M concentration and 298 K in THF (-7 kJ mol⁻¹), dioxane (-6 kJ mol⁻¹) and MeOH (-7 kJ mol⁻¹) are quite negative, while in water (7 kJ mol⁻¹) it is much higher (**Table 2-4**, Entry 1). This difference is caused by the low polarity of benzaldehyde, consisting of a nonpolar benzyl ring and a formyl group, leading to a much lower solubility in water (~7 g L⁻¹ at 298 K) than that in MeOH, THF, and dioxane (miscible solute).

Table 2-4. Summary of standard free energy for the states in Scheme 2^a.

	Standard free energy (kJ mol ⁻¹)	Dioxane	THF	Water	MeOH	Gas phase (solvent-free)
0	$\mu_{\text{BZH(g)}}^{\circ}$			0		
	$\mu_{\text{H}_2(\text{g})}^{\circ}$			0		
1^b	$\mu_{\text{BZH(solv)}}^{\circ}$	-7	-6	7	-7	-
2	$\mu_{\text{BZH(ad)}}^{\circ}$	-14	-7	1	-10	-17
3^c	$\mu_{\text{H}_2(\text{solv})}^{\circ}$	15	14	18	14	-
4	$\mu_{\text{H(ad)}}^{\circ}$	-5	0	2	10	-7
5	$\mu_{\text{GS}}^{\circ} = \mu_{\text{BZH(ad)}}^{\circ} + 2\mu_{\text{H(ad)}}^{\circ}$	-24	-7	5	10	-31
6	μ_{TS}°	52	59	63	54	37
7	$\Delta G^{\ddagger\circ} = \mu_{\text{TS}}^{\circ} - \mu_{\text{BZH(ad)}}^{\circ} - 2\mu_{\text{H(ad)}}^{\circ}$	76	66	58	44	68
8	$\mu_{\text{TS}}^{\circ} - \mu_{\text{BZH(ad)}}^{\circ}$	66	66	62	64	54

^a All standard chemical potentials are referred to BZH(g) at saturated vapor pressure (1.3 mbar) and H₂ (g) at 1 bar, which are treated here as zero (Entry 0). ^b The standard chemical potential for dissolved benzaldehyde is calculated based on the measured benzaldehyde partial pressure equilibrated with 1 M solution in MeOH, THF and dioxane, and from the solubility of benzaldehyde in water, and the ideal chemical potential is calculated based on the molar ratio of benzaldehyde to solvent (chemical potential of liquid benzaldehyde was denoted as zero). ^c The standard chemical potential for dissolved hydrogen is calculated based on hydrogen solubility at 1 bar H₂ and 298 K^{45 46}.



Scheme 2-2. Standard free energy profile of the benzaldehyde hydrogenation. (a) Standard free energy (standard chemical potential) profile during benzaldehyde hydrogenation in a certain solvent. Measured results (derived from thermodynamic and kinetic parameters) shown with solid lines while assumed values shown using dashed lines. (b) Simplified energy profile showing specified energy states and species in above Scheme 2a in different solvents and in gas phase representing solvent-free conditions.

Sorbed benzaldehyde on Pd has a standard chemical potential ($\mu^{\circ}_{BZH(ad)}$) of -17 kJ mol^{-1} in the absence of a solvent (gas-solid interface). The presence of the solvent destabilizes the sorbed benzaldehyde, increasing the $\mu^{\circ}_{BZH(ad)}$ to -14 kJ mol^{-1} in dioxane, to -10 kJ mol^{-1} in

MeOH, -7 kJ mol^{-1} in THF and 1 kJ mol^{-1} in water (**Table 2-4**, Entry 2).

The adsorbed H on Pd has also significant different standard chemical potentials $\mu_{\text{H(ad)}}^{\circ}$ among the four solvents, changing from -5 kJ mol^{-1} in dioxane to 10 kJ mol^{-1} in MeOH (**Table 2-4**, Entry 4). Compared to that in solvent-free condition which has $\mu_{\text{H(ad)}}^{\circ}$ of -7 kJ mol^{-1} , all the four solvents destabilized the sorbed H to different extents. The destabilization is strongest in MeOH, followed by water, THF and dioxane, although dissolved H_2 in the all the four solvents are destabilized to the same extent (**Table 2-4**, Entry 3). Therefore, the H coverage is orders of magnitude smaller in MeOH and water in comparison with dioxane and THF.

The standard chemical potential of the reacting ground state μ_{GS}° (adsorbed benzaldehyde + 2 adsorbed H) is the sum of $\mu_{\text{BZH(ad)}}^{\circ}$ and $2 \mu_{\text{H(ad)}}^{\circ}$ (**Table 2-3**, Entry 5). It showed the same trend as that for H^* ($\mu_{\text{H(ad)}}^{\circ}$), i.e., it was the highest in MeOH followed by water, THF, dioxane and the lowest under solvent-free condition. In contrast, the standard chemical potential of the transition state μ_{TS}° was the highest in water (63 kJ mol^{-1}) followed by THF (59 kJ mol^{-1}), MeOH (54 kJ mol^{-1}), dioxane (52 kJ mol^{-1}) and solvent-free condition (37 kJ mol^{-1}) (**Table 2-4**, Entry 6), in the same sequence as that for adsorbed benzaldehyde $\mu_{\text{BZH(ad)}}^{\circ}$ (water > THF > MeOH > dioxane > solvent-free). The reaction free energy barrier ($\Delta G^{\ddagger\circ}$) is the standard chemical potential difference between the transition state and ground state (Equation 4).

$$\Delta G^{\ddagger\circ} = \mu_{\text{TS}}^{\circ} - \mu_{\text{GS}}^{\circ} \quad (4)$$

Dioxane shows the highest $\Delta G^{\ddagger\circ}$ (76 kJ mol^{-1}), while MeOH shows the lowest (44 kJ mol^{-1}) among the four solvents (**Table 2-4**, Entry 7). It is interesting to note that the barriers from sorbed benzaldehyde to the transition state ($\mu_{\text{TS}}^{\circ} - \mu_{\text{BZH(ad)}}^{\circ}$) are identical for the four solvents ($62\text{-}66 \text{ kJ mol}^{-1}$) (**Scheme 2-2b**, **Table 2-4** Entry 8).

To further explore the impact of solvent on the hydrogenation of benzaldehyde, the free energy of solvation was calculated by the difference between the standard free energy in a specific solvent ($\mu_{\text{(solv)}}^{\circ}$) and that under solvent-free condition ($\mu_{\text{(solv-free)}}^{\circ}$) (Equation 5). This free energy, representing the extent of the interaction between solvent molecules and reacting substrates, is also known as the excess free energy ($\Delta G_{\text{(solv)}}^{\text{excess}}$) or excess chemical potential ($\mu_{\text{(solv)}}^{\text{excess}}$).

$$\mu_{\text{(solv)}}^{\text{excess}} = \mu_{\text{(solv)}}^{\circ} - \mu_{\text{(solv-free)}}^{\circ} \quad (5)$$

For example, the sorbed H on Pd in MeOH has the standard chemical potential ($\mu_{\text{H(ad)}}^{\circ}$) of 10 kJ mol^{-1} , which is 17 kJ mol^{-1} higher than the counterpart under solvent-free condition (-

7 kJ mol⁻¹). Therefore, its excess chemical potential ($\mu_{\text{H(ad)}}^{\text{excess}}$) is 17 kJ mol⁻¹, quantifying the extent of the interaction between the solvent MeOH molecules and H*. The values of μ^{excess} for the four solvents of H*, sorbed benzaldehyde, the reacting ground state and the transition state are summarized in **Table 2-5**.

Table 2-5. Summary of excess chemical potential in different solvents for the states in Scheme 2-2.

Excess chemical potential (free energy of solvation, kJ mol ⁻¹)		Dioxane	THF	Water	MeOH
1	$\mu_{\text{BZH(ad)}}^{\text{excess}}$	3	10	18	7
2	$\mu_{\text{H(ad)}}^{\text{excess}}$	2	7	9	17
3	$\mu_{\text{GS}}^{\text{excess}} = \mu_{\text{BZH(ad)}}^{\text{excess}} + 2\mu_{\text{H(ad)}}^{\text{excess}}$	7	24	36	41
4	$\mu_{\text{TS}}^{\text{excess}}$	15	22	26	17
5	$\Delta G^{\ddagger\text{excess}} = \mu_{\text{TS}}^{\text{excess}} - \mu_{\text{GS}}^{\text{excess}}$	8	-2	-10	-24

The μ^{excess} are all positive in all solvents for all the species/states on Pd surface including H*, benzaldehyde, reacting ground state and transition state, highlighting the easier adsorption and desorption in the solvents (**Table 2-5**, Entries 1-4). For dioxane, the transition state is destabilized more than the ground state, thus, the excess free energy barrier ($\Delta G^{\ddagger\text{excess}}$) is increased. However, it is inverse for THF, water and methanol, i.e., the ground state is destabilized more than the transition state (**Table 2-5**, Entry 5), leading to a lower reaction barrier in presence of solvent.

The $\mu_{\text{H(ad)}}^{\text{excess}}$ shows an inverse linear correlation with $\Delta G^{\ddagger\text{excess}}$ (**Figure 2-5a**), indicating that the solvation destabilizes adsorbed H and reduces the reaction free energy barrier. On the contrary, the $\Delta G^{\ddagger\text{excess}}$ does not show a correlation with $\mu_{\text{BZH(ad)}}^{\text{excess}}$ (**Figure 2-5b**). This is attributed to the fact that the transition state resembles the ground state, i.e., both change similarly (**Figure 2-5b** inset). This is more evident when reformulating $\Delta G^{\ddagger\text{excess}}$ as Equation 6 to separate the solvation of sorbed benzaldehyde and H contributions in the ground state (**Table 2-5**, Entry 3).

$$\Delta G^{\ddagger\text{excess}} = \mu_{\text{TS}}^{\text{excess}} - \mu_{\text{GS}}^{\text{excess}} = \left(\mu_{\text{TS}}^{\text{excess}} - \mu_{\text{BZH(ad)}}^{\text{excess}} \right) - 2\mu_{\text{H(ad)}}^{\text{excess}} \quad (6)$$

Although both values of $\mu_{\text{TS}}^{\text{excess}}$ and $\mu_{\text{BZH(ad)}}^{\text{excess}}$ vary largely with solvents, their difference ($\mu_{\text{TS}}^{\text{excess}} - \mu_{\text{BZH(ad)}}^{\text{excess}}$) is quite similar, i.e., 12 kJ mol⁻¹ for both dioxane and THF, 8 and 10 kJ mol⁻¹ for water and MeOH (Entries 1 and 4 in **Table 2-5**). Consequently only the solvation of surface H affects the energy barrier via the term $\mu_{\text{H(ad)}}^{\text{excess}}$. This also explains the observed slope of -2.1 in **Figure 2-**

5a, which agrees well with the value of -2 that is deduced from Equation 6.

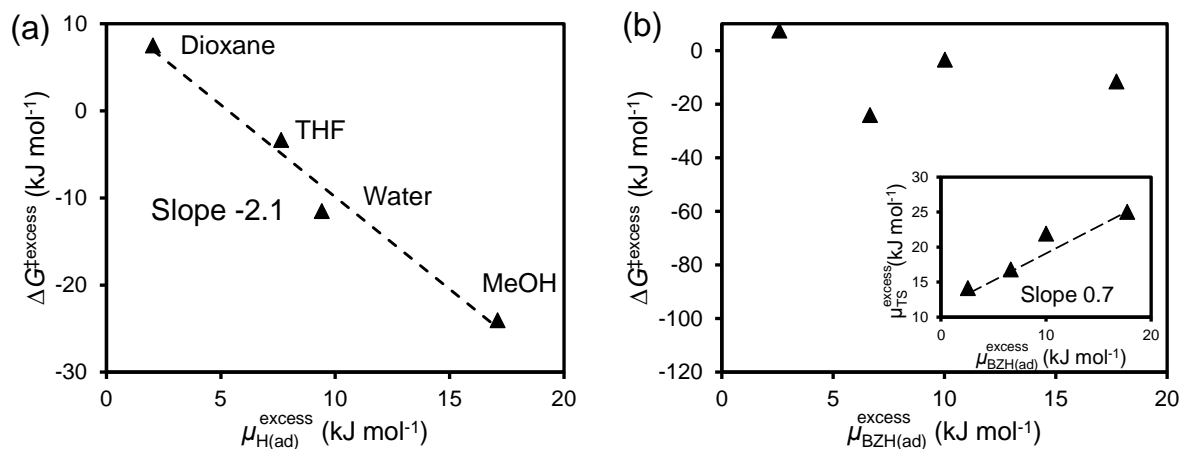


Figure 2-5. Dependence of reaction barrier on sorbed H / sorbed benzaldehyde. (a) Excess free energy barrier from ground state to transition state, $\Delta G_{\ddagger}^{\text{excess}}$, as a function of excess chemical potential for sorbed H, $\mu_{\text{H(ad)}}^{\text{excess}}$; (b) $\Delta G_{\ddagger}^{\text{excess}}$ as a function of excess chemical potential for sorbed benzaldehyde, $\mu_{\text{BZH(ad)}}^{\text{excess}}$; the inset graph shows the correlation between $\mu_{\text{BZH(ad)}}^{\text{excess}}$ and the excess chemical potential of transition state $\mu_{\text{TS}}^{\text{excess}}$.

2.4 Conclusions

Solvents strongly affect the hydrogenation rate of benzaldehyde to benzyl alcohol on Pd/C. From dioxane and THF to water and MeOH, the rate increased by one order of magnitude. We have established unequivocally that the elementary steps and their kinetic relevance do not vary, i.e., that the catalytic cycle is initiated by (dissociative) adsorption of H_2 and benzaldehyde on Pd, followed by stepwise additions of H^* adatoms. The first H^* is added to the O, forming a hydroxyl intermediate, before the second H^* is being added to the C of the formyl group. The pathway by adding H^* first to the carbonyl carbon atom, occurs only to a minor extent. A proton coupled electron transfer pathways has been excluded using isotope labelling and kinetic isotope effects.

The kinetic analysis shows that the dissociative adsorption of H_2 on Pd is quasi-equilibrated in dioxane and THF, while it deviates from equilibrium in water and MeOH. The first H addition to benzaldehyde on Pd is quasi-equilibrated, while the second H addition is rate-determining in all solvents.

The solvents influence the adsorbed reactants as well as the transition state. In general binding to the surface relative to the fluid phase is drastically weaker for all reactants. Because of the absence of an apparent influence of the binding of benzaldehyde on the reaction rate (standard free energy barrier), leads us to the conclusion that the similarity of adsorbed benzaldehyde with the partly hydrogenated intermediate is influenced nearly identical with all

solvents. In contrast, the differences in the stabilization of binding of H^* to the catalyst surface determine the reaction rates. Weaker binding to the surface (higher relative excess potentials) of H^* leads to higher reaction rates, i.e., methanol and water being by far more active solvents than the aprotic THF and dioxane.

The results show that the impact of solvents on the rates of hydrogenation of aldehyde functional groups can be quantitatively linked to the state of adsorbed hydrogen, which is transferred as atomic hydrogen. Weaker hydrogen bonding to the metal is positive for the rate of hydrogenation. For the concentration range of the hydronium ions investigated, the coupled transfer of protons and electrons has not found to be operative.

2.5 Appendix

A2-1 Characterization of Pd/C

Table A2-1. Textural properties of the activated carbon supported Pd catalysts.

Catalyst	Metal loading (wt.%)	BET surface area ($\text{m}^2\cdot\text{g}^{-1}$)	Particle size (nm) ^a	Dispersion (%) ^b
Pd/C	5	1034	3.3	33

^a measured by TEM.

^b measured by hydrogen chemisorption.

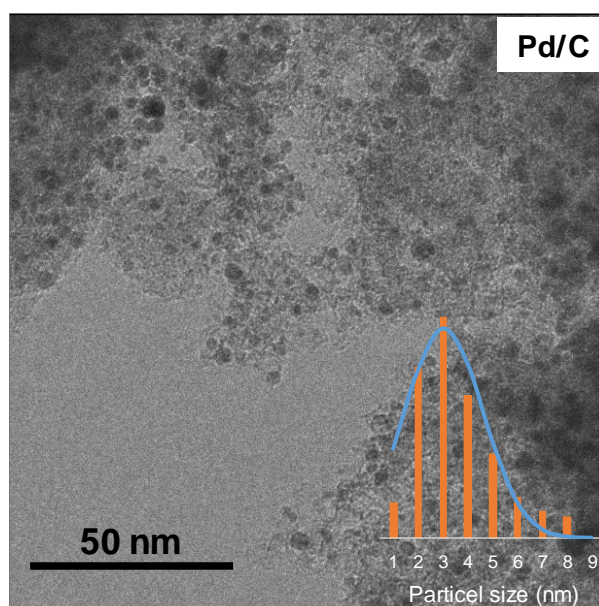


Figure A2-1. Representative TEM images of Pd/C.

A2-2 Solvents effect on TON and reaction orders of benzaldehyde hydrogenation

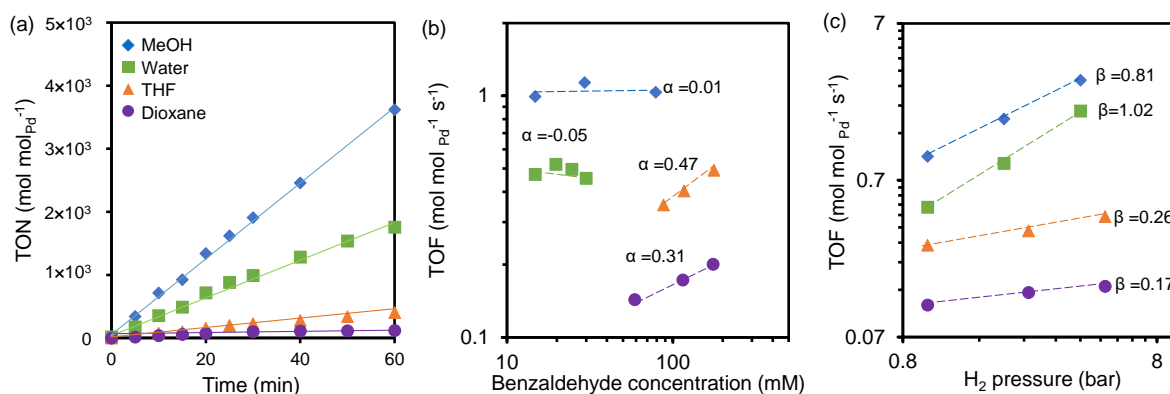


Figure A2-2. (a) Turnover number (TON) per exposed Pd atom for the formation of benzyl alcohol in H_2O , methanol (MeOH), tetrahydrofuran (THF), and dioxane at 1 bar H_2 and 298 K with an initial benzaldehyde concentration of 14.8 mM; (b) TOF as a function of benzaldehyde concentration at 1 bar H_2 in water and MeOH and at 5 bar H_2 in THF and dioxane; (c) TOF as a function of H_2 pressure with the initial benzaldehyde concentration of 115 mM in dioxane and THF and 14.8 mM in MeOH and water. α and β refers to the apparent reaction orders with respect to benzaldehyde and hydrogen.

A2-3 Derivation of rate equation

The sum of the fractional coverages for species i (θ_i), which include the adsorbed H adatom (H^*), adsorbed benzaldehyde (BZH^*), partially hydrogenated benzaldehyde intermediates ($BZH-H^*$), together with that of the unoccupied site ($*$), equals unity:

$$\theta_H + \theta_{BZH} + \theta_{BZH-H} + \theta_* = 1 \quad (A1)$$

Pseudo steady-state approximation, carried out on the elementary steps in **Scheme 2-1**, gives the fractional coverage of adsorbed benzaldehyde:

$$\theta_{BZH} = K_{BZH}^0 C_{BZH} \theta_* \quad (A2)$$

Pseudo steady-state approximation of the reactive H^* adatoms, taken into consideration of all rates that form and consume the H^* , which include H_2 dissociative adsorption (forward of step a, $r_{a,f}$), decomposition of partially hydrogenated benzaldehyde intermediates (reverse of step c, $r_{c,r}$), and either desorbed as hydrogen (reverse of step a, $r_{a,r}$) or undergoes hydrogenation to form partially hydrogenated benzaldehyde intermediates (forward of step c, $r_{c,f}$) or benzyl alcohol (step d, r_d), gives

$$2r_{a,f} + r_{c,r} = 2r_{a,r} + r_{c,f} + r_d \quad (A3)$$

$$r_{a,f} = k_H P_{H_2} \theta_*^2 \quad (A4)$$

$$r_{a,r} = k_{-H} \theta_H^2 \quad (A5)$$

$$r_{c,f} = k_1 \theta_H \theta_{BZH-H} \quad (A6)$$

$$r_{c,r} = k_{-1} \theta_{BZH-H} \theta_* \quad (A7)$$

$$r_d = k_2 \theta_H \theta_{BZH-H} \quad (A8)$$

and then leading to the equation A9,

$$2k_H P_{H_2} \theta_*^2 + k_{-1} \theta_{BZH-H} \theta_* = 2k_{-H} \theta_H^2 + k_1 \theta_H \theta_{BZH-H} + k_2 \theta_H \theta_{BZH-H} \quad (A9)$$

Next, the pseudo steady-state treatment of the $BZH-H^*$ intermediates leads to Equation A10 and A11, upon rearrangement, Equation A12, since the partially hydrogenated benzaldehyde intermediates (forward of step c, $r_{c,f}$) either undergo sequential hydrogenation to benzyl alcohol (step d, r_d) or dehydrogenate back to benzaldehyde (reverse of step c, $r_{c,r}$):

$$r_{c,f} = r_{c,r} + r_d \quad (A10)$$

$$k_1 \theta_H \theta_{BZH} = k_{-1} \theta_{BZH-H} \theta_* + k_2 \theta_H \theta_{BZH-H} \quad (A11)$$

$$\theta_{\text{BZH-H}} = \frac{k_1 \theta_{\text{H}} \theta_{\text{BZH}}}{k_{-1} \theta_* + k_2 \theta_{\text{H}}} \quad (\text{A12})$$

Substituting Equation A11 in Equation A9:

$$k_{\text{H}} P_{\text{H}_2} \theta_*^2 = k_{-\text{H}} \theta_{\text{H}}^2 + k_2 \theta_{\text{H}} \theta_{\text{BZH-H}} \quad (\text{A13})$$

We defined η_{H} for the H_2 adsorption (step a) and η_1 for the initial benzaldehyde hydrogenation step (step c) by the ratio of the reverse rate ($r_{-\text{H}}, r_{-1}$) divided by the forward rate (r_{H}, r_1) of their respective steps:

$$\eta_{\text{H}} = \frac{r_{-\text{H}}}{r_{\text{H}}} = \frac{k_{-\text{H}} \theta_{\text{H}}^2}{k_{\text{H}} P_{\text{H}_2} \theta_*^2} \quad (\text{A14})$$

$$\eta_1 = \frac{r_{-1}}{r_1} = \frac{k_{-1} \theta_{\text{BZH-H}} \theta_*}{k_1 \theta_{\text{H}} \theta_{\text{BZH}}} \quad (\text{A15})$$

η_{H} and η_1 are the rigorous measures on the reversibility of their respectively step and can range from zero to one; when η approaches zero, the step is irreversible, but as it approaches unity, the step becomes quasi-equilibrated.

Rearranging Equation A14, the fractional coverage of H^* is

$$\frac{\theta_{\text{H}}^2}{\theta_*^2} = K_{\text{H}_2}^{\circ} P_{\text{H}_2} \eta_{\text{H}} \quad (\text{A16a})$$

$$\theta_{\text{H}} = \sqrt{K_{\text{H}_2}^{\circ} P_{\text{H}_2} \eta_{\text{H}}} \theta_* \quad (\text{A16b})$$

$$\text{Where } K_{\text{H}_2}^{\circ} = \frac{k_{\text{H}}}{k_{-\text{H}}} \quad (\text{A16c})$$

Rearranging Equation A13,

$$k_{\text{H}} P_{\text{H}_2} = k_{-\text{H}} \frac{\theta_{\text{H}}^2}{\theta_*^2} + k_2 \frac{\theta_{\text{H}} \theta_{\text{BZH-H}}}{\theta_*^2} \quad (\text{A17})$$

Substituting Equation A15, A16a and A2 in Equation A17,

$$\eta_{\text{H}} = \frac{k_{-\text{H}}}{k_{-\text{H}} + k_2 K_1^{\circ} \eta_1 K_{\text{BZH}}^{\circ} C_{\text{BZH}}} \quad (\text{A18a})$$

$$\text{where } K_1^\circ = \frac{k_1}{k_{-1}} \quad (\text{A18b})$$

Substituting Equation A16b and A2 in Equation A15, the fractional coverage of BZH-H* is

$$\theta_{\text{BZH-H}} = K_1^\circ \eta_1 \sqrt{K_{\text{H}_2}^\circ P_{\text{H}_2} \eta_{\text{H}}} K_{\text{BZH}}^\circ C_{\text{BZH}} \theta^* \quad (\text{A19})$$

Substituting in Equation A2, A19, and A16b in Equation A1, the fraction of unoccupied Pd sites is:

$$\theta^* = \left(1 + \sqrt{K_{\text{H}_2}^\circ P_{\text{H}_2} \eta_{\text{H}}} + K_{\text{BZH}}^\circ C_{\text{BZH}} + K_1^\circ \eta_1 \sqrt{K_{\text{H}_2}^\circ P_{\text{H}_2} \eta_{\text{H}}} K_{\text{BZH}}^\circ C_{\text{BZH}} \right)^{-1} \quad (\text{A20})$$

Substituting Equation A16b, A19 and A20 in Equation A8, the benzyl alcohol formation rate can be written as:

$$r_d = \frac{k_2 \sqrt{K_{\text{H}_2}^\circ P_{\text{H}_2} \eta_{\text{H}}} K_1^\circ \eta_1 \sqrt{K_{\text{H}_2}^\circ P_{\text{H}_2} \eta_{\text{H}}} K_{\text{BZH}}^\circ C_{\text{BZH}}}{\left(1 + \sqrt{K_{\text{H}_2}^\circ P_{\text{H}_2} \eta_{\text{H}}} + K_{\text{BZH}}^\circ C_{\text{BZH}} + K_1^\circ \eta_1 \sqrt{K_{\text{H}_2}^\circ P_{\text{H}_2} \eta_{\text{H}}} K_{\text{BZH}}^\circ C_{\text{BZH}} \right)^2} \quad (\text{A21})$$

Substituting Equation A18a in Equation A21, the full rate expression for benzaldehyde hydrogenation is

$$r_d = \frac{k_2 K_1^\circ \eta_1 K_{\text{BZH}}^\circ C_{\text{BZH}} K_{\text{H}_2}^\circ P_{\text{H}_2} \frac{k_{-H}}{k_{-H} + k_2 K_1^\circ \eta_1 K_{\text{BZH}}^\circ C_{\text{BZH}}}}{\left(1 + \sqrt{K_{\text{H}_2}^\circ P_{\text{H}_2} \frac{k_{-H}}{k_{-H} + k_2 K_1^\circ \eta_1 K_{\text{BZH}}^\circ C_{\text{BZH}}}} + K_{\text{BZH}}^\circ C_{\text{BZH}} + K_1^\circ \eta_1 \sqrt{K_{\text{H}_2}^\circ P_{\text{H}_2} \frac{k_{-H}}{k_{-H} + k_2 K_1^\circ \eta_1 K_{\text{BZH}}^\circ C_{\text{BZH}}}} K_{\text{BZH}}^\circ C_{\text{BZH}} \right)^2} \quad (\text{A22})$$

This rate expression contains the rate constant of the kinetically relevant step (k_2), equilibrium constants for the adsorption of reactants (K_{BZH}° , K_1° , $K_{\text{H}_2}^\circ$), and also those related to the adsorption of the various species occupying the Pd sites (θ^* , θ_{H} , θ_{BZH} , $\theta_{\text{BZH-H}}$), and the approaches-to-equilibrium (η_{H} and η_1). Each term in the denominator of the rate expressions denotes the relative abundances of a type of surface species to the unoccupied Pd sites during steady-state catalysis.

A2-4 Competitive adsorption of benzaldehyde and benzyl alcohol and kinetic fitting

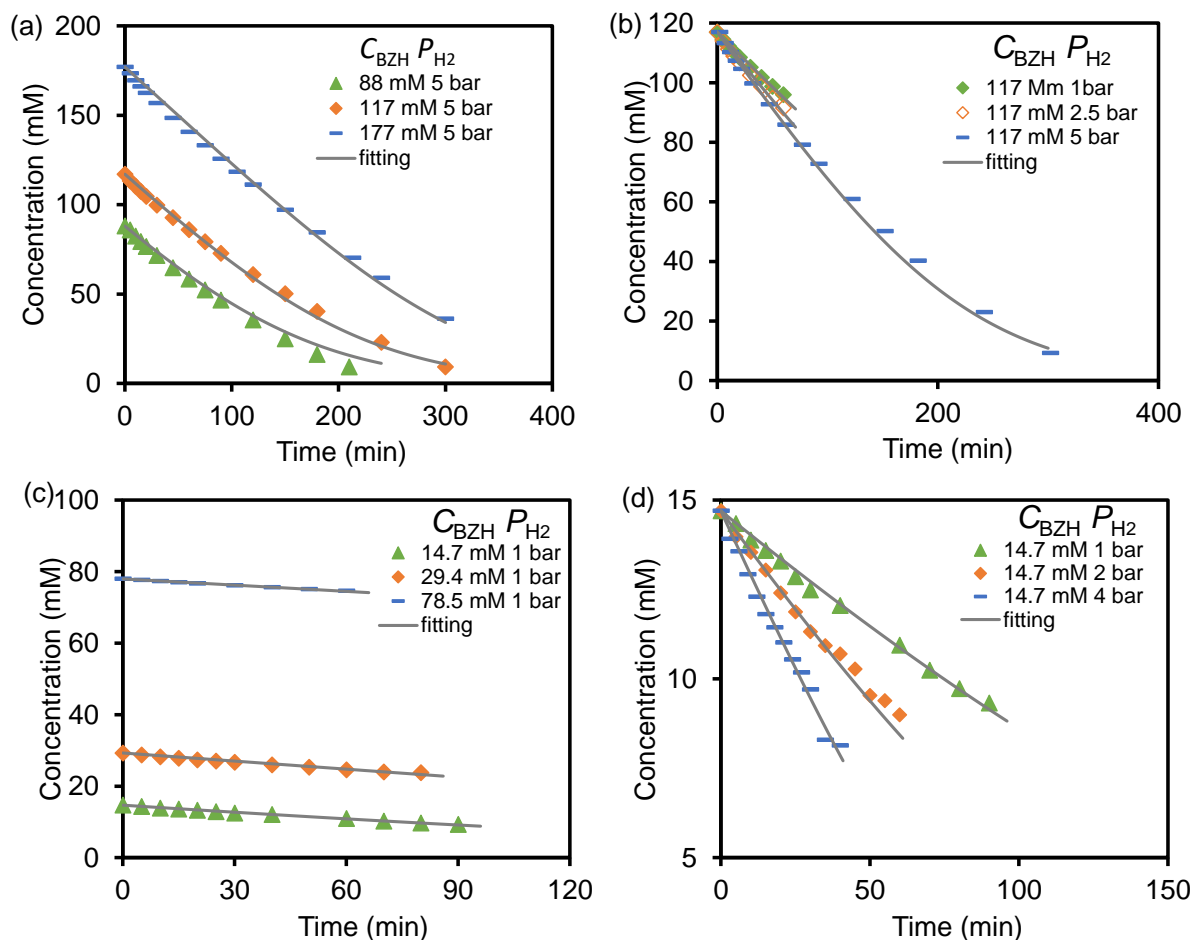


Figure A2-3. (a) Time-dependent concentration of benzaldehyde as a function of time with different initial concentration in THF (15 mg Pd/C) at 298 K and 5 bar H_2 . (b) Time-dependent concentration of benzaldehyde as a function of hydrogen pressure in dioxane (117 mM, 15 mg Pd/C) at 298 K. (c) Time-dependent concentration of benzaldehyde as a function of time with different initial concentration in MeOH (1 mg Pd/C) at 298 K and 1 bar H_2 . (d) Time-dependent concentration of benzaldehyde as a function of hydrogen pressure in dioxane (14.8 mM, 1 mg Pd/C) at 298 K.

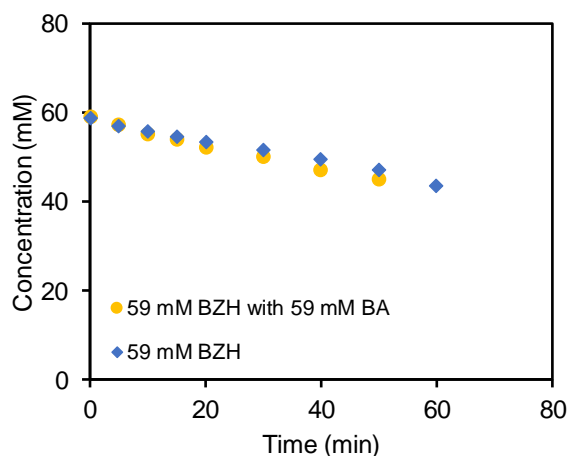


Figure A2-4. Concentration of benzaldehyde as a function of time with and without benzyl alcohol in dioxane (20 mg Pd/C) at 298 K and 1 bar H_2 .

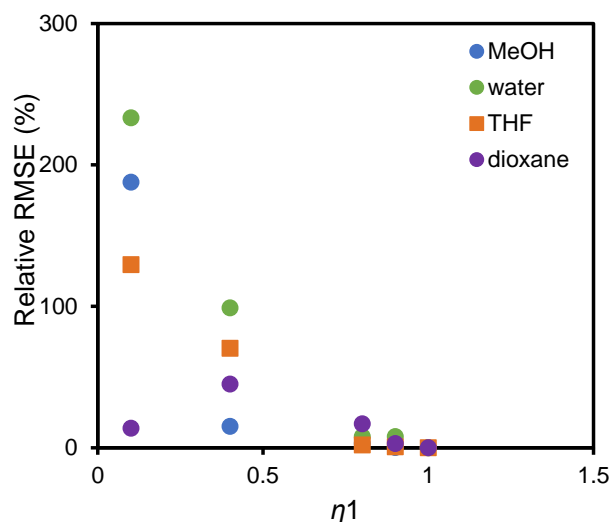


Figure A2-5. Relative root mean square error (RMSE) as a function of η_1 .

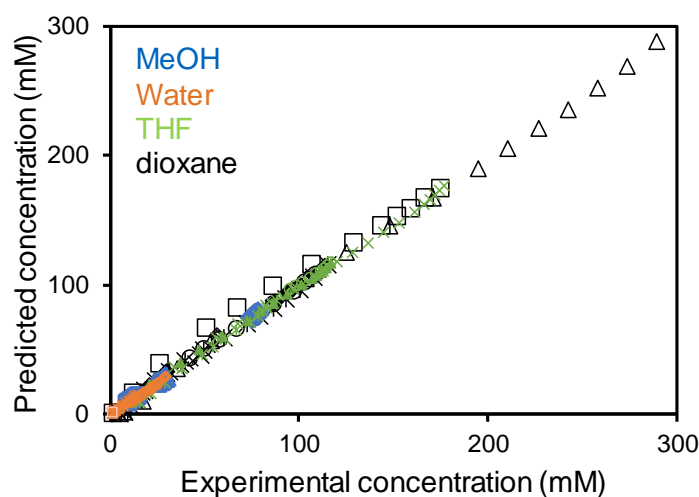


Figure A2-6. Parity plot comparing predicted concentration and experimental results in dioxane (black points), THF (green points), MeOH (blue points) and water (orange points).

A2-5 Determination of equilibrium constant of H_2 , benzaldehyde and rate constant in Solvent-free conditions

The equilibrium constant of H_2 adsorption ($K^{\circ}_{H_2}$) and benzaldehyde adsorption (K°_{BZH}) on Pd in gas phase were determined by measuring adsorption isotherm of H_2 and gaseous benzaldehyde on Pd. The experiment procedure is described in Section 2-7.

The adsorption isotherm of H_2 is shown in **Figure A2-7a** and that of benzaldehyde is shown in **Figure A2-7b**. After analysis of obtained adsorption isotherm using Equation A23 and A24, the adsorption constants are obtained as 396 ± 98 for $K^{\circ}_{H_2}$ corresponding a chemical potential of $-14.8 \pm 0.6 \text{ kJ mol}^{-1}$ for H_2 adsorption, and K°_{BZH} of 942 ± 49 corresponding a chemical potential

of $-17 \pm 0.3 \text{ kJ mol}^{-1}$ for benzaldehyde adsorption. Here, gaseous benzaldehyde at saturated vapor pressure and H_2 at 1 bar are denoted as standard state.

$$K_{\text{H}_2}^\circ = \frac{\theta_{\text{H}}^2}{P_{\text{H}_2} (1 - \theta_{\text{H}})^2} \quad (\text{A23})$$

$$K_{\text{BZH}}^\circ = \frac{\theta_{\text{BZH}}}{P_{\text{BZH}} (1 - \theta_{\text{BZH}})} \quad (\text{A24})$$

The reaction rate of benzaldehyde hydrogenation under solvent-free condition is represented by the reaction in gas phase measured in a CSTR reactor. The reaction result is shown in **Table A2-3**. It is widely accepted that the dissociative adsorption of hydrogen in hydrogenation is equilibrated for gas phase reaction, thus, η_{H} (Equation A14) equals to 1. Based on the fact that the η_1 approaches to 1 in the reactions in all the solvents, we assume the same for gas phase reaction. In the following equations for the gas phase reaction, P_{BZH} is used to express benzaldehyde pressure instead of C_{BZH} used in the former equations in the liquid phase. Thus, Equation A20, A21 can be written as

$$\theta_*^{-1} = 1 + \sqrt{K_{\text{H}_2}^\circ P_{\text{H}_2}} + K_{\text{BZH}}^\circ P_{\text{BZH}} + K_1 \sqrt{K_{\text{H}_2}^\circ P_{\text{H}_2}} K_{\text{BZH}}^\circ P_{\text{BZH}} \quad (\text{A25})$$

$$r_d = \frac{k_2 K_1 K_{\text{H}_2}^\circ P_{\text{H}_2} K_{\text{BZH}}^\circ P_{\text{BZH}}}{\left(1 + \sqrt{K_{\text{H}_2}^\circ P_{\text{H}_2}} + K_{\text{BZH}}^\circ P_{\text{BZH}} + K_1 \sqrt{K_{\text{H}_2}^\circ P_{\text{H}_2}} K_{\text{BZH}}^\circ P_{\text{BZH}}\right)^2} \quad (\text{A26})$$

Substituting the denominator in Equation A26 by Equation A25, we got

$$r_d = k_2 K_1 K_{\text{H}_2}^\circ P_{\text{H}_2} K_{\text{BZH}}^\circ P_{\text{BZH}} \theta_*^2 \quad (\text{A27})$$

Rearrange Equation A2, we obtained

$$\theta_* = \frac{\theta_{\text{BZH}}}{K_{\text{BZH}}^\circ P_{\text{BZH}}} \quad (\text{A28})$$

Substituting the θ_* in Equation A27 by Equation A28,

$$r_d = k_2 K_1 K_{\text{H}_2}^\circ P_{\text{H}_2} \frac{1}{K_{\text{BZH}}^\circ P_{\text{BZH}}} \theta_{\text{BZH}}^2 \quad (\text{A29})$$

Due to the strong adsorption of benzaldehyde on Pd in gas phase ($-17 \pm 0.3 \text{ kJ mol}^{-1}$), Pd surface is readily saturated by benzaldehyde at a benzaldehyde pressure of $0.025 P/P^0$ (**Figure A2-7b**). Accordingly, we assume that Pd is dominantly occupied by adsorbed benzaldehyde ($\theta_{\text{BZH}} \approx 1$) under present reaction conditions (benzaldehyde partial pressure $P/P^0 \geq 0.45$, **Table A2-3**). Thus, Equation A29 can be written into Equation A30,

$$r_d = k_2 K_1^\circ \frac{K_{H_2}^\circ P_{H_2}}{K_{BZH}^\circ P_{BZH}} \quad (\text{A30})$$

Equation A30 predicts the r_d increasing proportionally with the pressure ratio of H_2 to benzaldehyde (P_{H_2}/P_{BZH}). With the measured TOF under different P_{H_2} and P_{BZH} (Table A2-3), we plot the reaction rate (TOF) as a function of $K_{H_2}^\circ P_{H_2}/K_{BZH}^\circ P_{BZH}$ (Figure A2-8). It indeed shows a proportional increase as predicted in Equation S30. In particular, the slope is the value of $K_1^\circ \cdot k_2$, which is 4.5 s^{-1} . It should be noted here that with current data it is not possible to obtain the individual value of K_1° and k_2 . However, their product ($K_1^\circ \cdot k_2$) can still be useful for the analyse of reaction barriers.

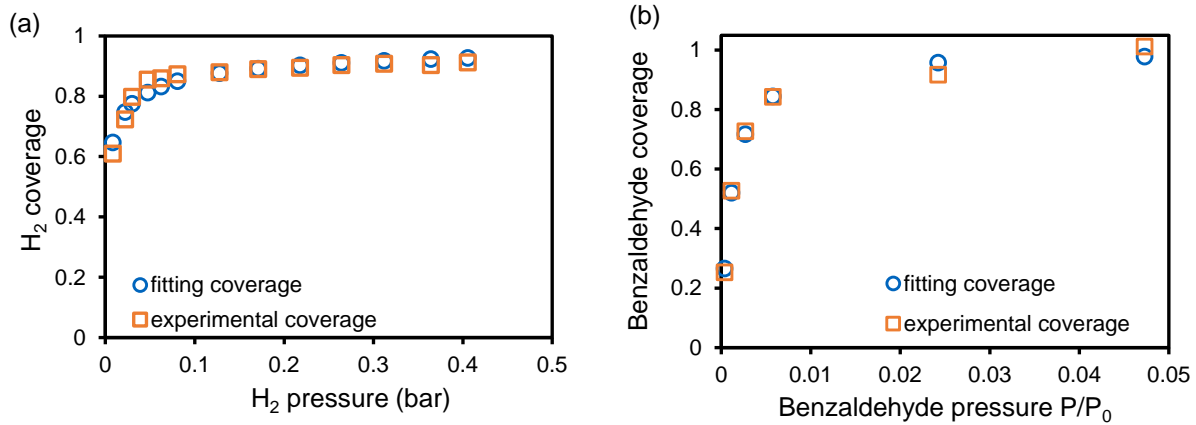


Figure A2-7. (a) Coverage of H_2 as a function of H_2 pressure on Pd/C at 298K; (b) Coverage of benzaldehyde as a function of benzaldehyde pressure on Pd black at 298K, P^0 is the saturated vapor pressure of benzaldehyde.

Table A2-2. Reaction results of benzaldehyde hydrogenation on Pd/C in gas phase.

H_2 pressure [bar]	0.02	0.03	0.04	0.05
Benzaldehyde pressure ^a [P^0]	0.98	0.97	0.96	0.95
Benzaldehyde pressure ^b [P^0]	0.96	0.85	0.6	0.45
TOF (s^{-1})	0.015	0.056	0.15	0.21

^a benzaldehyde pressure of the feedstock, P^0 is the saturated vapor pressure of benzaldehyde.

^b benzaldehyde pressure in the CSTR reactor, P^0 is the saturated vapor pressure of benzaldehyde.

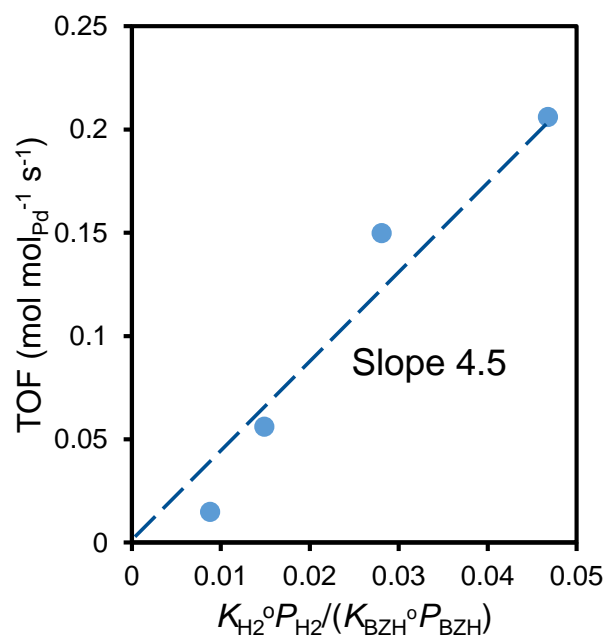


Figure A2-8. TOF as a function of $\frac{K_{H_2}^o P_{H_2}}{K_{BZH}^o P_{BZH}}$ for benzaldehyde hydrogenation in solvent-free condition (gas phase).

A2-6 Hydride desorption as H₂ after solvent evaporation

In **Figure A2-9a** and **A2-9b**, D₂ reacted the pre-adsorbed H to form HD and H₂ after switch from H₂ to D₂, and this transient reaction takes ~20 s. After this reaction, D₂ was switched to N₂ which is inert and can accelerate the evaporation of dioxane. After flowing N₂ for 2000s, a large amount of H₂ (176 μmol H) desorption was observed exactly after liquid dioxane totally evaporation, which is ~5 times of the surface Pd sites (38 μmol) and ~0.4 of the total amount of Pd in Pd black used (472 μmol). The later desorbed H can neither react with D₂ during the transient reaction nor desorbed in N₂ in presence of solvent, indicating this is the palladium hydride and trapped in subsurface of Pd in the presence of solvent. Thus, the measured H coverage using the transient method is surface H.

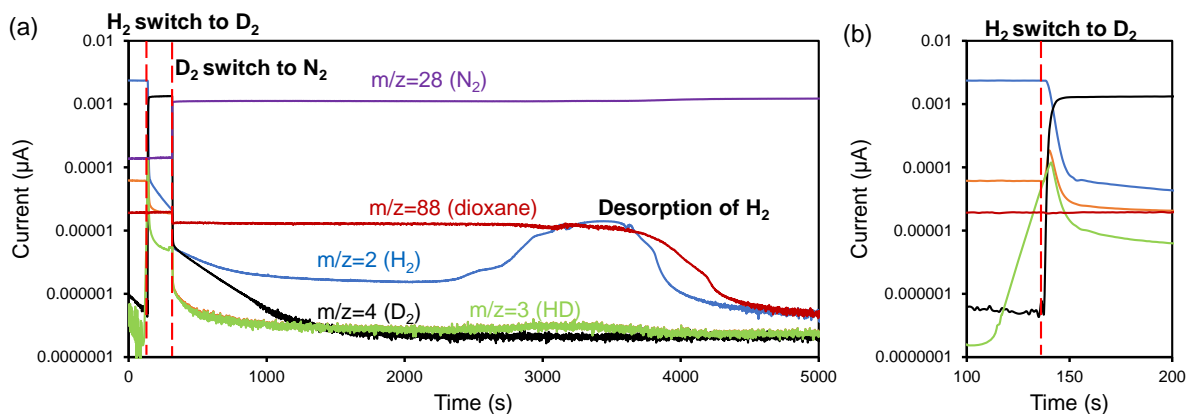


Figure A2-9. (a) Transient response of HD and H₂ following the switch from H₂ to D₂ in dioxane then flowing N₂ to accelerate the evaporation of dioxane. (b) showing the transient response during 100-200s. The dash line showing the gas switch during the reaction. The flow rate of H₂ and D₂ are 10 mL min and N₂ 32 mL min. Pd black used in this experiment is 50 mg.

A2-7 Sensitivity analyses of all estimated rate and equilibrium constant values

The sensitivity analyses of all estimated rate and equilibrium constants showed significant sensitivity differences in the root mean square error (RMSE) of the regressed kinetic fitting. For the benzaldehyde adsorption equilibrium constant, K_{BZH}° , a 30% change in its value causes the RMSE to increase by $76 \pm 35\%$ in dioxane and $78 \pm 44\%$ in THF and to a much lower extent of $37 \pm 8\%$ in water and $19 \pm 5\%$ in MeOH. The parameters for the H addition step, K_1° and k_2 , affect the rate values strongly, in aprotic solvent: 30% variation of K_1° and k_2 leading to a $\sim 107\% \pm 65\%$ and $\sim 350\% \pm 60\%$ increase of the RMSE, respectively. For the case of protic solvents, these changes lead the RMSE to increase by $\sim 22\% \pm 13\%$ and $\sim 80\% \pm 40\%$ with, respectively.

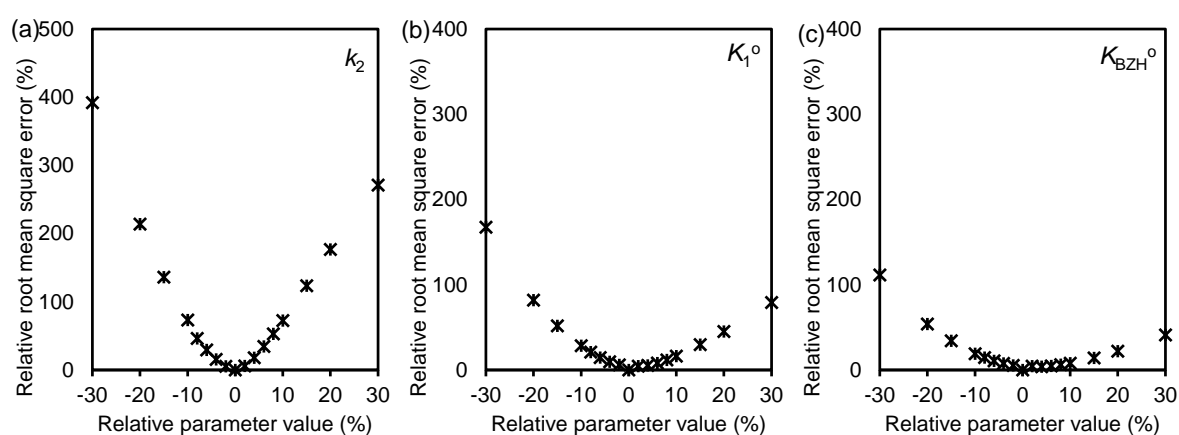


Figure A2-10. Sensitivity of the relative parameter values (a) rate constant of 2nd H addition step k_2 , (b) equilibrium constant of 1st H addition to benzaldehyde, (c) equilibrium constant of benzaldehyde adsorption K_{BZH}° on the root mean square error for benzaldehyde concentration predicted by Eq. 17 in dioxane.

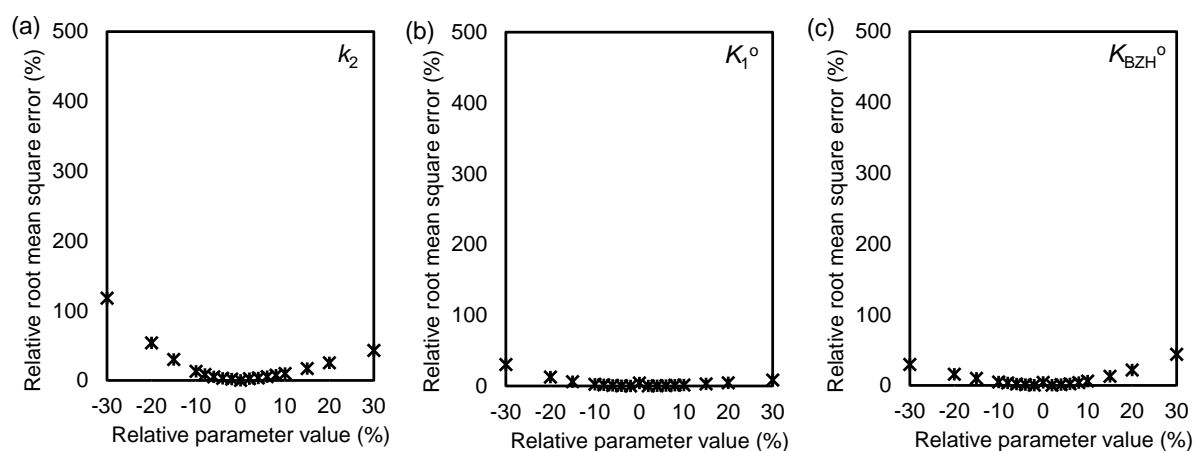


Figure A2-11. Sensitivity of the relative parameter values (a) rate constant of 2nd H addition step k_2 , (b) equilibrium constant of 1st H addition to benzaldehyde, (c) equilibrium constant of benzaldehyde adsorption K_{BZH}° on the root mean square error for benzaldehyde concentration predicted by Eq. 17 in water.

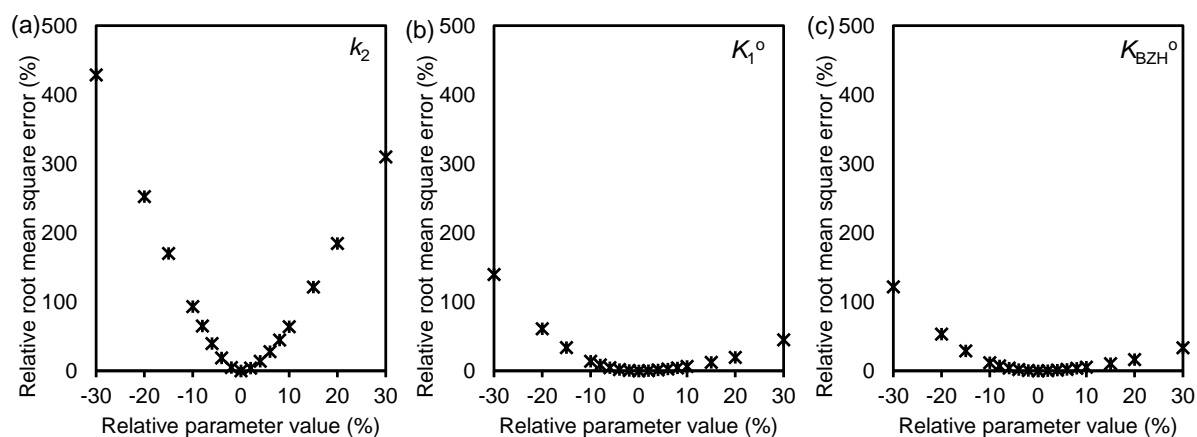


Figure A2-12. Sensitivity of the relative parameter values (a) rate constant of 2nd H addition step k_2 , (b) equilibrium constant of 1st H addition to benzaldehyde, (c) equilibrium constant of benzaldehyde adsorption K_{BZH}^0 on the root mean square error for benzaldehyde concentration predicted by Eq. 17 in THF.

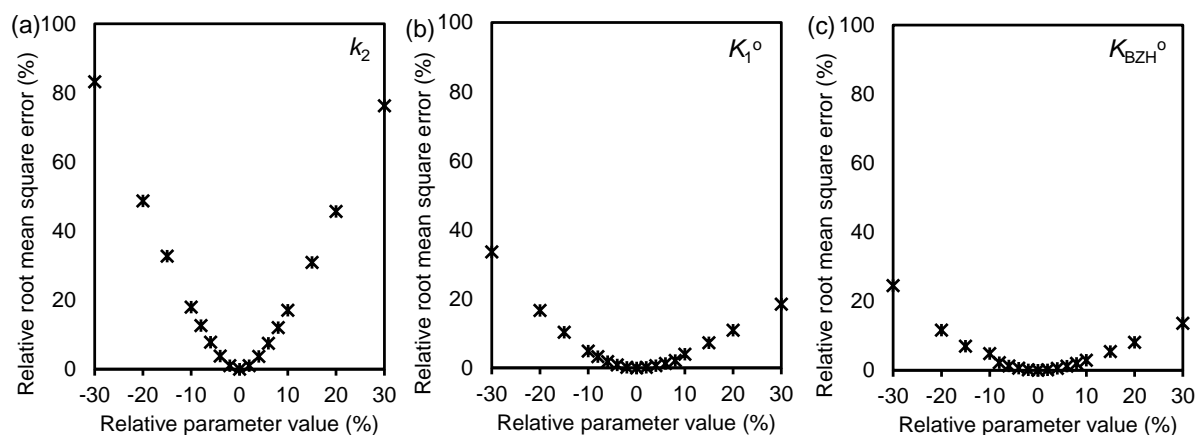


Figure A2-13. Sensitivity of the relative parameter values (a) rate constant of 2nd H addition step k_2 , (b) equilibrium constant of 1st H addition to benzaldehyde, (c) equilibrium constant of benzaldehyde adsorption K_{BZH}^0 on the root mean square error for benzaldehyde concentration predicted by Eq. 17 in MeOH.

Table A2-3. Summary of sensitivity analyses of parameters with a 30% change.

Solvent	Sensitivity of k_2	Sensitivity of K_1^0	Sensitivity of K_{BZH}^0
dioxane	$330 \pm 60\%$	$123 \pm 44\%$	$76 \pm 35\%$
THF	$370 \pm 60\%$	$92 \pm 48\%$	$78 \pm 44\%$
water	$80 \pm 40\%$	$19 \pm 11\%$	$37 \pm 8\%$
MeOH	$80 \pm 4\%$	$26 \pm 7\%$	$19 \pm 5\%$

A2-8 PCET in protic solvent

Table A2-4. Elementary steps of benzaldehyde hydrogenation and corresponding rate expressions based on proton coupled electron transfer mechanism.

Step No.	Description	Elementary step
a	H ₂ adsorption	$H_2 + 2 * \xrightleftharpoons{K_{H_2}} 2H^*$
b	benzaldehyde (BZH) adsorption	$BZH + * \xrightleftharpoons{K_{BZH}} BZH^*$
c	H ₃ O ⁺ formation	$H_2O + H^* \xrightleftharpoons{K_4} H_3O^+ + e^- + *$
d	1 st H addition	$BZH^* + H_3O^+ + e^- \xrightleftharpoons[k_{-1}]{k_1} BZH - H^* + H_2O$
e	2 nd H addition	$BZH - H^* + H_3O^+ + e^- \xrightarrow{k_2} BA^* + H_2O$
f	Benzyl alcohol (BA) desorption	$BA^* \xrightleftharpoons{K_{BA}} BA + *$

^a Key to symbols: *, an unoccupied metal site; $\xrightleftharpoons{\quad}$, a quasi-equilibrated step, $\xrightarrow{\quad}$ an irreversible step; and \rightarrow , an irreversible step.

2.6 Reference

1. Magano, J. & Dunetz, J. R. Large-scale carbonyl reductions in the pharmaceutical industry. *Organic Process Research & Development* **16**, 1156-1184 (2012).
2. Bychko, I. B., Abakumov, A. A., Lemesh, N. V. & Strizhak, P. E. Catalytic activity of multiwalled carbon nanotubes in acetylene hydrogenation. *ChemCatChem* **9**, 4470-4474, doi:https://doi.org/10.1002/cctc.201701234 (2017).
3. Song, S. *et al.* Heterostructured Ni/NiO composite as a robust catalyst for the hydrogenation of levulinic acid to γ -valerolactone. *Applied Catalysis B: Environmental* **217**, 115-124, doi:https://doi.org/10.1016/j.apcatb.2017.05.073 (2017).
4. Saadi, A., Rassoul, Z. & Bettahar, M. M. Gas phase hydrogenation of benzaldehyde over supported copper catalysts. *Journal of Molecular Catalysis A: Chemical* **164**, 205-216, doi:https://doi.org/10.1016/S1381-1169(00)00199-0 (2000).
5. Sitthisa, S., Sooknoi, T., Ma, Y., Balbuena, P. B. & Resasco, D. E. Kinetics and mechanism of hydrogenation of furfural on Cu/SiO₂ catalysts. *Journal of Catalysis* **277**, 1-13, doi:https://doi.org/10.1016/j.jcat.2010.10.005 (2011).
6. Mäki-Arvela, P., Hájek, J., Salmi, T. & Murzin, D. Y. Chemoselective hydrogenation of carbonyl compounds over heterogeneous catalysts. *Applied Catalysis A: General* **292**, 1-49, doi:https://doi.org/10.1016/j.apcata.2005.05.045 (2005).
7. Takenouchi, M., Kudoh, S., Miyajima, K. & Mafune, F. Adsorption and desorption of hydrogen by gas-phase palladium clusters revealed by in situ thermal desorption spectroscopy. *The Journal of Physical Chemistry A* **119**, 6766-6772 (2015).
8. Schennach, R., Eichler, A. & Rendulic, K. Adsorption and desorption of methanol on Pd (111) and on a Pd/V surface alloy. *The Journal of Physical Chemistry B* **107**, 2552-2558 (2003).
9. Pang, S. H., Román, A. M. & Medlin, J. W. Adsorption orientation-induced selectivity control of reactions of benzyl alcohol on Pd (111). *The Journal of Physical Chemistry C* **116**, 13654-13660 (2012).
10. Wan, H., Vitter, A., Chaudhari, R. V. & Subramaniam, B. Kinetic investigations of unusual solvent effects during Ru/C catalyzed hydrogenation of model oxygenates. *Journal of catalysis* **309**, 174-184 (2014).

11. Rajadhyaksha, R. & Karwa, S. Solvent effects in catalytic hydrogenation. *Chemical engineering science* **41**, 1765-1770 (1986).
12. Bertero, N. M., Trasarti, A. F., Apesteguía, C. R. & Marchi, A. J. Solvent effect in the liquid-phase hydrogenation of acetophenone over Ni/SiO₂: A comprehensive study of the phenomenon. *Applied Catalysis A: General* **394**, 228-238, doi:<https://doi.org/10.1016/j.apcata.2011.01.003> (2011).
13. Aramendia, M. A. *et al.* Reduction of Acetophenones over Pd/AlPO₄ Catalysts. Linear Free Energy Relationship (LFER). *Journal of Catalysis* **140**, 335-343, doi:<https://doi.org/10.1006/jcat.1993.1088> (1993).
14. Koppel, I. & Palm, V. in *Advances in linear free energy relationships* 203-280 (Springer, 1972).
15. Ide, M. S., Hao, B., Neurock, M. & Davis, R. J. Mechanistic insights on the hydrogenation of α , β -unsaturated ketones and aldehydes to unsaturated alcohols over metal catalysts. *ACS Catalysis* **2**, 671-683 (2012).
16. Herrerias, C. I., Yao, X., Li, Z. & Li, C.-J. Reactions of C–H bonds in water. *Chemical reviews* **107**, 2546-2562 (2007).
17. Butler, R. N. & Coyne, A. G. Water: Nature's reaction enforcer comparative effects for organic synthesis "In-Water" and "On-Water". *Chemical reviews* **110**, 6302-6337 (2010).
18. Akpa, B. S. *et al.* Solvent effects in the hydrogenation of 2-butanone. *Journal of Catalysis* **289**, 30-41, doi:<https://doi.org/10.1016/j.jcat.2012.01.011> (2012).
19. Singh, U. K. & Vannice, M. A. Kinetics of liquid-phase hydrogenation reactions over supported metal catalysts — a review. *Applied Catalysis A: General* **213**, 1-24, doi:[https://doi.org/10.1016/S0926-860X\(00\)00885-1](https://doi.org/10.1016/S0926-860X(00)00885-1) (2001).
20. Hibbitts, D. D., Loveless, B. T., Neurock, M. & Iglesia, E. Mechanistic role of water on the rate and selectivity of Fischer–Tropsch synthesis on ruthenium catalysts. *Angewandte Chemie International Edition* **52**, 12273-12278 (2013).
21. Wagner, F. T. & Moylan, T. E. Generation of surface hydronium from water and hydrogen coadsorbed on Pt(111). *Surface Science* **206**, 187-202, doi:[https://doi.org/10.1016/0039-6028\(88\)90021-0](https://doi.org/10.1016/0039-6028(88)90021-0) (1988).
22. Hensley, A. J. R., Bray, J., Shanguan, J., Chin, Y.-H. C. & McEwen, J.-S. Catalytic consequences of hydrogen addition events and solvent-adsorbate interactions during

- guaiacol-H₂ reactions at the H₂O-Ru(0001) interface. *Journal of Catalysis*, doi:https://doi.org/10.1016/j.jcat.2020.09.034 (2020).
23. Shangguan, J. *et al.* The role of protons and hydrides in the catalytic hydrogenolysis of guaiacol at the ruthenium nanoparticle–water interface. *ACS Catalysis* **10**, 12310-12332, doi:10.1021/acscatal.0c01963 (2020).
 24. Mayer, J. M., Hrovat, D. A., Thomas, J. L. & Borden, W. T. Proton-coupled electron transfer versus hydrogen atom transfer in benzyl/toluene, methoxyl/methanol, and phenoxy/phenol self-exchange reactions. *Journal of the American Chemical Society* **124**, 11142-11147, doi:10.1021/ja012732c (2002).
 25. Shangguan, J. & Chin, Y.-H. C. Kinetic significance of proton–electron transfer during condensed phase reduction of carbonyls on transition metal clusters. *ACS Catalysis* **9**, 1763-1778, doi:10.1021/acscatal.8b03470 (2019).
 26. Koh, K. *et al.* Electrochemically tunable proton-coupled electron transfer in Pd-catalyzed benzaldehyde hydrogenation. *Angewandte Chemie* **132**, 1517-1521 (2020).
 27. Scognamiglio, J., Jones, L., Vitale, D., Letizia, C. & Api, A. Fragrance material review on benzyl alcohol. *Food and Chemical Toxicology* **50**, S140-S160 (2012).
 28. Bertero, N. M., Trasarti, A. F., Apesteguía, C. R. & Marchi, A. J. Solvent effect in the liquid-phase hydrogenation of acetophenone over Ni/SiO₂: A comprehensive study of the phenomenon. *Applied Catalysis A: General* **394**, 228-238 (2011).
 29. Blaser, H., Jalett, H. & Wiehl, J. Enantioselective hydrogenation of α -ketoesters with cinchona-modified platinum catalysts: Effect of acidic and basic solvents and additives. *Journal of molecular catalysis* **68**, 215-222 (1991).
 30. Rautanen, P. A., Aittamaa, J. R. & Krause, A. O. I. Solvent effect in liquid-phase hydrogenation of toluene. *Industrial & engineering chemistry research* **39**, 4032-4039 (2000).
 31. Claus, P. Selective hydrogenation of α,β -unsaturated aldehydes and other C=O and C=C bonds containing compounds. *Topics in Catalysis* **5**, 51-62, doi:10.1023/a:1019177330810 (1998).
 32. Hub, S., Hilaire, L. & Touroude, R. Hydrogenation of but-1-yne and but-1-ene on palladium catalysts: particle size effect. *Applied catalysis* **36**, 307-322 (1988).

33. Neri, G., Musolino, M. G., Milone, C., Pietropaolo, D. & Galvagno, S. Particle size effect in the catalytic hydrogenation of 2, 4-dinitrotoluene over Pd/C catalysts. *Applied Catalysis A: General* **208**, 307-316 (2001).
34. Haffad, D., Kameswari, U., Bettahar, M. M., Chambellan, A. & Lavalley, J. C. Reduction of benzaldehyde on metal oxides. *Journal of Catalysis* **172**, 85-92, doi:<https://doi.org/10.1006/jcat.1997.1854> (1997).
35. Zhou, Y., Liu, J., Li, X., Pan, X. & Bao, X. Selectivity modulation in the consecutive hydrogenation of benzaldehyde via functionalization of carbon nanotubes. *Journal of Natural Gas Chemistry* **21**, 241-245, doi:[https://doi.org/10.1016/S1003-9953\(11\)60359-9](https://doi.org/10.1016/S1003-9953(11)60359-9) (2012).
36. Masson, J., Cividino, P. & Court, J. Selective hydrogenation of acetophenone on chromium promoted Raney nickel catalysts. III. The influence of the nature of the solvent. *Applied Catalysis A: General* **161**, 191-197, doi:[https://doi.org/10.1016/S0926-860X\(97\)00068-9](https://doi.org/10.1016/S0926-860X(97)00068-9) (1997).
37. Mukherjee, S. & Vannice, M. A. Solvent effects in liquid-phase reactions: I. Activity and selectivity during citral hydrogenation on Pt/SiO₂ and evaluation of mass transfer effects. *Journal of Catalysis* **243**, 108-130, doi:<https://doi.org/10.1016/j.jcat.2006.06.021> (2006).
38. Song, Y. *et al.* Hydrogenation of benzaldehyde via electrocatalysis and thermal catalysis on carbon-supported metals. *Journal of Catalysis* **359**, 68-75, doi:<https://doi.org/10.1016/j.jcat.2017.12.026> (2018).
39. Wu, Z. & Chin, Y.-H. C. Catalytic pathways and mechanistic consequences of water during vapor phase hydrogenation of butanal on Ru/SiO₂. *Journal of Catalysis*, doi:<https://doi.org/10.1016/j.jcat.2020.10.022> (2020).
40. Koh, K. *et al.* Electrochemically tunable proton coupled electron transfer in Pd-catalyzed benzaldehyde hydrogenation. *Angewandte Chemie* (2019).
41. Wu, P. *et al.* Formation of PdO on Au–Pd bimetallic catalysts and the effect on benzyl alcohol oxidation. *Journal of Catalysis* **375**, 32-43, doi:<https://doi.org/10.1016/j.jcat.2019.05.003> (2019).
42. Verma, A. M. & Kishore, N. Molecular simulations of palladium catalysed hydrodeoxygenation of 2-hydroxybenzaldehyde using density functional theory.

- Physical Chemistry Chemical Physics* **19**, 25582-25597, doi:10.1039/C7CP05113A (2017).
43. Kizhakevariam, N. & Stuve, E. M. Coadsorption of water and hydrogen on Pt(100): formation of adsorbed hydronium ions. *Surface Science* **275**, 223-236, doi:https://doi.org/10.1016/0039-6028(92)90796-9 (1992).
 44. Zhao, Z. *et al.* Solvent-mediated charge separation drives alternative hydrogenation path of furanics in liquid water. *Nature Catalysis* **2**, 431-436, doi:10.1038/s41929-019-0257-z (2019).
 45. Purwanto, Deshpande, R. M., Chaudhari, R. V. & Delmas, H. Solubility of hydrogen, carbon monoxide, and 1-octene in various solvents and solvent mixtures. *Journal of Chemical & Engineering Data* **41**, 1414-1417, doi:10.1021/je960024e (1996).
 46. Brunner, E. Solubility of hydrogen in 10 organic solvents at 298.15, 323.15, and 373.15 K. *Journal of Chemical & Engineering Data* **30**, 269-273, doi:10.1021/je00041a010 (1985).

Chapter 3

Role of solvents on the selective hydrogenation of cinnamaldehyde

Solvent properties e.g., like polarity can strongly influence the hydrogenation of cinnamaldehyde, a frequently used model substrate for hydrogenation reactions of α , β -unsaturated aldehydes, over noble and base metal catalysts using H_2 as reductive agent. Both the C=C and C=O bond hydrogenation rates are sensitive to the polarity in protic solvents, while show only a weak dependency in aprotic solvents. IR spectra indicates that the interaction of solvent and cinnamaldehyde is not the main reason leading to such a scenario. The reaction mechanism in protic solvents are different from that in aprotic solvents. Aprotic solvents can only enable the reaction mechanism of H_{ad} addition. In contrast, isotope labeling results suggest a reaction mechanism of H transfer addition in protic solvents.

This chapter is based on the article: Guanhua Cheng et al. Role of solvents on the selective hydrogenation of cinnamaldehyde (prepared for submission). Guanhua Cheng performed the experiments, did the data analysis and wrote the manuscript.

3.1 Introduction

Chemoselective reduction of C=O bond in presence of a C=C bond in α,β -unsaturated aldehydes is a critical step in flavor, fragrance, and pharmaceutical syntheses. The reaction suffers from poor selectivities, because the desired C=O bond hydrogenation is thermodynamically less favored than C=C bond hydrogenation by 35 kJ mol^{-1} . Among the various α,β -unsaturated aldehydes, cinnamaldehyde derived from cinnamon essential oil represents a particularly suitable model compound for probing the catalytic properties as it contains both the strong aromaticity and conjugated C=O and C=C double bonds.

Group VIII metals (Pt, Pd, Rh) are among the most frequently used catalysts for hydrogenation reactions². Attempts to promote the selectivities in C=O hydrogenation on these metals include: (i) the modification of the metal ensemble sites and the electron densities by incorporation of a secondary metal, such as Zn, Cr^{3,4}, (ii) the change of the metal cluster size and morphologies^{5,6}, (iii) the use of reducible carriers (CeO₂, ZnO, etc.) as support⁷⁻⁹ that interact strongly with the metal, (iv) the addition of alkali additives into the reaction medium to promote the adsorption of the carbonyl group and to suppress side reactions.

These modifications are proposed to alter the d-electron densities of transition metal, the size of the exposed metal ensemble, and in turn, the relative heats of α,β -unsaturated aldehyde adsorption, as they adsorb and interact with the metal sites via their C=O or C=C bonds. Delbecq et al. computed the binding energies of several α,β -unsaturated aldehydes (acrolein, crotonaldehyde, cinnamaldehyde, and propenol) on uncovered Pd₄₉ (111) (a Pd cluster of 49 atoms) surfaces and reported that the most stable adsorption configuration of these aldehydes is the $\eta_{4(\text{di-}\pi)}$ configuration, where two adjacent metal sites (Pd-Pd) interact with the C=C and C=O bonds, forming a four center Pd-(C-O)-(C-C)-Pd adsorbed intermediate¹⁰. Their computational results show, in general, a more exothermic and stronger binding of the metal to the C=C π bonds rather than to the C=O π bonds (by $\sim 14\text{-}61 \text{ kJ mol}^{-1}$). The strategies are to alter aldehyde adsorption configurations, the resulting relative surface abundance of these adsorbed aldehydes, and in turn their individual rates and selectivities. Another strategy is to incorporate Lewis-acid sites onto the metal support, which interact with C=O groups through the unshared electron pairs of carbonyl oxygen and thus lower the energy of the π_{CO^*} -orbital, which promotes the cinnamyl alcohol selectivity^{11,12}. Incorporating an electropositive promoter such as Fe or Sn enriches the d-electron density of the metals and promotes the backbonding interaction with π_{CO^*} to a larger extent than with π_{CC^*} , thus favoring C=O over C=C bond adsorption^{13,14}. For example, the addition of alkali ions (Na⁺) on Pt (5 wt%)/CeO₂-ZrO₂

enhances both the cinnamaldehyde conversion rates and selectivity to cinnamyl alcohol ⁷. In addition, larger metal particles will increase the selectivity of unsaturated alcohols due to the enhanced repulsive force between the large rigid phenyl ring and the flat surface^{5,6,15}.

Despite the extensive studies, there are little mechanistic insights at the molecular level on the catalytic requirements for these two competing hydrogenation steps. The hydrogenation occurs via either 1,2 addition that saturates the C=O bond or 3,4 addition that saturates the C=C bond initially, after which, secondary hydrogenation may occur, resulting in the saturated product. The relative rates and catalytic requirements for these primary and secondary hydrogen addition steps have not been systematically examined. In addition to the metal site and electron density requirements, the reactions typically occur in the presence of solvent, which may influence the adsorption configurations and free energies of the adsorbed α,β -unsaturated aldehyde reactants, their derived intermediates, and transition states. On Pd/C and Pt/C, Yamada et.al reported that in polar solvents the C=O polar bond is selectively activated, while in the contrasting case with non-polar solvents the C=C bond is activated ¹⁶. Pyridine as the solvent can assist with the selective hydrogenation of cinnamaldehyde to cinnamyl alcohol, because it competitively adsorbs on the metal surfaces and provides the steric hindrance for the adsorption of the C=C bond, that causes the cinnamaldehyde to adsorb through its C=O bond ¹⁷. These effects have neither been addressed systematically nor been examined at the molecular scale. To our best knowledge, there is no catalyst which would allow the selectively hydrogen attack to C=C or C=O bonds.

This work investigated the catalytic rates and mechanism cinnamaldehyde hydrogenation under different solvents (protic solvents and aprotic solvents) over Pd/C. With an attempt to study the solvent effects on selective hydrogenation of cinnamaldehyde, d-labeling study of hydrogenation products was performed to determine the reaction mechanism in protic solvents. In addition, kinetic analysis was used to study the solvent insensitivity of activity in aprotic solvents.

3.2 Experimental method

3.2.1 Chemicals

Nobel metal nanoparticles (Pd) with 5 wt.% metal loadings (CAS No. 205680) and particle sizes supported on high surface area carbon were purchased from Sigma Aldrich. Trans-Cinnamaldehyde (CA, $\geq 99.0\%$, CAS No. 239968), cinnamyl alcohol (CAL, $\geq 98.0\%$, CAS No. 108197), hydrocinnamaldehyde (HCA, $\geq 99.0\%$, CAS No. 93762), 3-phenyl propanol

(PPL, $\geq 98.0\%$, CAS No.140856), methanol (MeOH, $\geq 99.0\%$, CAS No. 322415), ethanol (EtOH, $\geq 99.0\%$, CAS No. 34852), n-Propanol (n-PrOH, $\geq 99.0\%$, CAS No. 23519779), isopropanol (iPrOH, $\geq 99.0\%$, CAS No. 278475), tert-Butanol (t-Butanol, $\geq 99.0\%$, CAS No. 360538), diethyl ether (Et₂O, $\geq 99.0\%$, CAS No. 32203), dimethyl sulfoxide (DMSO, $\geq 99.0\%$, CAS No. D4540), tetrahydrofuran (THF, $\geq 99.0\%$, CAS No. 186562), 1,4-dioxane ($\geq 99.0\%$, CAS No. 296309), N,N-dimethylformamide ($\geq 99.0\%$, CAS No. 51781), decalin ($\geq 99.0\%$, CAS No. 91178) and Trifluoroacetic acid (TFA, $\geq 99.9\%$ CAS No. 76051) were obtained from Sigma Aldrich and used without any further purification. High purity water, obtained with a Milli-Q water purification system with a resistivity of 18.2 M Ω ·cm, was used in all experiments. H₂ (Air Liquide, $> 99.99\%$) was used for thermal hydrogenation.

3.2.2 Catalyst Characterization

The dispersion of the noble metal nanoparticles was determined by H₂ chemisorption (20 %) performed on a Thermo Scientific Surfer Analyzer. Morphology and particle size of the supported noble metal nanoparticles were determined by transmission electron microscopy (TEM) recorded on a JEOL JEM-2011 with an accelerating voltage of 120 keV. Catalyst samples were mounted on the copper-coated carbon TEM grid. Statistical treatment of the metal particle size was carried out over at least 300 particles on representative micrographs. Electron paramagnetic resonance (ESR) spectra were recorded in perpendicular mode on an X-band Joel Jes Fa 200 spectrometer. The measurements were performed in a high-pressure quartz tube at 133 K (9.45 GHz, 1 mW microwave power) in order to identify transiently formed radicals as (paramagnetic) intermediates. The average particle size was determined to be 5 nm.

3.2.3 Thermal catalytic hydrogenation

Catalytic hydrogenation reactions were carried out in a double jacketed 100 mL glass batch reactor equipped with a magnetic stirrer and a pressure balanced glass valve for H₂ gas supply. In this reactor operating configuration, the H₂ pressure was kept constant, by introducing a continuous stream of H₂ into the reactor, whereas the liquid reaction mixture was constantly stirred. Typical measurements were performed at atmospheric pressure by using 10 mg of catalyst in 60 mL solution. The catalyst was added to the solution and reduced with H₂ for 30 min under continuous stirring (600 rpm) prior to adding CA reactant (66 mM) at 298 K. The temperature was controlled with a Julabo F25-ED cooling/heating circulator. The reaction time was recorded as soon as CA was added to the reaction mixture. For analyzing the composition of the reaction mixture, 1 mL sample was taken from the chemical reactor every 10 min and filtered with a minisart syringe filter prior to GC analysis using a wax capillary column (30 m

× 250 μm) and a flame ionization detector (FID). Blank tests of the catalyst were conducted with H₂ and a reaction mixture consisting of CA and solvent. For calibration all possible hydrogenation products of CA were purchased from Sigma Aldrich with high analytical purity (> 99.9 %). The reaction order in H₂ was determined at 298 K by systematically varying the H₂ pressure from 0.3 to 1 bar in the glass batch reactor using 33 mM CA and 10 - 20 mg 5 wt. % Pd/C in EtOH and dioxane. The reaction order in CA was determined by varying the CA concentration from 16 to 66 mM in the presence of 1 bar H₂ and 10 - 20 mg Pd/C (5 wt. %) in EtOH and dioxane.

3.2.4 ATR-IR measurement

Interactions between the CA substrate and solvents in the liquid phases were examined by attenuated total reflectance infrared spectroscopy (ATR-IR) using a Thermo Fischer Nicolet 6700 spectrometer at a resolution of 4 cm⁻¹ accumulating 100 scans at 296 K on a home-built ATR cell with a trapezoid ZnSe crystal as internal reflection element. For each experiment, a liquid mixture of CA and a solvent in a volume ratio similar to that used in the reaction was mixed using a magnetic stirrer and then loaded onto an ATR crystal.

3.2.5 Isotope-labeling experiments

The reactions in C₂H₅OD were carried out in a 100 mL Hastelloy PARR reactor. 33 mM cinnamaldehyde, 30 mL C₂H₅OD (99.8%, Sigma), 1 bar H₂ and 2 mg Pd/C were sealed in the reactor for reaction at 296 K and 750 rpm. Before the reaction, air was removed from the reactor by introducing 20 bar D₂, followed by depressurizing the reactor for three times. After the experiment, the product analysis was quantified using GC-MS equipped with a HP-5 capillary column. For the reference samples, standard hydrocinnamaldehyde and phenyl propanol were added into C₂H₅OD and measured using GC-MS after three days to make sure the completion of H-D exchange.

3.2.6 Measurement of equilibrium constant of H₂ adsorption

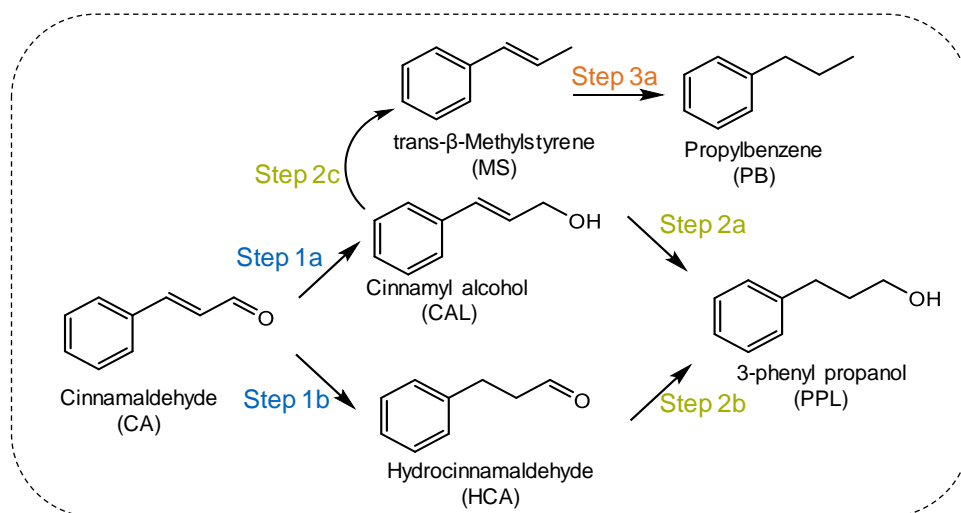
The measurement of equilibrium constant of H₂ adsorption in liquid was used a transient method as described in Chapter 2.

3.3 Results and Discussion

3.3.1 Catalytic pathways, rates, and chemical selectivity of cinnamaldehyde hydrogenation

Scheme 3-1 summarizes all reaction pathways and the associated products for

cinnamaldehyde hydrogenation on Pd/C catalysts. 1,2-Addition of hydrogen (Step 1a) produces the cinnamyl alcohol (CAL) as a desirable pathway. In competing to this pathway, 3,4-addition leads to the hydrocinnamaldehyde (HCA, Step 1b). The secondary hydrogen addition to either CAL or HCA (Steps 2a and 2b) forms the 3-phenyl propanol (PPL) as the common product. Hydrogenolysis of cinnamyl alcohol to *trans*- β -Methylstyrene (MS, Step 2c) and further hydrogenation to propylbenzene (PB, Step 3a) are not observed in present experiments due to the low proton concentration.



Scheme 3-1. Reaction pathways for the cinnamaldehyde hydrogenation over Pd/C and the TOF of different reaction steps measured in ethanol at 1 bar H₂ and 298.

Figure 3-1a shows the time-dependent concentration profiles of CA and hydrogenation products (HCA, CAL, PPL) during CA-H₂ reactions on Pd/C (5 wt.% Pd/C with an average particle size of 5.6 nm) at 1 bar H₂ and 298 K in EtOH. First, CA conversion leads to the formation of HCA, CAL and PPL, in which, the detected CAL is only in trace over the entire conversion range (0% - >80% conversion) (**Figure 3-1a**), suggesting a rapid sequential reaction from CAL to PPL. Second, the hydrogenation of HCA, an intermediate of CA hydrogenation, shows negligible rates under similar conditions, thus the sequential reaction (Step 2b) does not occur at kinetically significant extents (**Figure 3-1b**). This result also indicates the PPL is produced predominantly from the secondary hydrogenation of the CAL (Step 2a). Third, a separate reaction study with CAL-H₂ reactions has shown a much higher rate than that of CA (**Figure 3-1c**), with the rate ratio for Step 2a over Step 1a of ~15 times (**Table A3-2**), when comparing at identical cinnamaldehyde and cinnamyl alcohol concentration (33 mM). This explains why only traces of cinnamyl alcohol are detected during CA hydrogenation.

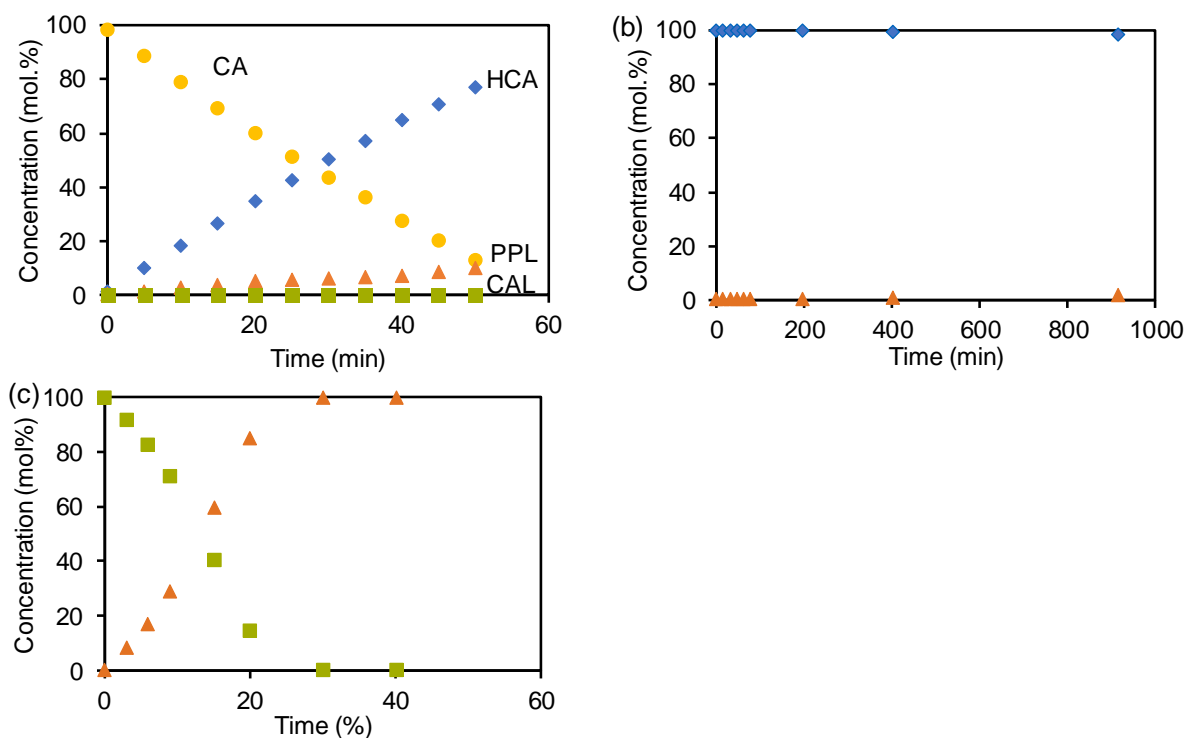


Figure 3-1. Time-dependent-profiles of the catalytic hydrogenation of 33 mM (a) cinnamaldehyde, (b) hydrocinnamaldehyde and (c) cinnamyl alcohol over 10 mg Pd/C (5 wt. %, 5 mg Pd/C for cinnamyl alcohol) in 60 ml EtOH at 298 K and 1 bar H₂.

3.3.2 Solvent effects on the C=C and C=O hydrogenation over Pd/C

Figures 3-2 captures the solvent identity effects for two group of solvents, protic vs. aprotic, on 5 wt.% Pd/C at 298 K and 1 bar H₂. In protic alcoholic solvent (blue points), the saturation rate for both C=O and C=C bonds varies with the solvent polarity, whereas that of C=O bond hydrogenation is more sensitive to the solvent properties. In the contrasting case of aprotic solvents (orange points), the hydrogenation rates of C=O and C=C do not exhibit a sensitivity on solvent polarity. Comparing the TOF values between the two series of solvents, both the C=O and C=C bond hydrogenation rates are significantly enhanced with the presence of H bonds prevalent in protic solvents.

Solvents can affect catalytic reaction rates by interacting with or reacting with surface-bound species, activating it towards reaction or deactivating it^{18,19}. The higher sensitivity of C=O bond to the solvent polarity may be caused by the destabilization of the C=O bond by the H bonds in solvent molecules, which leads to a lower activation energy and related higher hydrogenation rate. Not only the solvents, but also the functional group could affect C=C hydrogenation. The hydrogenation rate of C=C bond of CAL (**Figure 3-1c**, **Figure A3-1**) is one time higher than that of the C=C of CA, when comparing at a reactant concentration of 33 mM. Moreover, the hydrogenation rate of C=C bond in methylstyrene (MS) (**Figure A3-1**) is 2~3

times higher than that of CAL in alcoholic solvents (methanol, ethanol, isopropanol and tert-butanol). Thermodynamic arguments indicate that the isolated C=C bond should be the easiest to hydrogenate followed by the conjugated C=C bond and finally the C=O bond²⁰. Dyson et.al reported a higher selectivity of C=C saturation in polar solvents than in apolar solvents over Wilkinson's catalyst for the hydrogenation of alkenes containing aromatic nitro-groups, a speculation could be the alkene protons hydrogen-bond with the solvent thereby activating the unsaturated C=C bond rather than the nitro-group²¹. Here, we propose that the solvent can stabilize the transition state or destabilize the ground state to decrease the activation energy barrier, which could have an effect on both C=O and C=C hydrogenation.

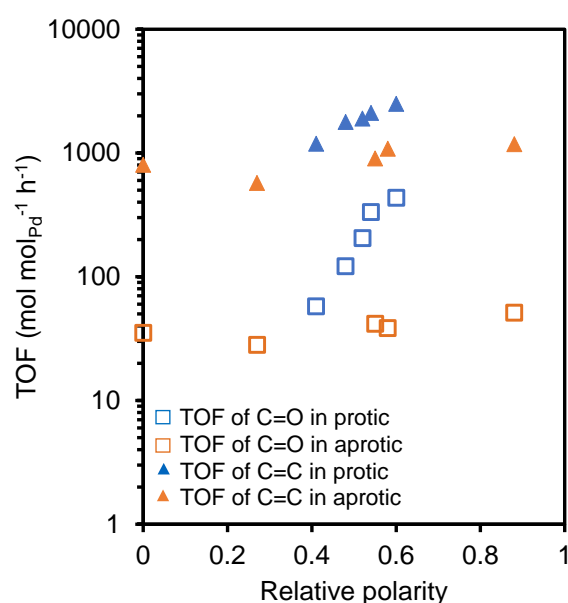


Figure 3-2. Turnover of frequency of C=C and C=O bonds hydrogenation in protic and aprotic solvents as a function of relative polarity (normalized to the polarity of water) of solvents.

3.3.3 Correlation of solvation effects on cinnamaldehyde molecular and hydrogenation rates

ATR-IR of C=O and C=C absorption bands of CA were measured by mixing CA with solvent molecules (80 mM, 150 mM in methanol) to check the substrate solvation in different solvents as shown in **Figure 3-3**. In gas phase, the C=O and C=C vibrational stretches of CA are located at 1705 and 1624 cm⁻¹²², respectively. In presence of solvents, the C=O vibrational stretch shifts to lower wavenumbers to different extent depending on the solvent chemical identity, while in contrast, the C=C absorption band remains almost unchanged at 1625 cm⁻¹ regardless of the solvent (**Figure 3-3a**). These results indicate that the solvents interact strongly with the carbonyl group but not with the C=C bond of CA. To quantitatively analyze the C=O band shift in the solvents, the band in gas phase was used as a reference. The observed red-shift

of C=O band indicates a strong correlation between the C=O stretching frequency and the hydrogen bonding of the solvents ¹⁶, and the larger the wavenumber red-shifted, the stronger the specific force (H-bonding) and non-specific force (non-specific dipolar and dispersion interactions of the solvent and the solute) between the carbonyl group and the solvent.

Figure 3-3b shows a plot of hydrogenation rates of C=O and C=C bonds against the extent of the red-shift in different solvents with respect to that in gas phase. For protic solvents, the C=O shift (stabilization trend by solvent) is in accordance with the hydrogenation rate of C=O. The stronger the interaction strength of CA with solvents, the higher the conversion rate. However, even no C=C band shift was observed in protic solvents, the activity of C=C bond hydrogenation follows the trend of C=O band shift. In aprotic solvents, even the C=O band is red-shifted, no significant effect on hydrogenation rate is observed. A possible explanation is that the solvent effect is different in protic and aprotic solvents. Moreover, the main influence of solvents on the reaction rate is not by the interaction with the substrate. Two solvents with the similar polarity, dioxane and EtOH, were chosen for further detailed study.

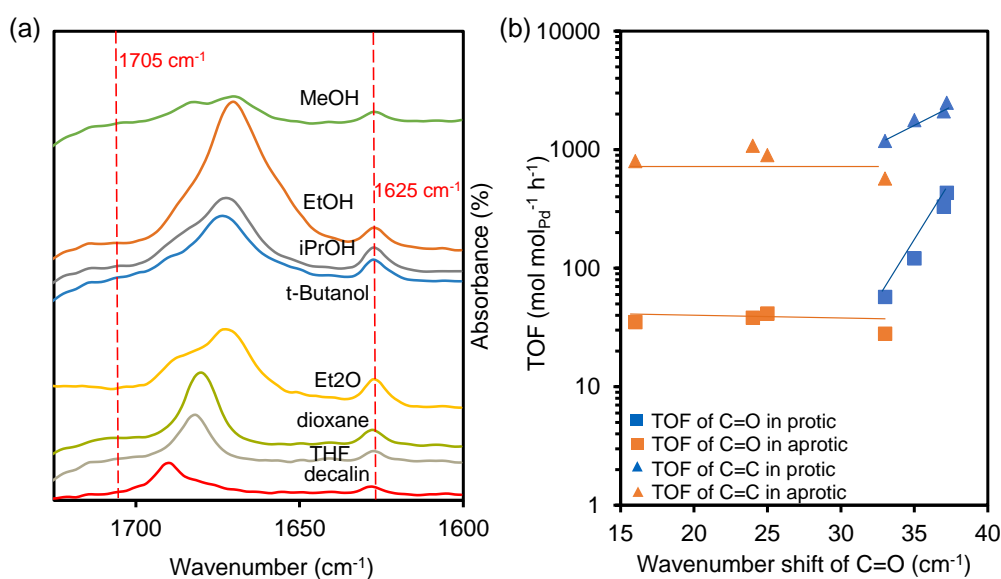


Figure 3-3. (a) ATR-IR spectra of pure cinnamaldehyde. (a) ATR-IR spectra of cinnamaldehyde measured in different solvents (80 mM, except in methanol 150 mM). (b) Turnover frequency of C=C and C=O bonds hydrogenation in protic and aprotic solvents as a function of wavenumber shift of C=O bond of cinnamaldehyde in different solvents by ATR-IR spectra using the band in gas phase as a reference.

3.3.4 Comparison of reaction orders in EtOH and dioxane

The reaction orders (R.O.) with respect to cinnamaldehyde and H₂ in EtOH and dioxane are shown in **Figure 3-4** and **Table 3-1**. For cinnamaldehyde, the reaction orders are near zero

in both EtOH (0.2) and dioxane (0.1), indicating a high coverage of cinnamaldehyde and cinnamaldehyde derived species. Separately, the reaction orders are the same for C=C saturation (0.1) in both solvents, while for C=O bond hydrogenation, a reaction order of 0.1 is observed in dioxane while much higher in EtOH (0.7). This indicates the solvent could affect C=O bond hydrogenation route or change the C=O bond saturation intermediates. In contrast, the hydrogen pressure affects C=O and C=C bonds hydrogenation routes parallelly in both solvents. The reaction order in H₂ is larger in EtOH (0.9) than that in dioxane (0.7), indicating a lower H coverage in EtOH compared that in dioxane.

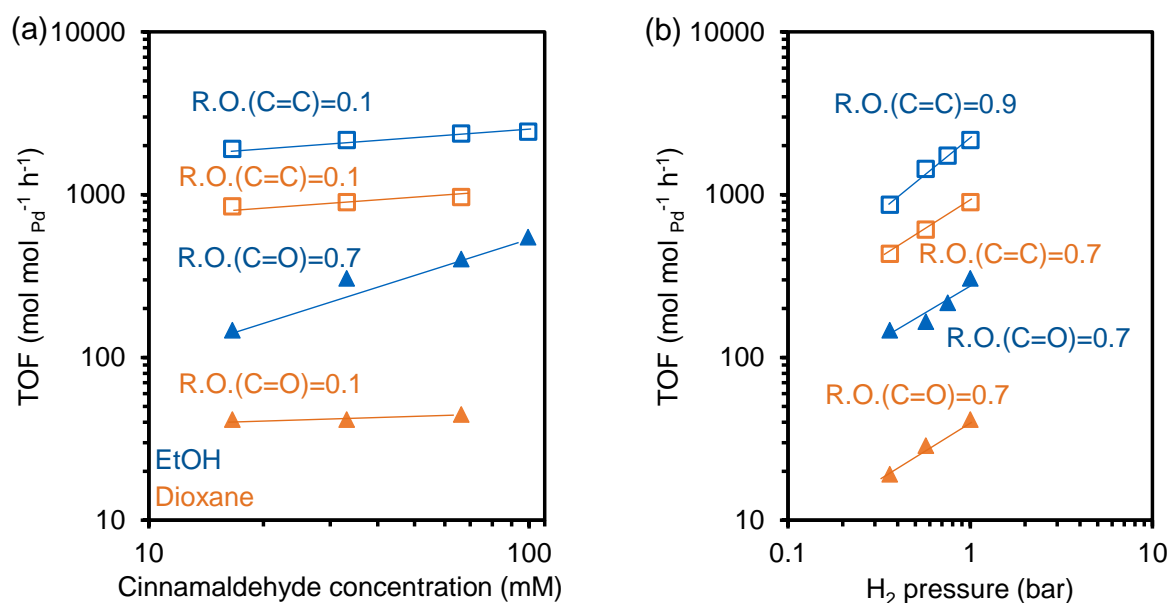


Figure 3-4. (a) TOF as a function of cinnamaldehyde (16-66 mM) at 1 bar H₂ and 298 K. (b) TOF as a function of H₂ (0.3-1 bar) at 33 mM cinnamaldehyde and 298 K.

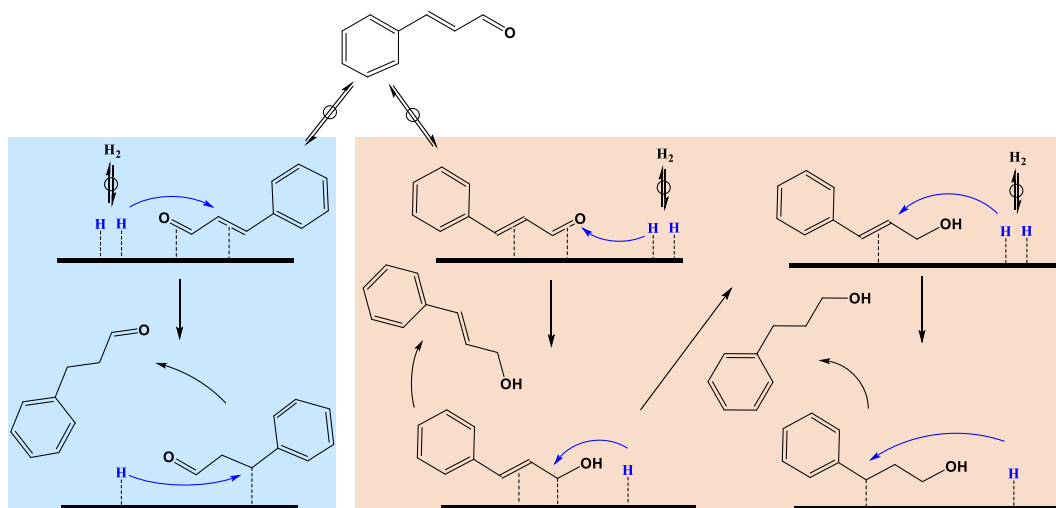
Table 3-1. Summary of reaction orders.

Solvent	Reaction order in CA	Reaction order of C=C in CA	Reaction order of C=O in CA	Reaction order in H ₂	Reaction order of C=C in H ₂	Reaction order of C=O in H ₂
EtOH	0.2	0.1	0.7	0.9	0.9	0.7
Dioxane	0.1	0.1	0.1	0.7	0.7	0.7

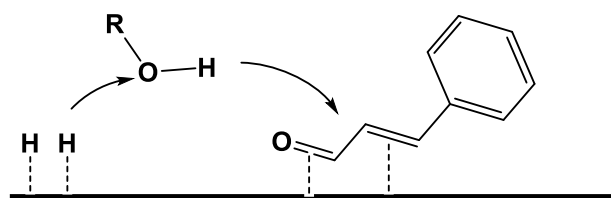
3.3.5 Effects of solvents on catalytic pathway of cinnamaldehyde hydrogenation

In aprotic solvents, there is no doubt that the solvent cannot directly participate in the elementary steps, and the reductive species is dissociatively adsorbed hydrogen (H_{ad}). **Scheme 3-2** shows the reaction mechanism for cinnamaldehyde hydrogenation in aprotic solvents, left pattern presents the C=C bond saturation and right pattern gives the reaction pathway of cinnamyl alcohol hydrogenation as well as further reaction to phenyl propanol. The steps of molecular cinnamaldehyde adsorption and H₂ dissociative adsorption are considered as quasi-

equilibrated. The reaction order in H_2 varies from 0.7 to 1 in aprotic solvents for both C=C and C=O bond hydrogenation (**Table A3-2**). Therefore, the 2nd H addition is considered as the rate-determining step, otherwise the reaction order should be 0.5 (derivation in **Appendix**). The adsorption configurations of cinnamaldehyde is assumed as $\eta_{4(di-\pi)}$, with both C=C and C=O bonds attaching on the Pd surface, because of the highest binding energy of this configuration¹⁰. HCA desorbs from Pd surface after C=C bond saturation. In comparison, CAL will react with H_{ad} further to yield PPL.



Scheme 3-2. Reaction mechanism based on Langmuir–Hinshelwood adsorption in aprotic solvents. Left pattern shows the C=C hydrogenation pathway and right pattern shows the C=O bond hydrogenation as well as further formation of phenyl propanol.



Scheme 3-3. Possible reaction mechanism with H transfer in protic solvents. $R=CH_3, C_2H_5, C_3H_7, C_4H_9$.

The presence of polar protic solvent enables the reaction pathway with hydrogen transfer between H_{ad} and solvent (**Scheme 3-3**)²³, and differs the sole pathway of H_{ad} addition in aprotic solvent. Therefore, the potential involvement of this reaction pathway in hydrogenation catalysis needs to be clarified, which could be determined by the analysis of D involvement in hydrogenation products of cinnamaldehyde in d-ethanol (C_2H_5OD)- H_2 . Considering phenyl propanol (PPL) only yield from cinnamyl alcohol (CAL) and the transformation rate is one order of magnitude larger than the formation rate of cinnamyl alcohol (**Table A3-1**), there is no need to analyze cinnamyl alcohol. The reference tests for exchange process were carried out in the absence of catalyst and H_2 . Based on the mass spectra of phenyl propanol (PPL), the

observation of m/z peak at 137 suggests the H-D exchange between d-ethanol and hydroxyl group of PPL compared to that in C_2H_5OH . The only one D detection indicates only H atom of hydroxyl group deuterated, while C-H was not attached. In comparison, the mass spectra of hydrocinnamaldehyde (HCA) in C_2H_5OD keeps the same as that in C_2H_5OH , confirming that C-H could not be exchanged with D from the solvent. The presence of m/z peak at 137 for PPL and 135 for HCA yielding from cinnamaldehyde hydrogenation in $(C_2H_5OD)-H_2$, suggesting the involvement of D from C_2H_5OD . It is hard to tell whether the D in PPL is from solvent involved reaction pathway or H-D exchange after PPL formation because less than one D deuterated into the PPL. It suggests that time is needed for the completion of H-D exchange process between d-ethanol and hydroxyl group of PPL, otherwise, the number of D in PPL should be one at least. The result for HCA confirmed the existence of a solvent involved reaction process. In addition, due to the involved D in HCA is less than one, the direct H_{ad} from H_2 dissociation addition also exists.

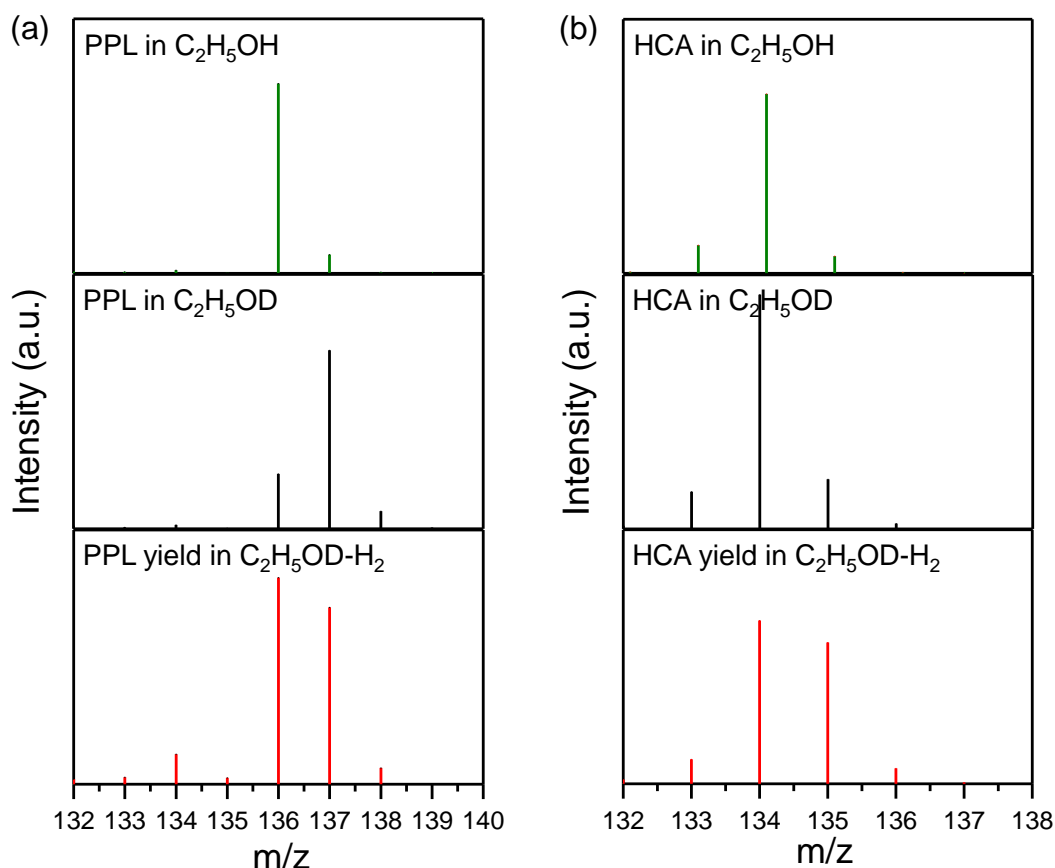


Figure 3-5. The mass spectra of (a) PPL and (b) HCA in C_2H_5OH and C_2H_5OD as well as hydrogenation products in $C_2H_5OD - H_2$ on Pd/C at 298K. The samples of PPL and HCA in C_2H_5OD without Pd/C were exchanged for 3 days at 298K.

Based on the deuterium study, we can confirm the existence of the reaction pathway in which the solvent is involved in cinnamaldehyde hydrogenation in protic solvent. This explains the higher reaction rate in protic solvents than that in aprotic solvents (**Figure 3-2**). Moreover, the enhancement present in both C=C and C=O hydrogenation, suggesting this reaction pathway exists in both reactions. The ability of H transfer is related to proton affinity of the protic solvents, therefore, it is methanol > ethanol > propanol > butanol ²⁴, which is in accordance with the reaction activity. This activity trend is also related to the larger destabilization of sorbed H in methanol (**Table A3-3**) which attributes to a smaller energy barrier. A higher selectivity of cinnamyl alcohol is observed in methanol > ethanol > propanol = butanol (**Table A3-4**), a possible explanation is that methanol can better activate C=O bond to increase the selectivity (**Figure 3-3**).

Considering the 2nd H addition is rate-determining step in aprotic solvents, the rate is related to the activation barrier as well as coverages of H and substrate, then the rate equation can be expressed in the Arrhenius equation (the expression cannot distinguish C=C and C=O hydrogenation)

$$r = A \frac{\theta_{\text{H}}^2 \theta_{\text{CA}}}{\theta^*} e^{-E_a/RT} \quad (1)$$

Where E_a is the activation barrier, A is an independent prefactor including the activation entropy, and θ_{H} and θ_{CA} are the coverages of adsorbed hydrogen and adsorbed cinnamaldehyde. The aprotic solvents present possess similar standard entropy in gas phase (303 J mol⁻¹ K⁻¹ for dioxane, 301.7 J mol⁻¹ K⁻¹ for THF, 333 J mol⁻¹ K⁻¹ for decalin and 306 J mol⁻¹ K⁻¹ for DMF) ^{25,26}. Based on the equation describing the standard entropies of adsorbed molecules ($\Delta S_{\text{ads}}^\circ$) linearly depend on those of the gas-phase molecules (S_{gas}°) at the same temperature on flat surface ($-\Delta S_{\text{ads}}(T) = 0.3S_{\text{gas}}(T) + 3.3R$) reported by Campbell and Sellers ²⁷, the adsorption entropy of these solvents are essentially the same at 298 K considering the Pd surface is not confined environment. we assume the entropy of H₂ adsorption is relative constant in various solvents. Here, we assumed that the entropy of the adsorbed species are independent on solvent. This expression applies for both C=C and C=O hydrogenation, while E_a is different for the reaction pathways. The enthalpy change (ΔH_r) for the hydrogenation of either C=C and C=O is

$$\Delta H_r = \Delta H_{\text{CA}-2\text{H}}^\circ - \Delta H_{\text{CA}}^\circ - \Delta H_{\text{H}_2}^\circ \quad (2)$$

$\Delta H_{H_2}^\circ$ is standard enthalpy of H_2 adsorption, ΔH_{CA}° is standard enthalpy of CA adsorption and ΔH_{CA-2H}° is standard enthalpy of intermediate with two H addition. According to Evans–Polanyi principle, the activation energy of the rate-determining step varies linearly with its reaction enthalpy:

$$\begin{aligned} E_a &= \alpha + \beta \Delta H_r \\ &= \alpha + \beta (\Delta H_{CA-2H}^\circ - \Delta H_{CA}^\circ - \Delta H_{H_2}^\circ) \quad (3) \end{aligned}$$

where β is constant between 0 and 1, α is a constant. It is likely that the solvent effect on sorbed CA and the intermediate to the same extent ($\Delta H_{CA-H_2}^\circ - \Delta H_{CA}^\circ \approx \text{constant}$) due to the similar structure, and main effect on the adsorption enthalpy of H_2 . Substitute E_a in Equation 3 into Equation 1,

$$\begin{aligned} r &= A \frac{\theta_H^2 \theta_{CA}}{\theta^*} e^{-(\alpha + \beta (\Delta H_{CA-2H}^\circ - \Delta H_{CA}^\circ - \Delta H_{H_2}^\circ))/RT} \\ &= A' \frac{\theta_H^2 \theta_{CA}}{\theta^*} e^{\beta \Delta H_{H_2}^\circ / RT} \quad (4) \end{aligned}$$

where A' is a new constant. If we substitute the expression of θ_H , θ_{CA} and θ^* (deviation in the SI) into Equation 4,

$$r = A' \frac{K_{H_2}^\circ P_{H_2} K_{CA}^\circ C_{CA} e^{\beta \Delta H_{H_2}^\circ / RT}}{(1 + K_{H_2}^{\circ 1/2} P_{H_2}^{1/2} + K_{CA}^\circ C_{CA} + K_1 K_{H_2}^{\circ 1/2} P_{H_2}^{1/2} K_{CA}^\circ C_{CA})^2} \quad (5)$$

The equilibrium constant of hydrogen adsorption can be expressed using enthalpy of hydrogen adsorption,

$$K_{H_2}^\circ = B e^{-\Delta H_{H_2}^\circ / RT} \quad (6)$$

In which B is a constant. Considering the reaction order in cinnamaldehyde is near 0 while that in H_2 is near 1, coverage of substrate is higher than that of H, then

$$K_{CA}^\circ C_{CA} \gg K_{H_2}^{\circ 1/2} P_{H_2}^{1/2} \quad (7)$$

combined with Equation 6, Equation 5 can be simplified as

$$r = C e^{(\beta-1)\Delta H_{H_2}^\circ / RT} \quad (8)$$

Taking the natural log of both sides gives Equation 8,

$$\ln r = \ln C + (\beta - 1) \Delta H_{\text{H}_2}^{\circ} / RT \quad (9)$$

As mentioned above, we assume the entropy of H₂ adsorption is relative constant in various solvents. Therefore, the free energy of H₂ adsorption can be used to represent $\Delta H_{\text{H}_2}^{\circ}$. **Figure 3-6** presents the relation of ln TOF as a function of free energy of H₂ adsorption for both C=C and C=O hydrogenation. According to the slope of 0, β is 1.0 in Equation 8, suggesting a late transition state for the rate-determining step. Thus, the transition state resembles the product (hydrocinnamaldehyde and cinnamyl alcohol) on the aspects of energy and structure and the enthalpies of sorbed products are not sensitive to the solvents. Therefore, the hydrogenation rate is relative constant in aprotic solvents (**Figure 3-2**).

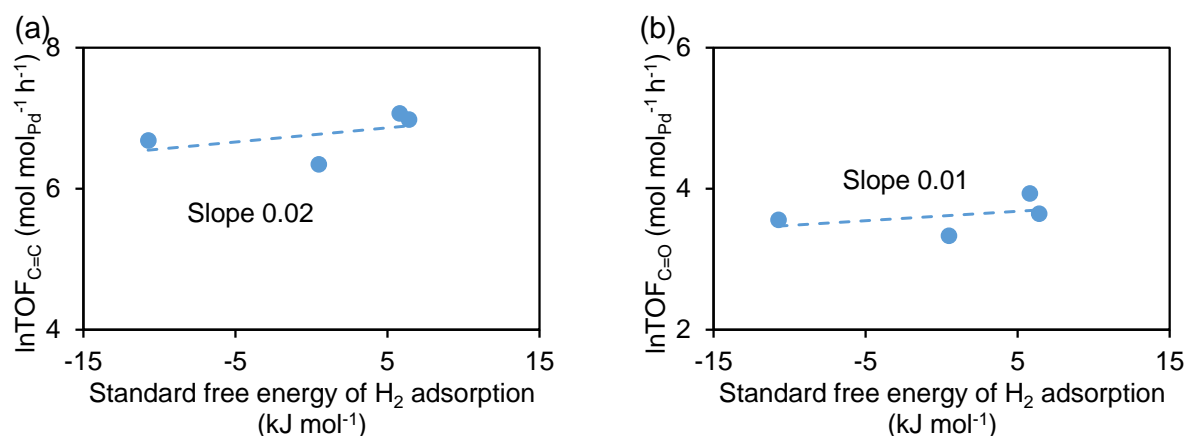


Figure 3-6. ln TOF as a function of free energy of H₂ adsorption. (a) C=C bond hydrogenation and (b) C=O bond hydrogenation. The method to obtain the free energy of H₂ adsorption in the liquid is as described in Chapter 2

3.4 Conclusions

The nature of the solvent plays an important role in the hydrogenation rate of cinnamaldehyde on Pd/C. The hydrogenation rate of cinnamaldehyde is much higher in protic solvents than that in aprotic solvents. The isotope labeling result shows that reaction mechanisms with H transfer and direct H_{ad} addition coexist in protic solvents. In contrast, aprotic solvents only enable H_{ad} addition pathway. Protic solvents with higher proton affinity facilitate the reaction pathway with H transfer leading to a higher activity. In addition, the solvent with higher polarity destabilizes the adsorbed C=O bond in cinnamaldehyde via hydrogen bonding facilitating C=O bond hydrogenation resulting in a higher selectivity in C=O bond saturation. A late transition state of rate determining step is suggested based on the kinetic analysis. The insensitivity of hydrogenation rate in aprotic solvents is attributed to the similar enthalpy of sorbed product.

3.5 Appendix

Table A3-1. Hydrogenation rate and selectivity of CA, CAL and HCA on Pd/C.

Reactant	Selectivity at 20% conversion		TOF (mol mol _{Pd} ⁻¹ h ⁻¹)	Formation rate (mol mol _{Pd} ⁻¹ h ⁻¹)		
	C=C	C=O		HCA	PPL	CAL
CA	87	13	2438	2121	293	24
CAL	100	0	4463	0	4463	0
HCA	0	100	0.2	0	0.2	0

Reaction condition: the hydrogenation of cinnamaldehyde (CA) and hydrocinnamaldehyde (HCA) were performed over 10 mg Pd/C and cinnamyl alcohol (CAL) over 5 mg Pd/C (5wt.%) in EtOH at 298 K, 1 bar of H₂ flow and stirring speed of 600 rpm.

Table A3-2. Summary of reaction orders in aprotic solvents.

Solvent	Reaction order in CA	Reaction order of C=C in CA	Reaction order of C=O in CA	Reaction order in H ₂	Reaction order of C=C in H ₂	Reaction order of C=O in H ₂
THF	0.02	0.02	0.00	0.79	0.72	1.01
dioxane	0.09	0.09	0.05	0.72	0.72	0.76
DMF	0.14	0.11	0.86	0.91	0.98	1.02
decalin	0.02	0.02	0.03	0.91	0.98	0.62

Table A3-3. Equilibrium constant* of H₂ adsorption in protic solvents on Pd.

Solvent	methanol	ethanol	isopropanol	tert-butanol
$K_{H_2}^{\circ}$ (bar)	4.0×10^{-4}	6.9×10^{-4}	1.2×10^{-3}	-

*The equilibrium constant of H₂ adsorption was measured on Pd black at 298 K and 1 bar pressure. A transient method was used in which to react the presorbed H using D₂, with the quantification of formed HD and H₂ to determine the H coverage on Pd black in different solvents. The equilibrium constant of H₂ adsorption was calculated based on the H coverage.

Table A3-4. Selectivity of C=C and C=O bond hydrogenation.

Solvent	C=C saturation	C=O saturation
methanol	85%	15%
ethanol	87%	13%
isopropanol	93%	7%
n-propanol	93%	7%
tert-butanol	93%	7%
THF	97%	3%
dioxane	93%	7%
DMF	96%	4%
decalin	96%	4%

*The selectivities were determined under a conversion of 20% at 1 bar H₂ and 298 K.

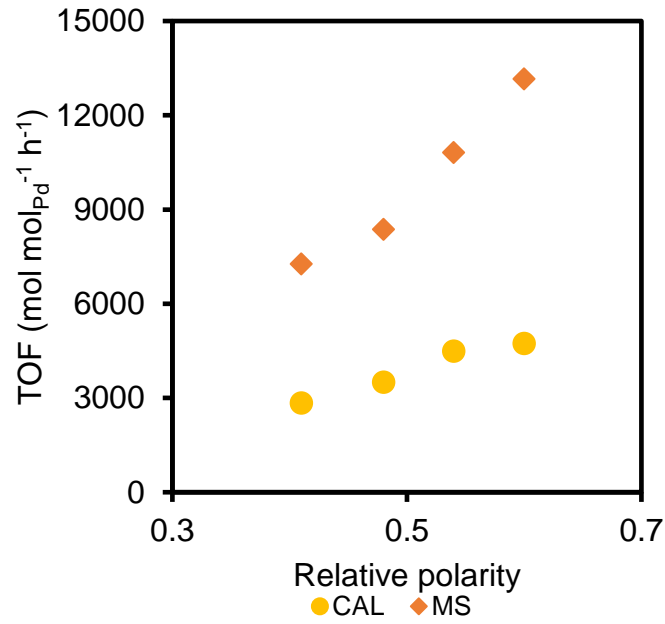


Figure A3-1. TOF of cinnamyl alcohol and trans- β -methyl styrene consumption rate as a function of relative polarity in alcoholic solvents at a concentration of 66 mM, 298 K and 1 bar H_2 .

A3.1 Derivation of rate equation

A3.1.1 power law and general reaction order expression

Rate equation of cinnamaldehyde hydrogenation based on power law,

$$r = k_{\text{lumped}} P_{H_2}^{\gamma} C_{CA}^{\eta} \quad (\text{A1})$$

Thus, the reaction order in hydrogen and cinnamaldehyde can be expressed as,

$$\gamma = \left(\frac{\partial \ln r}{\partial \ln P_{H_2}} \right)_{C_{CA}} \quad (\text{A2})$$

$$\eta = \left(\frac{\partial \ln r}{\partial \ln C_{CA}} \right)_{P_{H_2}} \quad (\text{A3})$$

k_{lumped} denotes the lumped rate constant, which equals the rate constant of the kinetically relevant step multiplied by the respective equilibrium constants of reactants for the various elementary steps that are required to form the surface precursor (prior to the kinetically relevant step). γ and η are reaction orders of hydrogen and cinnamaldehyde, respectively.

A3.1.2 Reaction order expression for 2nd H addition as rate determining step

The sum of the fractional coverages for species i (θ_i), which include the adsorbed H atom (H^*), adsorbed cinnamaldehyde (CA^*), the partially hydrogenated cinnamaldehyde intermediates ($CA-H^*$) for both $CA-Hc^*$ (partially C=C bond hydrogenated cinnamaldehyde intermediates) and $CA-Ho^*$ (partially C=O bond hydrogenated cinnamaldehyde intermediates) considering the rate equation cannot distinguish from C=C hydrogenation to C=O

hydrogenation, together with that of the unoccupied site (*), equals unity:

$$\theta_H + \theta_{CA} + \theta_{CA-H} + \theta_* = 1 \quad (A4)$$

Pseudo steady-state approximation, carried out on the elementary steps in Scheme 2 gives the fractional coverage of H atoms, adsorbed cinnamaldehyde and partially hydrogenated cinnamaldehyde intermediated,

$$\theta_H = K_{H_2}^{\circ 1/2} P_{H_2}^{1/2} \theta_* \quad (A5)$$

$$\theta_{CA} = K_{CA}^{\circ} C_{CA} \theta_* \quad (A6)$$

$$\theta_{CA-H} = K_1 \theta_H \theta_{CA} / \theta_* \quad (A7)$$

Substituting Equation A5 and A6 in Equation A7 leading to equation A8 ,

$$\theta_{CA-H} = K_1 K_{H_2}^{\circ 1/2} P_{H_2}^{1/2} K_{CA}^{\circ} C_{CA} \theta_* \quad (A8)$$

Substituting Equation A5, A6 and A8 into Equation A4,

$$\theta_* + K_{H_2}^{\circ 1/2} P_{H_2}^{1/2} \theta_* + K_{CA}^{\circ} C_{CA} \theta_* + K_1 K_{H_2}^{\circ 1/2} P_{H_2}^{1/2} K_{CA}^{\circ} C_{CA} \theta_* = 1 \quad (A9)$$

$$\theta_* = (1 + K_{H_2}^{\circ 1/2} P_{H_2}^{1/2} + K_{CA}^{\circ} C_{CA} + K_1 K_{H_2}^{\circ 1/2} P_{H_2}^{1/2} K_{CA}^{\circ} C_{CA})^{-1} \quad (A10)$$

The reaction rate expression is

$$\begin{aligned} r &= k_2 \theta_{CA-H} \theta_H \\ &= \frac{k_2 K_{H_2}^{\circ} P_{H_2} K_{CA}^{\circ} C_{CA}}{(1 + K_{H_2}^{\circ 1/2} P_{H_2}^{1/2} + K_{CA}^{\circ} C_{CA} + K_1 K_{H_2}^{\circ 1/2} P_{H_2}^{1/2} K_{CA}^{\circ} C_{CA})^2} \quad (A11) \end{aligned}$$

In the rate expressions, k_2 the rate constant of the kinetically relevant step; $K_{H_2}^{\circ}$ equilibrium constants for the adsorption of H_2 ; K_{CA}° equilibrium constants for the adsorption of CA; K_1 is rate constants for first H addition.

Based on Equation A3,

$$\gamma = \left(\frac{\partial \ln r}{\partial \ln P_{H_2}} \right)_{C_{CA}} = 1 - (\theta_H + \theta_{CA-H}) \quad (A12)$$

$$\eta = \left(\frac{\partial \ln r}{\partial \ln C_{CA}} \right)_{P_{H_2}} = 1 - 2(\theta_{CA} + \theta_{CA-H}) \quad (A13)$$

A3.1.3 Reaction order expression for 1st H addition as rate determining step

If the first H addition step is the rate determining step, then the surface is mainly saturated by adsorbed H adatom (H^*), adsorbed cinnamaldehyde (CA^*), together with that of the

unoccupied site (*), equals unity:

$$\theta_H + \theta_{CA} + \theta_* = 1 \quad (\text{A14})$$

Substituting Equation S5 and S6 Equation S14, the expression of empty site is

$$\theta_* = (1 + K_{H_2}^o 1/2 P_{H_2} 1/2 + K_{CA}^o C_{CA})^{-1} \quad (\text{A15})$$

The reaction rate expression is

$$\begin{aligned} r &= k_1 \theta_{CA} \theta_H \\ &= \frac{k_1 K_{H_2}^o 1/2 P_{H_2} 1/2 K_{CA}^o C_{CA}}{(1 + K_{H_2}^o 1/2 P_{H_2} 1/2 + K_{CA}^o C_{CA})^2} \quad (\text{A16}) \end{aligned}$$

In the rate expressions, k_1 the rate constant of the kinetically relevant step.

Based on Equation A3,

$$\gamma = \left(\frac{\partial \ln r}{\partial \ln P_{H_2}} \right)_{C_{CA}} = 0.5 - \theta_H \quad (\text{A17})$$

$$\eta = \left(\frac{\partial \ln r}{\partial \ln C_{CA}} \right)_{P_{H_2}} = 1 - 2\theta_{CA} \quad (\text{A18})$$

Considering the smallest coverage is 0 for all the species, therefore, γ is 0.5 at largest if 1st H addition is rate determining step.

3.6 Reference

1. Mäki-Arvela, P., Hájek, J., Salmi, T. & Murzin, D. Y. Chemoselective hydrogenation of carbonyl compounds over heterogeneous catalysts. *Applied Catalysis A: General* **292**, 1-49 (2005).
2. Trost, B. M. & Kulawiec, R. J. Chemoselectivity in the ruthenium-catalyzed redox isomerization of allyl alcohols. *Journal of the American Chemical Society* **115**, 2027-2036 (1993).
3. Vicente, A., Lafaye, G., Especel, C., Marécot, P. & Williams, C. T. The relationship between the structural properties of bimetallic Pd–Sn/SiO₂ catalysts and their performance for selective citral hydrogenation. *Journal of catalysis* **283**, 133-142 (2011).
4. Ramos-Fernández, E., Ferreira, A., Sepúlveda-Escribano, A., Kapteijn, F. & Rodríguez-Reinoso, F. Enhancing the catalytic performance of Pt/ZnO in the selective hydrogenation of cinnamaldehyde by Cr addition to the support. *Journal of Catalysis* **258**, 52-60 (2008).
5. Galvagno, S., Capannelli, G., Neri, G., Donato, A. & Pietropaolo, R. Hydrogenation of cinnamaldehyde over Ru/C catalysts: effect of Ru particle size. *Journal of molecular catalysis* **64**, 237-246 (1991).
6. Giroir-Fendler, A., Richard, D. & Gallezot, P. Chemoselectivity in the catalytic hydrogenation of cinnamaldehyde. Effect of metal particle morphology. *Catalysis letters* **5**, 175-181 (1990).
7. Bhogeswararao, S. & Srinivas, D. Intramolecular selective hydrogenation of cinnamaldehyde over CeO₂–ZrO₂-supported Pt catalysts. *Journal of catalysis* **285**, 31-40 (2012).
8. Piqueras, C. M., Gutierrez, V., Vega, D. A. & Volpe, M. A. Selective hydrogenation of cinnamaldehyde in supercritical CO₂ over Pt/SiO₂ and Pt/HS-CeO₂: An insight about the role of carbonyl interaction with supercritical CO₂ or with ceria support sites in cinamyl alcohol selectivity. *Applied Catalysis A: General* **467**, 253-260 (2013).
9. Han, X., Zhou, R., Yue, B. & Zheng, X. Selective hydrogenation of cinnamaldehyde over Pt/ZrO₂ catalyst modified by Cr, Mn, Fe, Co and Ni. *Catalysis letters* **109**, 157-161 (2006).

10. Delbecq, F. & Sautet, P. Competitive C=C and C=O Adsorption of α - β -unsaturated aldehydes on Pt and Pd surfaces in relation with the selectivity of hydrogenation reactions: A theoretical approach. *Journal of Catalysis* **152**, 217-236, doi:<https://doi.org/10.1006/jcat.1995.1077> (1995).
11. Szöllösi, G., Török, B., Baranyi, L. & Bartók, M. Chemoselective hydrogenation of cinnamaldehyde to cinnamyl alcohol over Pt/K-10 catalyst. *Journal of Catalysis* **179**, 619-623 (1998).
12. Gallezot, P. & Richard, D. Selective hydrogenation of α , β -unsaturated aldehydes. *Catalysis Reviews* **40**, 81-126 (1998).
13. Marinelli, T., Nabuurs, S. & Ponec, V. Activity and selectivity in the reactions of substituted α , β -unsaturated aldehydes. *Journal of Catalysis* **151**, 431-438 (1995).
14. Marinelli, T. & Ponec, V. A Study on the selectivity in acrolein hydrogenation on platinum catalysts: a model for hydrogenation of α , β -unsaturated aldehydes. *Journal of Catalysis* **156**, 51-59 (1995).
15. Jiang, F., Cai, J., Liu, B., Xu, Y. & Liu, X. Particle size effects in the selective hydrogenation of cinnamaldehyde over supported palladium catalysts. *RSC Advances* **6**, 75541-75551 (2016).
16. Nie, B., Stutzman, J. & Xie, A. A vibrational spectral marker for probing the hydrogen-bonding status of protonated Asp and Glu residues. *Biophysical journal* **88**, 2833-2847 (2005).
17. Li, Y. *et al.* Solvent effects on heterogeneous catalysis in selective hydrogenation of cinnamaldehyde over a conventional Pd/C catalyst. *Catalysis Science & Technology* (2018).
18. Faheem, M., Suthirakun, S. & Heyden, A. New implicit solvation scheme for solid surfaces. *The Journal of Physical Chemistry C* **116**, 22458-22462, doi:[10.1021/jp308212h](https://doi.org/10.1021/jp308212h) (2012).
19. Roudgar, A., Eikerling, M. & van Santen, R. Ab initio study of oxygen reduction mechanism at Pt₄ cluster. *Physical Chemistry Chemical Physics* **12**, 614-620, doi:[10.1039/B914570B](https://doi.org/10.1039/B914570B) (2010).
20. Singh, U. K. & Vannice, M. A. Kinetics of liquid-phase hydrogenation reactions over supported metal catalysts—a review. *Applied Catalysis A: General* **213**, 1-24 (2001).

21. Dyson, P. J. & Jessop, P. G. Solvent effects in catalysis: rational improvements of catalysts via manipulation of solvent interactions. *Catalysis Science & Technology* **6**, 3302-3316, doi:10.1039/C5CY02197A (2016).
22. Trans-Cinanaldehyde. Published by John Wiley & Sons, Inc. URL <https://spectrabase.com/spectrum/JKs54SH6SPB>. Access date 30th April 2021.
23. Dai, Y. *et al.* On the role of water in selective hydrogenation of cinnamaldehyde to cinnamyl alcohol on PtFe catalysts. *Journal of Catalysis* **364**, 192-203, doi:<https://doi.org/10.1016/j.jcat.2018.05.008> (2018).
24. Marcus, Y. The properties of organic liquids that are relevant to their use as solvating solvents. *Chemical Society Reviews* **22**, 409-416, doi:10.1039/CS9932200409 (1993).
25. Ghahremanpour, M. M., Maaren, P. J. v., Ditz, J. C., Lindh, R. & Spoel, D. v. d. Large-scale calculations of gas phase thermochemistry: Enthalpy of formation, standard entropy, and heat capacity. *The Journal of Chemical Physics* **145**, 114305, doi:10.1063/1.4962627 (2016).
26. *Tetrahydrofuran*, Published by Wikipedia, [https://en.wikipedia.org/wiki/Tetrahydrofuran_\(data_page\)](https://en.wikipedia.org/wiki/Tetrahydrofuran_(data_page)). Access date 30th April 2021.
27. Campbell, C. T. & Sellers, J. R. V. The Entropies of Adsorbed Molecules. *Journal of the American Chemical Society* **134**, 18109-18115, doi:10.1021/ja3080117 (2012).

Chapter 4

Understanding of the rate-enhancement with hydronium ions on the hydrogenolysis of benzyl alcohol over Pd/C

Acidity can significantly promote the hydrogenolysis reaction of benzylic alcohol, reductively converting C-O bonds to the corresponding C-H bonds. There are three plausible reaction pathways for benzyl alcohol hydrogenolysis: 1) a one-step attack in which the adsorbed H displaces the carbonyl group to form toluene; 2) a partial hydrogenation of the benzene ring providing a β -H leading intra-molecular dehydration forming an olefin which is further hydrogenated to toluene; 3) protonated benzyl alcohol dehydrates to benzylic carbenium followed by a hydride addition to form toluene. Combining low H coverage and 0th reaction order of H₂ under the benzyl alcohol concentration present as well as the negligible kinetic isotope effects of H₂ and D₂ during reaction in H₂O or D₂O, we confirm that adsorbed H is not involved in the rate-determining step. Moreover, isotope-labeling analysis of the products indicate that benzene ring hydrogenation is not an elementary step in benzyl alcohol hydrogenolysis under the conditions present. Thus the reaction follows the protonation-dehydration-hydride addition pathway. An analysis of the rate equation shows that the spontaneous electric potential on Pd in aqueous solution plays an important role in the catalytic reaction which can influence the relative stability of transition state and ground state. Both H₂ and H⁺ can affect the reaction by tuning the electric potential on Pd. The enhanced reaction rate at low pH is attributed to the increasing concentration of transition state though the negative effect on increasing the activation barrier.

This chapter is based on the article: Guanhua Cheng et al. Understanding of the rate-enhancement with hydronium ions on the reaction of benzyl alcohol hydrogenolysis over Pd/C (prepared for submission). Guanhua Cheng performed the experiments, did the data analysis and wrote the manuscript.

4.1 Introduction

Catalytic reactions catalyzed by transition metals, e.g. hydrogenolysis and reduction, are fundamental in both, chemical production and energy conversion¹⁻³. The activity of the catalytic reactions is highly dependent on the interactions between the key reaction agents and the metal surfaces as well as the interfacial medium surrounding (solvent). The catalytic rate can be enhanced by destabilization of reactant or / and stabilization of transition state so that to decrease the activation energy barrier^{4,5}.

The gas-solid interfacial reactions have been extensively explored and well understood⁶⁷. However, the presence of aqueous electrolytes, on one hand, results in the formation of a metal-liquid interface capable of catalyzing complex multi-proton-coupled electron transfer (PCET) reactions⁸⁻¹⁰. On the other hand, the generation of electrostatic potential gradient from metal surface to bulk solution caused by the polarization of the electrode surface, which contributes to the chemical potentials of charged species as well as the arrangement of the hydrated ions and molecules¹¹. Therefore, not only the chemisorbed species on the metal surfaces which can directly involve in the reaction, but also nonspecifically adsorbed hydrated ions / molecules at the outer Helmholtz plane, especially the hydronium ions, play an important role in the catalytic reaction. It has been reported that hydronium ions can greatly enhance reactions catalyzed by Pt and Pt-group metals, by an energy-favored PCET pathway¹²⁻¹⁴ or by weakening of the H-metal bond, which decreases the activation barrier¹⁵. The growing understanding of the processes on the interface indicates that the proton activity at the electrode surface plays a central role in kinetics, thermodynamics, and reaction mechanisms^{16,17}.

The reductive conversion of C-O bonds to the corresponding C-H bonds can be achieved by hydrogenolysis using molecular hydrogen as the reductant. It was reported that the activity and selectivity for C-O bond cleavage is sensitive to the acidity of the catalyst support or of the solvents¹⁸⁻²³, and that neutralizing the acid sites by bases will remove the enhancement^{21,24}. Extensive investigations on the reaction mechanism were performed in order to understand the promoter effect of acidity on benzylic alcohol hydrogenolysis. There are two main reaction mechanisms proposed. One is that the C-O bond scission proceeds via a dehydration-hydrogenation route, e.g. 1-(4-isobutylphenyl) ethanol converting to 4-isobutylethylbenzene on Pd supported on acid functionalized activated carbon¹⁸ or 1-phenylethanol to ethylbenzene on a bi-functional Pd/HMOR catalyst at 303 K²⁵. The other is a direct C-OH bond breaking by an incoming hydrogen^{26,27}, for example, the reactions of 1-(4-isobutylphenyl) ethanol on Pd/SiO₂ and Pd black¹⁸ and 1-Indanol over Rh²¹. Therefore, the acidic sites either catalyzes the

dehydration reaction or makes the carbonyl a better leaving group.

However, the individual contributions of hydronium ions and the metallic function on the kinetics of benzylic alcohol hydrogenolysis as well as the elementary steps are still unclear. Moreover, the role of electrostatic (metal-ion) force on catalytic reaction is not discussed. Thus making the elucidation of the reaction pathway and elementary steps are important for the understanding of interfacial reactions.

In this work, we describe the role of the hydronium ions and metal sites at the interface of metal surface and outer Helmholtz plane for benzyl alcohol hydrogenolysis over Pd/C in aqueous buffer solution. Pd is chosen due to its high activity and selectivity towards C-O bond cleavage²⁸. Reaction pathway identified proceeds via the protonation of the OH group makes a better leaving group (OH_2^+) leading to the formation benzylic carbocation, and toluene yield after a hydride addition. Through kinetic analysis and the study of kinetic isotope effects, we confirmed that dehydration of the protonated alcohol is the rate-determining step. Hydronium ions affect the reaction by changing the electric potential on Pd as well as the transition state concentration. While H_2 is basically through influencing the electric potential which is equivalent as directly applying an electric potential.

4.2 Experimental method

4.2.1 Chemicals and Catalyst

Pd/C catalyst with a Pd content of 5 wt. % was purchased from Sigma Aldrich. All chemicals were obtained from commercial suppliers and used as received, including benzyl alcohol (Sigma-Aldrich, $\geq 99.0\%$) and chemicals for buffer solutions (Sigma-Aldrich, $\geq 99.9\%$ e.g. HClO_4 , H_3PO_4 , NaH_2PO_4 , Na_2HPO_4 , H_2SO_4 , Na_2SO_4 , CH_3COOH , CH_3COONa), NaCl (Sigma-Aldrich, $\geq 99.9\%$), ethyl acetate (Sigma-Aldrich, $\geq 99.9\%$, HPLC), and 2-cyclohexen-1-one (Sigma Aldrich, $>99\%$). High purity water, treated with a Milli-Q water purification system until a resistivity of $18.2 \text{ M}\Omega\cdot\text{cm}$, was used in all experiments. H_2 (Air Liquide, $>99.99\%$) was used for hydrogenation.

4.2.2 Catalyst characterization

The specific surface area of the catalyst was determined (according to BET) from N_2 physisorption, which were measured at 77 K on a PMI automated BET sorptometer. The samples were first outgassed at 523 K in vacuum ($< 0.001 \text{ mbar}$) for 20h before measurement.

The dispersion of the metals was determined by H_2 chemisorption on Thermo Scientific Surfer Analyzer. The Pd/C catalysts were treated in vacuum at 588 K for 1h and then cooled to 313 K.

A first set of H₂ adsorption isotherm was measured from 1 to 40 kPa. Afterwards, the samples were outgassed at the same temperature for 1 h to remove the physisorbed H₂, followed by a second set of isotherms being measured, which corresponded to physisorbed H₂. The difference of the two isotherms was the chemisorbed hydrogen on Pd. The concentrations of surface Pd atoms were determined by extrapolating the saturated region of the difference isotherms to zero hydrogen pressure and using the value as the number of surface Pd atoms assuming a stoichiometry of one hydrogen to one Pd atom. Then the dispersion of Pd was calculated by comparing the surface Pd atoms to the total Pd atoms.

The size of Pd particle was determined by transmission electron microscopy (TEM, JEOL JEM-2011) with an accelerating voltage of 120 keV. Statistical treatment of the metal particle size was done by counting at least 300 particles detected in several places of the grid.

4.2.3 Catalytic reaction measurements under OCV (open circuit potential)

Benzyl alcohol hydrogenolysis was carried out in a batch reactor with 5-10 mg Pd/C (5 wt.% Pd loading) in 0.2 M buffer solution. Typical measurements under atmospheric pressure were performed with H₂ or diluted H₂ using N₂ (flow rate of 10 mL·min⁻¹) flowing through the reactant solution at 296 K and 600 rpm. Reactions at higher H₂ pressures were performed in a 300 mL Hastelloy PARR reactor, and air was removed from the reactor by introducing 20 bar H₂, followed by depressurizing the reactor for three times. The benzyl alcohol concentration was 20 mM. After the reaction, the solution was extracted using ethyl acetate with 2-cyclohexen-1-one as the internal standard for quantification. NaCl was used to increase the extraction efficiency. The extracted ethyl acetate was treated with Na₂SO₄ to remove dissolved water. Quantitative analyses of the samples were performed by gas chromatography equipped with a Wax capillary column (30m x 250 μm) and a flame ionization detector (FID). Reaction orders of H₂ were determined by changing H₂ pressure from 0.1 bar to 20 bar.

The reactions in D₂O or/and D₂ were carried out in a 100 mL Hastelloy PARR reactor. 20mM benzyl alcohol, 30 mL 0.2 M D₃PO₄ solution in D₂O (99.8%, Sigma), 1 bar D₂ and 10 mg Pd/C were sealed in the reactor for reaction at 296 K and 750 rpm. Before the reaction, air was removed from the reactor by introducing 20 bar D₂, followed by depressurizing the reactor for three times. After the experiment, ethyl acetate was used to extract the chemical species and then were quantified using GC-MS equipped with a HP-5 capillary column.

4.2.4 Electrocatalytic reaction

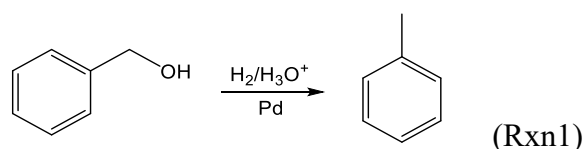
Experiments were carried out in a H cell with a Nafion 117 proton exchange membrane (Ion Power, Inc.) to separate the cathodic and anodic compartments. An electrochemical workstation VSP-300, Bio Logic was used to perform electrochemical procedures. A piece of carbon felt (Alfa Aesar >99.0%, 3.2 mm thickness) infiltrated with 10 mg Pd/C connected to a graphite rod (Sigma Aldrich, 99.99%) was used as working electrode in the cathode compartment. A platinum wire (Alfa Aesar, 99.9 %) was used as counter electrode in the anodic compartment. Ag/AgCl was used as a reference electrode. The cathode and anode compartments were filled with 60 mL 0.2 M H₃PO₄ solution as electrolyte solution. All reactions were performed at atmospheric pressure at constant potential referred to the reverse hydrogen electrode (RHE). The catalyst was first activated under a constant current of -40 mA for 10 min before adding benzyl alcohol (20 mM) into the cathode compartment. Then an electric potential was applied for reaction. Product analysis is the same as performed in the catalytic reaction under OCV.

4.2.5 Cyclic Voltammetry

The coverage of benzyl alcohol on Pd surface was determined via cyclic voltammetry in a Teflon H-cell with a Nafion 117 proton exchange membrane to separate cathodic and anodic compartments. 20 mg Pd/C (30 wt %, Sigma Aldrich) on carbon felt (Alfa Aesar >99.0%, 3.2 mm thickness) was used as working electrode, a Ag/AgCl electrode with double-junction was used as reference electrode, and a platinum wire (Alfa Aesar, 99.9 %) was used as counter electrode. The electrolytes are phosphate buffer (pH 2.5) and acetate buffer (pH 5). The cyclic voltammetry was measured at 5 mV s⁻¹ with 20 mL min⁻¹ N₂ bubbling, and under different concentrations of benzyl alcohol. The sites blocked by benzyl alcohol (benzyl alcohol coverage) was calculated based on the area difference of the underpotentially deposited hydrogen (H_{upd}) peak before and after the benzyl alcohol addition³³. The same measurement was also performed on Pd/C (5 wt.%), but it was difficult to distinguish the H_{upd} peak from the double layer capacitance background current induced by the carbon support.

4.3 Results and discussion

4.3.1 pH effect on TOF and reaction orders for Pd/C catalyzed benzyl alcohol hydrogenolysis in buffer solution



Reductive elimination of benzyl alcohol over Pd/C (5 wt.% with a particle size of ~ 3 nm, SI) was investigated in 0.2 M aqueous buffer solution as a function of the pH value at room temperature and atmospheric pressure of H_2 . In this reaction, the C-O bond in benzyl alcohol was selectively cleaved to form toluene under present reaction conditions as shown in the reaction equation Rxn 1. During the reaction, products resulting from the hydrogenation of the aromatic ring, e.g. cyclohexylmethanol and methylcyclohexane, were not observed, with toluene was the only product. The dependency of turnover frequency (TOF) on the pH value is shown in **Figure 4-1a**. At a pH above 5 the TOF was very low and with the decreasing pH it increased from 15 h^{-1} at pH 7 to 878 h^{-1} at pH 0.63, independently of the type of buffer solution used. This significant dependence of the conversion rates on the pH suggests a strong role of hydronium ions on the rate of the reaction. It has to be mentioned that in the absence of Pd, benzyl alcohol was not converted in acidic media (pH 1). Thus, the conversion of benzyl alcohol to toluene requires both the presence of Pd and acids. An apparent reaction order in hydronium ion of approximate 0.3 was observed for this reaction during the whole pH range (see **Figure 4-1b**). The close relation of the rate of alcohol hydrogenolysis on the pH was also observed by Ryu et al. in the hydrogenation / hydrogenolysis of cis-2-butene-1 over Pt. They quantified changes in interfacial pH local to the electrochemical double layer by using a concurrent non-faradaic probe reaction, however, they didn't focus on the hydrogenolysis mechanism in presence of hydronium ions ¹⁷.

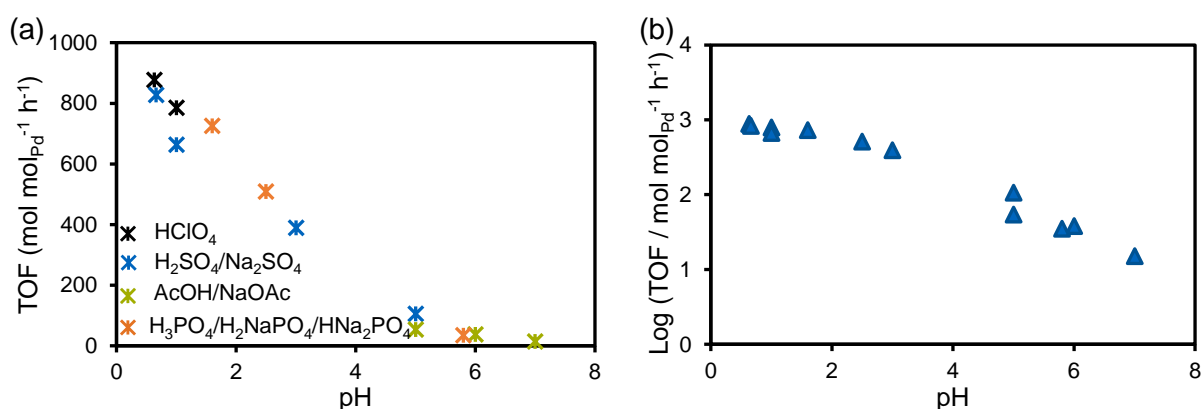


Figure 4-1. (a) TOF as a function of pH in the catalytic conversion of benzyl alcohol to toluene on Pd/C. (b) Log TOF as a function of pH to obtain the apparent reaction order in bulk hydronium ion. Reaction condition: 0.2 M buffer solution, 298 K and 1 bar H_2 . The legend indicates different buffer compositions.

Considering that hydronium ions are involved in the reaction, we assume that the elementary steps occur between the Pd surface and the outer Helmholtz plane. In this case the rate equation for the reaction (r_{BA} , where subscript BA denotes benzyl alcohol) is:

$$r_{\text{BA}} = -\frac{dC_{\text{BA}}}{dt} = k_{\text{eff}} C_{\text{BA}}^{\alpha} P_{\text{H}_2}^{\beta} a_{\text{H}^+}^{\gamma} \quad (1)$$

k_{eff} is the effective rate constant; a_{H^+} is the hydronium ion activity in the bulk phase, α , β and γ are the apparent reaction orders with respect to benzaldehyde, H_2 and hydronium ions.

The reaction orders for both benzyl alcohol and H_2 were measured at pH 2.5 and pH 5, as shown in **Figure A4-2** and **Table 4-1**. At pH 2.5, the reaction order in benzyl alcohol is slightly positive ($\alpha=0.17$, **Figure A4-2**) and near 0th order with respect to H_2 ($\beta=0.09$, **Figure A4-2b**). At pH 5, the reaction order with respect to both benzyl alcohol and hydrogen are near 0 (**Figure A4-2c** and **Figure A4-2d**). The reaction order being zero or close to zero for organic substrate is common in hydrogenation and hydrogenolysis reactions^{27,29-31}, which is the result of the high coverage of substrate on the catalyst. Due to the competitive adsorption of hydrogen and the substrate, such reaction order of 0th for H_2 indicates that either H coverage on Pd surface is also very high, or the adsorbed H does not participate in the rate determining step.

Table 4-1. Summary of reaction rates and reaction orders.

pH	TOF (mol mol _{Pd} ⁻¹ h ⁻¹) *	Reaction order in benzyl alcohol (α)	Reaction order in H_2 (β)
2.5	527	0.08	0.09
5	162	-0.01	0.09

* TOF at 1 bar H_2 and 298 K with a benzyl alcohol concentration of 20 mM.

In order to justify whether the Pd surface has a substantial coverage of H, cyclic voltammetry on Pd/C (20 mg, 30 wt.%) with different concentrations of benzyl alcohol was measured at pH 2.5 (**Figure 4-2a**) and pH 5 (**Figure 4-2b**). In presence of benzyl alcohol, the peak of hydrogen underpotential deposition is reduced (H_{upd} , 0.06 V to 0.34 V vs. RHE at pH 2.5 and 0.09 V to 0.43 V vs. RHE at pH 5), and totally disappears at a concentration of 500 μM (**Figure 4-2a-b**). Comparing the H_{upd} current in presence and absence of benzyl alcohol allows to determine the fraction of H that was inhibited (blocked) by benzyl alcohol molecules (**Figure 4-2c-d**). The drastically decreased H_{upd} with increasing benzyl alcohol concentration indicates that benzyl alcohol binds much stronger than H on Pd, which will lead to a full coverage of the Pd surface by benzyl alcohol and a very low coverage with H under our reaction condition (benzyl alcohol concentration between 10 mM and 40 mM). Therefore, the possibility of a high coverage of H can be excluded, and the observed near zero reaction order of H_2 in benzyl alcohol reaction indicates that the H atoms are only involved in elementary steps after the rate

determining step. If this is the case, benzyl alcohol conversion should only have a small kinetic isotope effect for gaseous H_2 vs. D_2 (as shown in **Figure 4-3**). The conversion rate of benzyl alcohol remains essentially the same for reactions with H_2 and D_2 in either H_2O or D_2O at 298 K and 1 bar pressure. In comparison, the rate in H_2O compared to that in D_2O is 1.4 in H_2 and 1.3 in D_2 . That is to say, the reaction has a stronger isotope effect for the solvent than the gas, indicating that the solvent is involved in the kinetic relevant step.

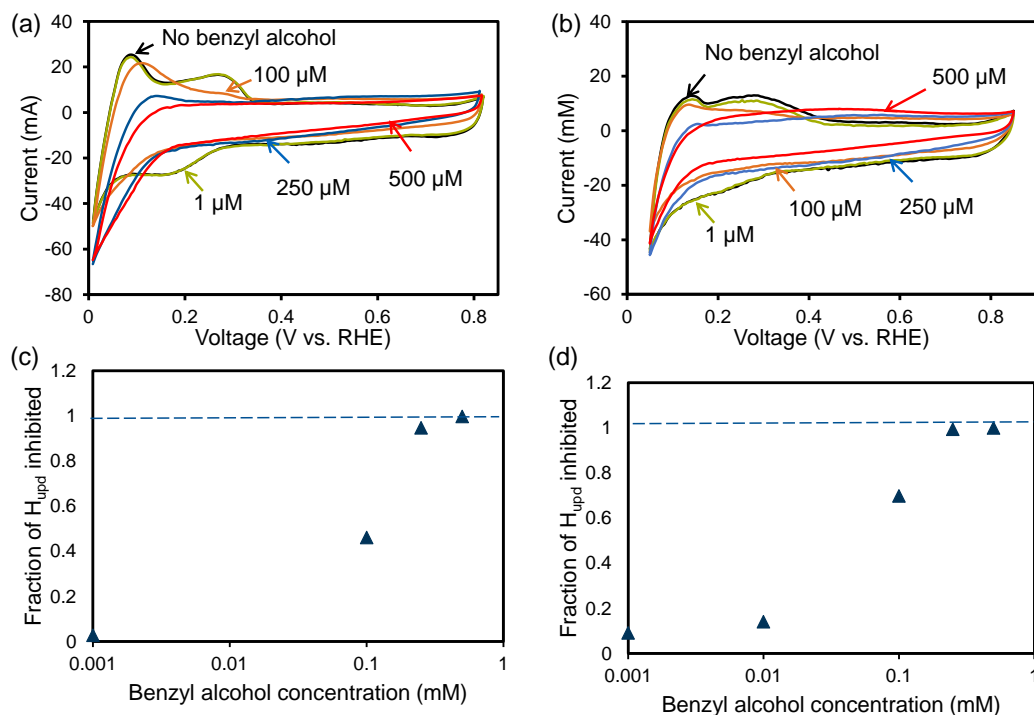


Figure 4-2. Cyclic voltammograms at a scan rate of 5 mV s^{-1} showing hydrogen underpotential deposition on Pd/C (30 wt.%) at room temperature with benzyl alcohol concentration varying from $0 \text{ } \mu\text{M}$ to $500 \text{ } \mu\text{M}$ at (a) pH 2.5 in phosphate buffer solution and (b) pH 5 in acetate buffer solution. The calculated fraction of underpotentially deposited hydrogen that is inhibited on Pd vs benzyl alcohol concentration (c) pH 2.5 in phosphate buffer solution and (d) pH 5 in acetate buffer solution, which is calculated from the decrease in H_{upd} charge relative to that without benzyl alcohol obtained from (a) and (b), respectively.

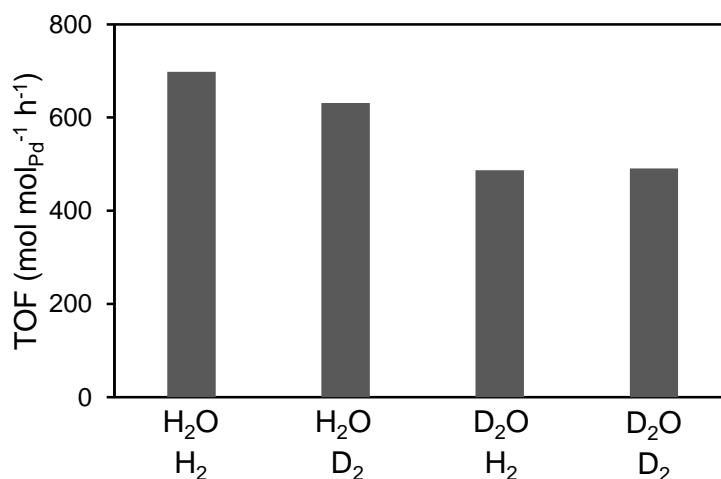


Figure 4-3. Turnover rates of benzyl alcohol hydrogenolysis in H₂O-H₂, H₂O-D₂, D₂O-H₂ and D₂O-D₂. Reaction condition: at 298 K and atmospheric pressure with a benzyl alcohol concentration of 20 mM on Pd/C and 0.2 M phosphoric acid.

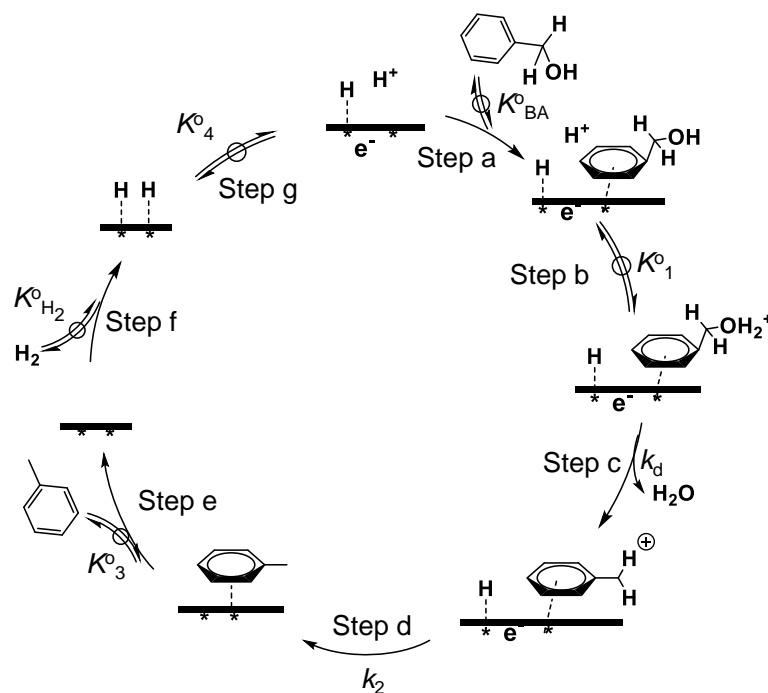
4.3.2 Reaction pathways

Three pathways are possible to convert benzyl alcohol to toluene: (1) direct hydrogenolysis, (2) hydrogenation-dehydration-hydrogen scrambling (**Scheme A4-1**) and (3) protonation-dehydration-hydride addition (**Scheme 4-1**). In the first pathway, molecular benzyl alcohol adsorbs on the Pd surface (BA_{ad}), and dissociatively adsorbed H₂ as the reduced agent (H_{ad}), which directly attacks the hydroxyl group of the benzylic carbon leading to the formation of toluene and water. However, for this pathway, the elementary step of hydrogenolysis, which is a slower step, involves H_{ad}, and the low coverage conflicts with the small reaction order in H₂ observed.

In the second reaction pathway, benzyl alcohol and H₂ are adsorbed and the aromatic ring of benzyl alcohol is partial hydrogenated. The intramolecular dehydration yields the stable olefin product, followed by hydrogen scrambling leading to toluene formation or hydrogenation to 5-methylcyclohexa-1,3-diene. This mechanism was similar to that reported for C–O bond cleavage of 1-(4-isobutylphenyl) ethanol over Pd supported on acidic carbon¹⁸. However, benzyl alcohol does not have a hydrogen in the β position for dehydration. If the aromatic ring undergoes partial hydrogenation, it can provide the hydrogen needed to complete the intermolecular dehydration, in analogy to the reductive solvolysis that has been observed for C–O bond cleavage of aryl ethers^{3,32}. This reaction pathway has been excluded because 5-methylcyclohexa-1,3-diene was not detected, in addition, deuterium was not observed in the aromatic ring for reactions performed in D₂ and D₂O (**Appendix, Section A4-3**). The third pathway, water elimination upon protonation of the hydroxyl group to a carbocation in presence of hydronium ions, which yields toluene via hydride addition will be described in detail in the following part.

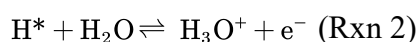
4.3.3 The role of acid in benzyl alcohol hydrogenolysis

Considering the results described above, not only the metal site is necessary for benzyl alcohol hydrogenolysis, but also hydronium ions are required in the reaction. Therefore, a metal-acid bifunctional catalytic mechanism is proposed via the elementary steps shown in **Scheme 4-1**.



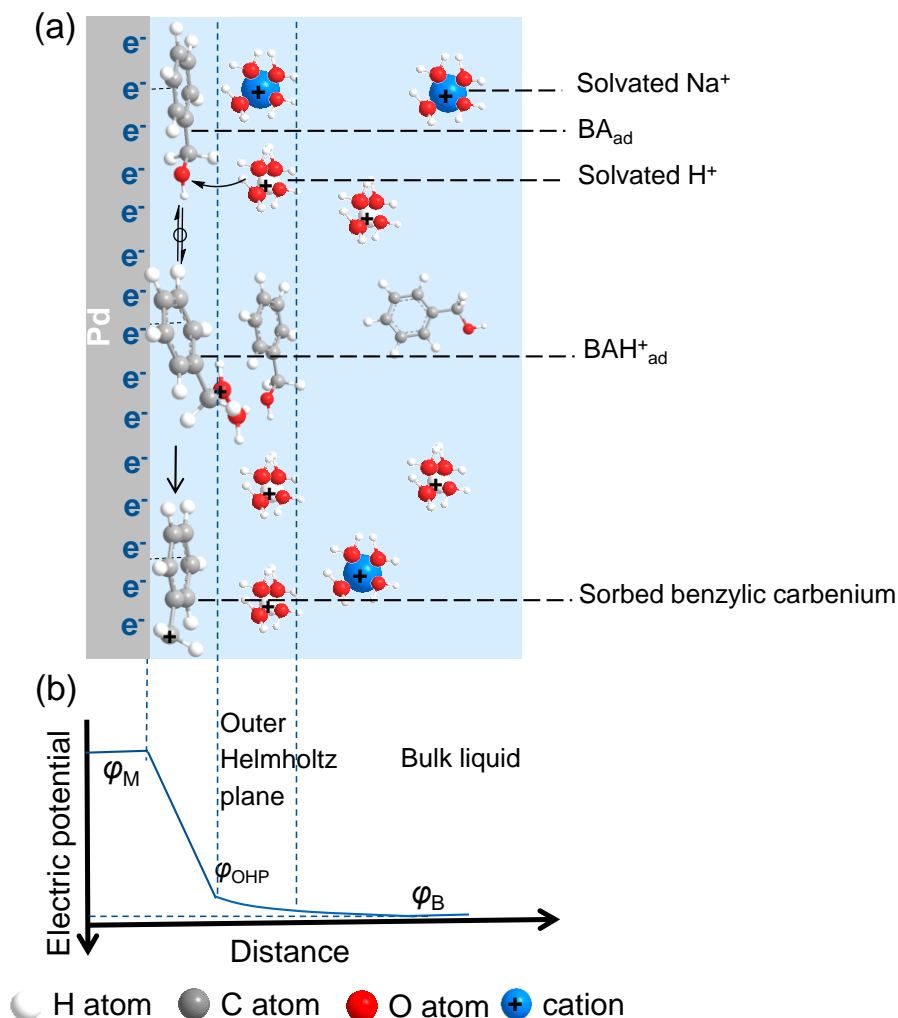
Scheme 4-1. Reaction pathway of benzyl alcohol hydrogenolysis via protonation dehydration-hydrogenation pathway on Pd and acids. The hydronium ion is expressed as proton in the scheme.

Under a certain H_2 pressure and hydronium ion concentration, an electrochemical equilibrium will be established between these two species on the metal surface as shown in the reaction equation Rxn 2 (Step g in **Scheme 4-1**). This is known as the hydrogen electrode reaction.



The catalytic cycle starts with benzyl alcohol adsorption on vacant Pd sites (*) (Step a), afterwards, the adsorbed benzyl alcohol (BA^*) gets protonated (Step b, $C_6H_5CH_2OH_2^+$, BAH^+*) and then eliminate the OH group as a water molecule via dehydration to benzyl carbocation ($C_6H_5CH_2^+$) (Step c). Toluene is then produced through a H addition combining charge neutralization with an electron (hydride) (Step d) and then desorbs from the Pd surface (Step e). H_2 dissociative adsorption on a Pd site pair (*-*), forming two adsorbed H atoms (H^*) (Step f). The adsorption-desorption steps (Step a, e and f) were generally accepted to occur much

faster than the surface reaction, thus they are considered quasi-equilibrated in the kinetic treatment. While the dehydration step (Step e) is considered as rate-determining step when deriving the rate equation.



Scheme 4-2. (a) Schematically showing the reaction mechanism of benzyl alcohol hydrogenolysis (Step b-c) between Pd surface and Helmholtz plane. (b) Potential profile as a function of distance from Pd surface. ϕ_M , ϕ_{OHP} , ϕ_B are potentials on Pd surface, at outer Helmholtz plane and in the bulk, respectively.

The catalytic reaction occurs at the Pd-water interface. **Scheme 4-2a** shows the reaction elementary steps (Step b-c) in the space between the metal surface and outer Helmholtz plane (OHP). The chemisorbed species, possessing chemical interactions with the surface, are located in the inner Helmholtz plane (IHP), while the nonspecifically adsorbed ions like hydrated hydronium ions and hydrated cations are located at the outer Helmholtz plane. The electric potential on Pd surface is determined by the equilibrium between H₂ and hydronium ion, i.e. hydrogen electrode reaction (Rxn 2). Under open circuit potential (OCP), the electric potential on Pd surface is expressed by Nernst Equation (Equation 2),

$$\varphi_M = \varphi_{\text{SHE}} + \frac{RT}{F} \ln \frac{a_{\text{H}^+}}{\sqrt{P_{\text{H}_2}}} \quad (2)$$

in which φ_{SHE} is standard hydrogen electrode potential (SHE), which is often used as a reference and generally defined as 0 V for convenience. The a_{H^+} is the hydronium ion activity in the bulk solution. It should be noted that φ_M is the electric potential difference between Pd surface and electrolyte. The electric potential decays with the distance away from Pd surface until reaching the level of the bulk solution, which is considered as 0 V (**Figure 4-2b**).

Pd surface is covered with adsorbed H (H_{ad}), adsorbed benzyl alcohol (BA_{ad}), protonated benzyl alcohol (BAH^+_{ad}), together with that of the unoccupied site (*). During the reaction, there is also a very small concentration of transition state (TS) at the interface. The expressions of chemical potentials for all the species are

$$\mu_{\text{BA}_{\text{aq}}} = \mu_{\text{BA}_{\text{aq}}}^{\circ} + RT \ln C_{\text{BA}_{\text{aq}}} \quad (3)$$

$$\mu_{\text{BA}_{\text{ad}}} = \mu_{\text{BA}_{\text{ad}}}^{\circ} + RT \ln \frac{\theta_{\text{BA}_{\text{ad}}}}{\theta^*} \quad (4)$$

$$\mu_{\text{H}_2} = \mu_{\text{H}_2}^{\circ} + RT \ln P_{\text{H}_2} \quad (5)$$

$$\mu_{\text{H}_{\text{ad}}} = \mu_{\text{H}_{\text{ad}}}^{\circ} + RT \ln \frac{\theta_{\text{H}_{\text{ad}}}}{\theta^*} \quad (6)$$

$$\mu_{\text{BAH}^+_{\text{ad}}} = \mu_{\text{BAH}^+_{\text{ad}}}^{\circ} + RT \ln \frac{\theta_{\text{BAH}^+_{\text{ad}}}}{\theta^*} + F\varphi_{\text{BAH}^+_{\text{ad}}} \quad (7)$$

$$\mu_{\text{H}^+} = \mu_{\text{H}^+}^{\circ} + RT \ln a_{\text{H}^+} + F\varphi_{\text{B}} \quad (8)$$

$$\mu_{\text{TS}} = \mu_{\text{TS}}^{\circ} + RT \ln \frac{\theta_{\text{TS}}}{\theta^*} + F\varphi_{\text{TS}} \quad (9)$$

The $\mu_{\text{BA}_{\text{aq}}}$, $\mu_{\text{BA}_{\text{ad}}}$, μ_{H_2} , $\mu_{\text{H}_{\text{ad}}}$, μ_{H^+} , $\mu_{\text{BAH}^+_{\text{ad}}}$ and μ_{TS} are chemical potential of benzyl alcohol in bulk, sorbed benzyl alcohol, gas H_2 , sorbed H, hydronium ion in bulk, sorbed protonated benzyl alcohol and transition state, respectively. The transition state (TS) and sorbed protonated benzyl alcohol (BAH^+_{ad}) are positively charged species, thus they are considered to locate closer to the outer Helmholtz plane (**Scheme 4-2a**). The $\varphi_{\text{BAH}^+_{\text{ad}}}$, φ_{B} and φ_{TS} are the electrochemical potential at the position of BAH^+_{ad} , bulk solution and transition state. Generally, φ_{B} is denoted as 0 V. Chemical potential of the charged species BAH^+_{ad} , H^+ and TS are affected by not only the activity but also the electric potential at their located position.

Because the dehydration step (Step e) is the RDS, the adsorption of substrate (Step a) and H_2 (Step f) as well as the protonation of benzyl alcohol (Step b) are considered as quasi-

equilibrated. Thus giving the following relations of chemical potentials,

$$\mu_{\text{BA}_{\text{aq}}} = \mu_{\text{BA}_{\text{ad}}} \quad (10)$$

$$\mu_{\text{H}_2} = 2\mu_{\text{H}_{\text{ad}}} \quad (11)$$

$$\mu_{\text{BA}_{\text{ad}}} + \mu_{\text{H}^+} = \mu_{\text{BAH}^+_{\text{ad}}} = \mu_{\text{TS}} \quad (12)$$

With these equations, the reaction rate is derived as (see derivation details in **Appendix**):

$$\begin{aligned} r &= \frac{k_B T}{h} \cdot \theta_{\text{TS}} \\ &= \frac{k_B T}{h} \cdot \frac{\exp\left(\frac{\mu_{\text{TS}} - \mu_{\text{TS}}^{\circ} - F\varphi_{\text{TS}}}{RT}\right)}{1 + \exp\left(\frac{\mu_{\text{H}_{\text{ad}}} - \mu_{\text{H}_{\text{ad}}}^{\circ}}{RT}\right) + \exp\left(\frac{\mu_{\text{BA}_{\text{ad}}} - \mu_{\text{BA}_{\text{ad}}}^{\circ}}{RT}\right) + \exp\left(\frac{\mu_{\text{BAH}^+_{\text{ad}}} - \mu_{\text{BAH}^+_{\text{ad}}}^{\circ} - F\varphi_{\text{BAH}^+_{\text{ad}}}}{RT}\right)} \quad (13a) \end{aligned}$$

In which, r is benzyl alcohol conversion rate, k_B is Boltzmann constant, T is the temperature and h is Planck constant. Substitute μ_{TS} with $(\mu_{\text{BA}_{\text{aq}}} + \mu_{\text{H}^+})$, $\mu_{\text{H}_{\text{ad}}}$ with $1/2\mu_{\text{H}_2}$, $\mu_{\text{BA}_{\text{ad}}}$ with $\mu_{\text{BA}_{\text{aq}}}$ and $\mu_{\text{BAH}^+_{\text{ad}}}$ with $(\mu_{\text{BA}_{\text{aq}}} + \mu_{\text{H}^+})$ in Equation 13a,

$$r = \frac{k_B T}{h} \cdot \frac{\exp\left(\frac{\mu_{\text{BA}_{\text{aq}}} + \mu_{\text{H}^+} - \mu_{\text{TS}}^{\circ} - F\varphi_{\text{TS}}}{RT}\right)}{1 + \exp\left(\frac{1/2\mu_{\text{H}_2} - \mu_{\text{H}_{\text{ad}}}^{\circ}}{RT}\right) + \exp\left(\frac{\mu_{\text{BA}_{\text{aq}}} - \mu_{\text{BA}_{\text{aq}}}^{\circ}}{RT}\right) + \exp\left(\frac{\mu_{\text{BA}_{\text{aq}}} + \mu_{\text{H}^+} - \mu_{\text{BAH}^+_{\text{ad}}}^{\circ} - F\varphi_{\text{BAH}^+_{\text{ad}}}}{RT}\right)} \quad (13b)$$

Apparently, the reaction rate (Equation 13b) is affected by the chemical potentials of aqueous benzyl alcohol ($\mu_{\text{BA}_{\text{aq}}}$), hydronium ion (μ_{H^+}) and H_2 (μ_{H_2}) as well as φ_{TS} and $\varphi_{\text{BAH}^+_{\text{ad}}}$. The chemical potentials are dependent on the benzyl alcohol concentration, hydronium ion concentration and gases hydrogen pressure, respectively. Then individually to see how each of the parameter influences the reaction,

$$\frac{\partial \ln r}{\partial \ln C_{\text{BA}_{\text{aq}}}} = \frac{\partial \ln r}{\partial \left(\frac{\mu_{\text{BA}_{\text{aq}}} - \mu_{\text{BA}_{\text{aq}}}^{\circ}}{RT}\right)} = RT \frac{\partial \ln r}{\partial \mu_{\text{BA}_{\text{aq}}}} = 1 - \theta_{\text{BA}} - \theta_{\text{BAH}^+_{\text{ad}}} \quad (14)$$

$$\frac{\partial \ln r}{\partial \ln P_{\text{H}_2}} = -\frac{1}{2}\theta_{\text{H}_{\text{ad}}} + \frac{\partial \varphi_{\text{TS}}}{2\partial \varphi_{\text{M}}} - \theta_{\text{BAH}^+_{\text{ad}}} \frac{\partial \varphi_{\text{BAH}^+_{\text{ad}}}}{2\partial \varphi_{\text{M}}} \quad (15)$$

$$\frac{\partial \ln r}{\partial \ln a_{\text{H}^+}} = 1 - \theta_{\text{BAH}^+_{\text{ad}}} - \frac{\partial \varphi_{\text{TS}}}{\partial \varphi_{\text{M}}} + \theta_{\text{BAH}^+_{\text{ad}}} \frac{\partial \varphi_{\text{BAH}^+_{\text{ad}}}}{\partial \varphi_{\text{M}}} \quad (16)$$

$$\frac{\partial \ln r}{\partial \varphi_{\text{M}}} = \frac{F}{RT} \left(-\frac{\partial \varphi_{\text{TS}}}{\partial \varphi_{\text{M}}} + \theta_{\text{BAH}^+_{\text{ad}}} \frac{\partial \varphi_{\text{BAH}^+_{\text{ad}}}}{\partial \varphi_{\text{M}}} \right) \quad (17)$$

Actually, Equation 14, 15 and 16 give the reaction order with respect to benzyl alcohol, H_2 and H^+ . It is noticeable that their reaction orders are functions of the coverages of

corresponding species. In particular, the reaction orders of H_2 and hydronium ions contains term of φ_M (Eqs. 15 and 16), indicating that they can influence the reaction rate by changing the electric potential on Pd because they are involved in the hydrogen electrode reaction establishing the OCP. On the other hand, benzyl alcohol does not affect the electric potential, so its reaction order expression does not contain the φ_M term (Equation 14). The measured reaction order of benzyl alcohol was 0, indicating the $(\theta_{BA} + \theta_{BAH^{+ad}})$ being 1 according to Equation 15, and meaning Pd surface is fully covered by benzyl alcohol and its protonated form BAH^+ . This is in accordance with the CV measurements (Figure 2) that Pd surface is saturated with benzyl alcohol and derived species.

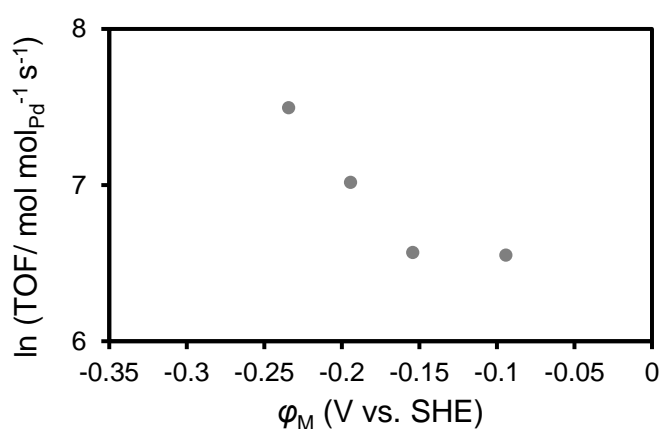


Figure 4-4. lnTOF as a function of electric potential of Pd at pH 1.6. Reaction condition: 10 mg Pd/C (5wt.%) at 298K.

The influence of electric potential φ_M on the rate is expressed in Equation 17. It implies to change the reaction rate by externally giving an electric potential on Pd. To verify it, Pd/C was loaded on an electrode and exposed to a negative electric potential (vs. SHE). Figure 4 shows the conversion rate of benzyl alcohol to toluene at pH 1.6 under different electric potentials. A larger reaction rate was obtained under a more negative electric potential. Therefore, we can reasonably assume that transition state is closer to Pd surface compared to protonated benzyl alcohol (BAH^+), so that transition state is stabilized more than ground state to decrease the activation energy barrier.

H_2 competes the active sites on Pd, while this effect is negligible under reaction conditions due to the small coverage of H_{ad} . Therefore, the main effect of H_2 on the reaction rate is by tuning φ_M (Equation 15), and a higher H_2 pressure is equivalent to a more negative φ_M (Equation 2). H^+ concentration is directly related to the concentration of BAH^+_{ad} , and the reaction order in H^+ can partially reflect the relative abundance of BA_{ad} and BAH^+_{ad} on Pd surface (the none electric potential related part in Equation 16). This explains the changing reaction order in H^+

during the whole pH range from pH 0.6 to pH 7 (**Figure 4-1b**) and why a smaller reaction order was obtained at a lower pH. However, increasing H^+ concentration also increases φ_M , which inhibits the reaction. As shown in **Figure 4-5**, for each pH, the reaction rate increases with H_2 pressure increasing, which results from the decreasing of electric potential. The black line with arrow schematically shows the effect of H_2 pressure increasing (or φ_M decreasing) on reaction rate. In comparison, to decrease pH (showing with the blue line with arrow) can be decomposed into two parts, BAH^+_{ad} coverage (or transition state concentration) increasing (red dash line with arrow) and φ_M increasing (black dash line with arrow). Apparently, the increase in BAH^+_{ad} coverage overcomes the negative influence by the electric potential increasing, and shows an increased reaction rate with decreasing pH.

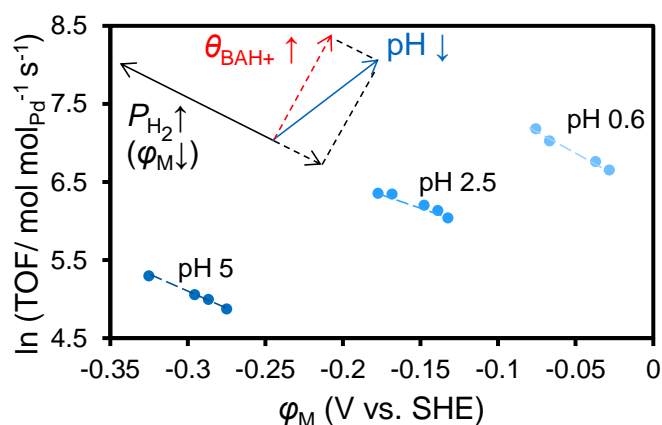


Figure 4-5. lnTOF as a function of electric potential on Pd at OCP under pH 0.6 (0.5-20 bar), pH 2.5 (0.3-10 bar) and pH 5 (0.2-10 bar) on Pd/C (5wt.%) at 298K.

4.4 Conclusions

The reductive elimination of benzyl alcohol is catalyzed by Pd/C in aqueous buffer solution. The conversion rate of benzyl alcohol hydrogenolysis is accelerated by 2-3 orders of magnitude with increasing the hydronium ion concentration. A reaction mechanism is proposed that the reaction proceeds through dehydration of the protonated benzyl alcohol and forming toluene before a hydride addition, and dehydration of the protonated benzyl alcohol step is considered as kinetic relevant. Because the transition state (TS) and sorbed protonated benzyl alcohol (BAH^+_{ad}) are positively charged species, the electric potential in the region between Pd surface and outer Helmholtz plane can directly influence their chemical potential. In addition, the transition state can be stabilized better than the ground state (BAH^+_{ad}) so that to decrease the activation barrier under a more negative electric potential. H_2 affects the reaction rate mainly through changing the electric potential on Pd, which is equivalent to directly applying an electric potential. In comparison, hydronium ion affects not only the electric potential but also

the abundance of transition state. The influence on increasing the transition state concentration by decreasing pH overcomes the negative effect on electric potentials, and gives an accelerating reaction rate.

4.5 Appendix

A4-1 Characterization of Pd/C

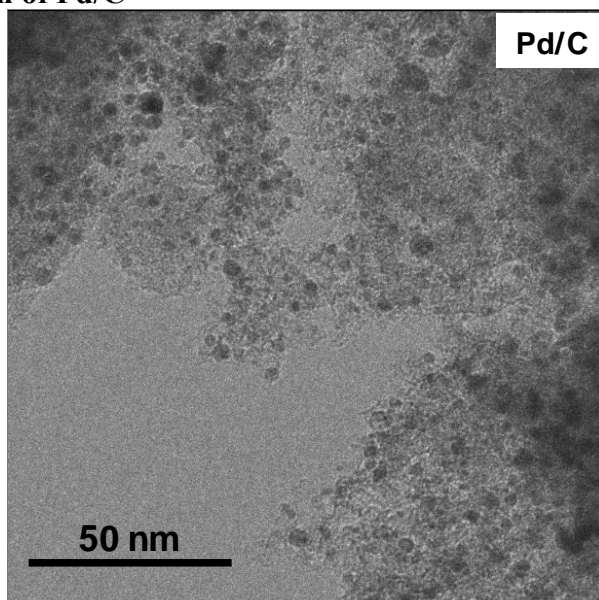


Figure A4-1. Representative TEM images of Pd/C.

Table A4-1. Textural properties of the Pd supported catalysts.

Catalyst	Metal loading (wt.%)	BET surface area ($\text{m}^2\cdot\text{g}^{-1}$)	Particle size (nm) ^a	Dispersion (%) ^b
Pd/C	5	1034	2.9	33

^a measured by TEM.

^b measured by hydrogen chemisorption.

A4-2 Reaction order in benzyl alcohol and hydrogen

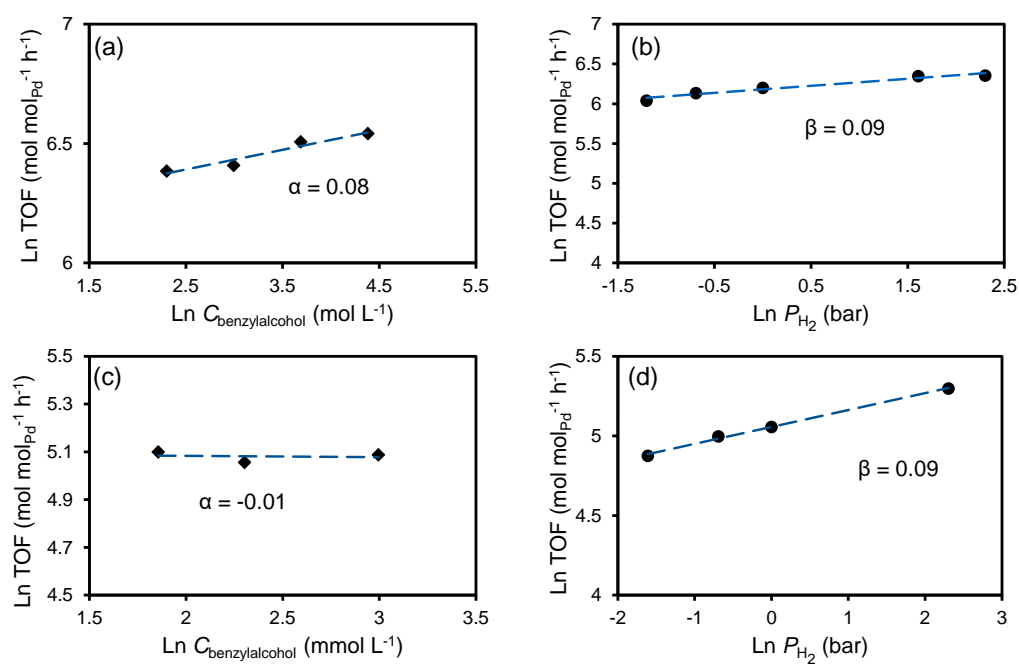
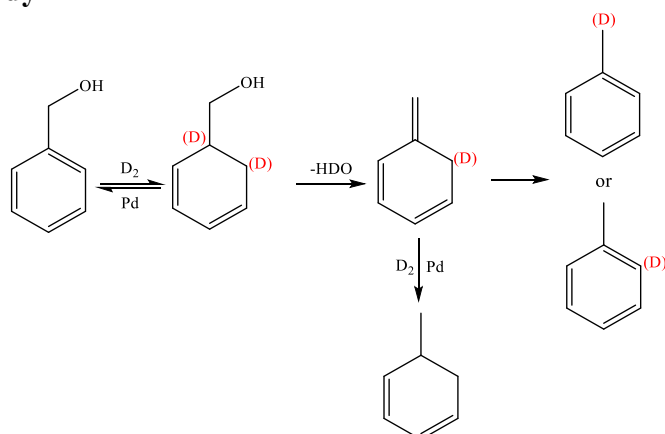


Figure A4-2. (a) TOF as a function of benzyl alcohol concentration (6.4-20 mM) at 1 bar H₂ and (b) TOF as a function of hydrogen pressure (0.3-1bar) with the benzyl alcohol concentration of 10 mM in 0.2 M phosphate buffer (pH=2.5). (c) TOF as a function of benzyl alcohol concentration (10-32 mM) at 1 bar H₂ and (d) TOF as a function of hydrogen pressure (0.3-1bar) with the benzyl alcohol concentration of 10 mM in 0.2 M acetate buffer (pH=5).

A4-3 Deuterium study



Scheme A4-1. Reaction mechanism of benzyl alcohol reductive elimination through hydrogenation-dehydration-hydrogen scrambling.

Deuterium study was performed to probe the pathway of partial hydrogenation-dehydration-hydrogen scrambling. If hydrogenation of the aromatic ring occurs during the conversion of benzyl alcohol, we should observe the aromatic rings of product with D- incorporation (Scheme S1). However, comparing mass spectra of the toluene converted from benzyl alcohol and standard toluene, it indicates no deuterium involves on the aromatic ring. (Figure S3).

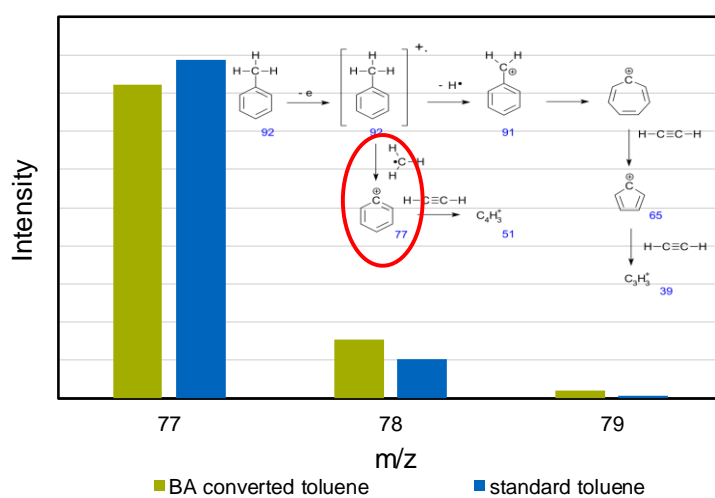


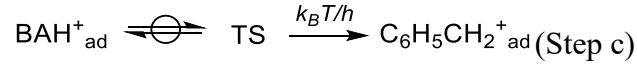
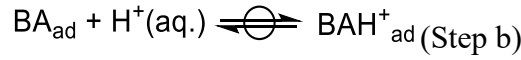
Figure A4-3. Mass spectra of aromatic ring from toluene yield from benzyl alcohol conversion and standard toluene.

A4-4 Derivation of the rate equation

The sum of the fractional coverages for species i (θ_i), which include the adsorbed H atom (H_{ad}), adsorbed benzyl alcohol (BA_{ad}), protonated benzyl alcohol (BAH^+_{ad}), together with that of the unoccupied site (*), equals unity:

$$\theta^* + \theta_{H_{ad}} + \theta_{BA_{ad}} + \theta_{BAH^+_{ad}} = 1 \quad (A1)$$

According to the elementary steps, the relations can be obtained as below,



Therefore, based on the equilibrium, the chemical potential of the species above shows the relation as following,

$$\mu_{BA_{aq}} = \mu_{BA_{ad}} \quad (A2)$$

$$\mu_{BA_{ad}} + \mu_{H^+} = \mu_{BAH^+_{ad}} = \mu_{TS} \quad (A3)$$

$$\mu_{H_2} = 2\mu_{H_{ad}} \quad (A4)$$

In which $\mu_{BA_{aq}}$, $\mu_{BA_{ad}}$, μ_{H_2} , $\mu_{H_{ad}}$, μ_{H^+} , $\mu_{BAH^+_{ad}}$ and μ_{TS} are chemical potential of benzyl alcohol in bulk, sorbed benzyl alcohol, gas H_2 , sorbed H, hydronium ion in bulk, sorbed protonated benzyl alcohol and transition state, respectively. The expressions for each chemical potential are

$$\mu_{BA_{aq}} = \mu_{BA_{aq}}^{\circ} + RT \ln C_{BA_{aq}} \quad (A5)$$

$$\mu_{H_{ad}} = \mu_{H_{ad}}^{\circ} + RT \ln \frac{\theta_{H_{ad}}}{\theta^*} \quad (A6a)$$

$$\frac{\theta_{H_{ad}}}{\theta^*} = \exp\left(\frac{\mu_{H_{ad}} - \mu_{H_{ad}}^{\circ}}{RT}\right) \quad (A6b)$$

$$\mu_{H_2} = \mu_{H_2}^{\circ} + RT \ln P_{H_2} \quad (A7)$$

$$\mu_{BA_{ad}} = \mu_{BA_{ad}}^{\circ} + RT \ln \frac{\theta_{BA_{ad}}}{\theta^*} \quad (A8a)$$

$$\frac{\theta_{BA_{ad}}}{\theta^*} = \exp\left(\frac{\mu_{BA_{ad}} - \mu_{BA_{ad}}^{\circ}}{RT}\right) \quad (A8b)$$

$$\mu_{BAH^+_{ad}} = \mu_{BAH^+_{ad}}^{\circ} + RT \ln \frac{\theta_{BAH^+_{ad}}}{\theta^*} + F\varphi_{BAH^+_{ad}} \quad (A9a)$$

$$\frac{\theta_{\text{BAH}^+_{\text{ad}}}}{\theta^*} = \exp\left(\frac{\mu_{\text{BAH}^+_{\text{ad}}} - \mu_{\text{BAH}^+_{\text{ad}}}^{\circ} - F\varphi_{\text{BAH}^+_{\text{ad}}}}{RT}\right) \quad (\text{A9b})$$

$$\mu_{\text{H}^+} = \mu_{\text{H}^+}^{\circ} + RT \ln a_{\text{H}^+} + F\varphi_{\text{B}} \quad (\text{A10})$$

$$\mu_{\text{TS}} = \mu_{\text{TS}}^{\circ} + RT \ln \frac{\theta_{\text{TS}}}{\theta^*} + F\varphi_{\text{TS}} \quad (\text{A11a})$$

$$\frac{\theta_{\text{TS}}}{\theta^*} = \exp\left(\frac{\mu_{\text{TS}} - \mu_{\text{TS}}^{\circ} - F\varphi_{\text{TS}}}{RT}\right) \quad (\text{A11b})$$

In which $\varphi_{\text{BAH}^+_{\text{ad}}}$, φ_{B} and φ_{TS} are the electrochemical potential at the position of BAH^+_{ad} , bulk phase and transition state. Generally, φ_{B} is denoted as 0. Substitute Equation A1, A6b, A8b and A9b in $1/\theta^*$, we can obtain

$$\begin{aligned} \frac{1}{\theta^*} &= \frac{\theta^* + \theta_{\text{H}_{\text{ad}}} + \theta_{\text{BA}_{\text{ad}}} + \theta_{\text{BAH}^+_{\text{ad}}}}{\theta^*} \\ &= 1 + \exp\left(\frac{\mu_{\text{H}_{\text{ad}}} - \mu_{\text{H}_{\text{ad}}}^{\circ}}{RT}\right) + \exp\left(\frac{\mu_{\text{BA}_{\text{ad}}} - \mu_{\text{BA}_{\text{ad}}}^{\circ}}{RT}\right) + \exp\left(\frac{\mu_{\text{BAH}^+_{\text{ad}}} - \mu_{\text{BAH}^+_{\text{ad}}}^{\circ} - F\varphi_{\text{BAH}^+_{\text{ad}}}}{RT}\right) \end{aligned} \quad (\text{A12})$$

Then substitute Equation A12 into Equation A11b, after arrangement, we can obtain the expression of θ_{TS} ,

$$\begin{aligned} \theta_{\text{TS}} &= \theta^* \cdot \exp\left(\frac{\mu_{\text{TS}} - \mu_{\text{TS}}^{\circ} - F\varphi_{\text{TS}}}{RT}\right) \\ &= \frac{\exp\left(\frac{\mu_{\text{TS}} - \mu_{\text{TS}}^{\circ} - F\varphi_{\text{TS}}}{RT}\right)}{1 + \exp\left(\frac{\mu_{\text{H}_{\text{ad}}} - \mu_{\text{H}_{\text{ad}}}^{\circ}}{RT}\right) + \exp\left(\frac{\mu_{\text{BA}_{\text{ad}}} - \mu_{\text{BA}_{\text{ad}}}^{\circ}}{RT}\right) + \exp\left(\frac{\mu_{\text{BAH}^+_{\text{ad}}} - \mu_{\text{BAH}^+_{\text{ad}}}^{\circ} - F\varphi_{\text{BAH}^+_{\text{ad}}}}{RT}\right)} \end{aligned} \quad (\text{A13})$$

Therefore, the rate equation is obtained as follows,

$$\begin{aligned} r &= \frac{k_{\text{B}}T}{h} \cdot \theta_{\text{TS}} \\ &= \frac{k_{\text{B}}T}{h} \cdot \frac{\exp\left(\frac{\mu_{\text{TS}} - \mu_{\text{TS}}^{\circ} - F\varphi_{\text{TS}}}{RT}\right)}{1 + \exp\left(\frac{\mu_{\text{H}_{\text{ad}}} - \mu_{\text{H}_{\text{ad}}}^{\circ}}{RT}\right) + \exp\left(\frac{\mu_{\text{BA}_{\text{ad}}} - \mu_{\text{BA}_{\text{ad}}}^{\circ}}{RT}\right) + \exp\left(\frac{\mu_{\text{BAH}^+_{\text{ad}}} - \mu_{\text{BAH}^+_{\text{ad}}}^{\circ} - F\varphi_{\text{BAH}^+_{\text{ad}}}}{RT}\right)} \quad (\text{A14a}) \\ r &= \frac{k_{\text{B}}T}{h} \cdot \frac{\exp\left(\frac{\mu_{\text{BA}_{\text{ad}}} + \mu_{\text{H}^+} - \mu_{\text{TS}}^{\circ} - F\varphi_{\text{TS}}}{RT}\right)}{1 + \exp\left(\frac{1/2\mu_{\text{H}_2} - \mu_{\text{H}_{\text{ad}}}^{\circ}}{RT}\right) + \exp\left(\frac{\mu_{\text{BA}_{\text{ad}}} - \mu_{\text{BA}_{\text{ad}}}^{\circ}}{RT}\right) + \exp\left(\frac{\mu_{\text{BA}_{\text{ad}}} + \mu_{\text{H}^+} - \mu_{\text{BAH}^+_{\text{ad}}}^{\circ} - F\varphi_{\text{BAH}^+_{\text{ad}}}}{RT}\right)} \\ &= \frac{k_{\text{B}}T}{h} \cdot \frac{\exp\left(\frac{\mu_{\text{BA}_{\text{aq}}} + \mu_{\text{H}^+} - \mu_{\text{TS}}^{\circ} - F\varphi_{\text{TS}}}{RT}\right)}{1 + \exp\left(\frac{1/2\mu_{\text{H}_2} - \mu_{\text{H}_{\text{ad}}}^{\circ}}{RT}\right) + \exp\left(\frac{\mu_{\text{BA}_{\text{aq}}} - \mu_{\text{BA}_{\text{ad}}}^{\circ}}{RT}\right) + \exp\left(\frac{\mu_{\text{BA}_{\text{aq}}} + \mu_{\text{H}^+} - \mu_{\text{BAH}^+_{\text{ad}}}^{\circ} - F\varphi_{\text{BAH}^+_{\text{ad}}}}{RT}\right)} \end{aligned}$$

(A14b)

Then with the rate equation, and partial derivative of $\ln r$ with respect to $\ln C_{\text{BA}_{\text{aq}}}$, $\ln P_{\text{H}_2}$, $\ln a_{\text{H}^+}$ and φ_{M} , we can obtain

$$\begin{aligned} \frac{\partial \ln r}{\partial \ln C_{\text{BA}_{\text{aq}}}} &= \frac{\partial \ln r}{\partial \left(\frac{\mu_{\text{BA}_{\text{aq}}} - \mu_{\text{BA}_{\text{aq}}}^{\circ}}{RT} \right)} = RT \frac{\partial \ln r}{\partial \mu_{\text{BA}_{\text{aq}}}} \\ &= \frac{\partial (\mu_{\text{BA}_{\text{aq}}} + \mu_{\text{H}^+} - F\varphi_{\text{TS}})}{\partial \mu_{\text{BA}_{\text{aq}}}} - \theta_{\text{BA}} \frac{\partial \mu_{\text{BA}_{\text{aq}}}}{\partial \mu_{\text{BA}_{\text{aq}}}} - \theta_{\text{BAH}^+_{\text{ad}}} \frac{\partial (\mu_{\text{BA}_{\text{aq}}} + \mu_{\text{H}^+} - F\varphi_{\text{BAH}^+_{\text{ad}}})}{\partial \mu_{\text{BA}_{\text{aq}}}} \\ &= 1 - \theta_{\text{BA}} - \theta_{\text{BAH}^+_{\text{ad}}} \end{aligned} \quad (\text{A15})$$

$$\begin{aligned} \frac{\partial \ln r}{\partial \ln P_{\text{H}_2}} &= \frac{\partial \ln r}{\partial \left(\frac{\mu_{\text{H}_2} - \mu_{\text{H}_2}^{\circ}}{RT} \right)} = RT \frac{\partial \ln r}{\partial \mu_{\text{H}_2}} \\ &= \frac{\partial (\mu_{\text{BA}_{\text{aq}}} + \mu_{\text{H}^+} - F\varphi_{\text{TS}})}{\partial \mu_{\text{H}_2}} - \frac{1}{2} \theta_{\text{H}_{\text{ad}}} \frac{\partial \mu_{\text{H}_2}}{\partial \mu_{\text{H}_2}} - \theta_{\text{BA}_{\text{ad}}} \frac{\partial \mu_{\text{BA}_{\text{ad}}}}{\partial \mu_{\text{H}_2}} - \theta_{\text{BAH}^+_{\text{ad}}} \frac{\partial (\mu_{\text{BA}_{\text{aq}}} + \mu_{\text{H}^+} - F\varphi_{\text{BAH}^+_{\text{ad}}})}{\partial \mu_{\text{H}_2}} \\ &= -\frac{1}{2} \theta_{\text{H}_{\text{ad}}} - F \frac{\partial \varphi_{\text{TS}}}{\partial \mu_{\text{H}_2}} + \theta_{\text{BAH}^+_{\text{ad}}} F \frac{\partial \varphi_{\text{BAH}^+_{\text{ad}}}}{\partial \mu_{\text{H}_2}} \end{aligned} \quad (\text{A16})$$

$$\begin{aligned} \frac{\partial \ln r}{\partial \ln a_{\text{H}^+}} &= \frac{\partial \ln r}{\partial \left(\frac{\mu_{\text{H}^+} - \mu_{\text{H}^+}^{\circ}}{RT} \right)} \\ &= \frac{\partial (\mu_{\text{BA}_{\text{aq}}} + \mu_{\text{H}^+} - F\varphi_{\text{TS}})}{\partial \mu_{\text{H}^+}} - \frac{1}{2} \theta_{\text{H}_{\text{ad}}} \frac{\partial \mu_{\text{H}_2}}{\partial \mu_{\text{H}^+}} - \theta_{\text{BA}_{\text{ad}}} \frac{\partial \mu_{\text{BA}_{\text{ad}}}}{\partial \mu_{\text{H}^+}} - \theta_{\text{BAH}^+_{\text{ad}}} \frac{\partial (\mu_{\text{BA}_{\text{aq}}} + \mu_{\text{H}^+} - F\varphi_{\text{BAH}^+_{\text{ad}}})}{\partial \mu_{\text{H}^+}} \\ &= 1 - \theta_{\text{BAH}^+_{\text{ad}}} - F \frac{\partial \varphi_{\text{TS}}}{\partial \mu_{\text{H}^+}} + \theta_{\text{BAH}^+_{\text{ad}}} F \frac{\partial \varphi_{\text{BAH}^+_{\text{ad}}}}{\partial \mu_{\text{H}^+}} \end{aligned} \quad (\text{A17})$$

$$\begin{aligned} \frac{\partial \ln r}{\partial \varphi_{\text{M}}} &= \frac{1}{RT} \left[\frac{\partial (\mu_{\text{BA}_{\text{aq}}} + \mu_{\text{H}^+} - F\varphi_{\text{TS}})}{\partial \varphi_{\text{M}}} - \frac{1}{2} \theta_{\text{H}_{\text{ad}}} \frac{\partial \mu_{\text{H}_2}}{\partial \varphi_{\text{M}}} - \theta_{\text{BA}_{\text{ad}}} \frac{\partial \mu_{\text{BA}_{\text{ad}}}}{\partial \varphi_{\text{M}}} - \theta_{\text{BAH}^+_{\text{ad}}} \frac{\partial (\mu_{\text{BA}_{\text{aq}}} + \mu_{\text{H}^+} - F\varphi_{\text{BAH}^+_{\text{ad}}})}{\partial \varphi_{\text{M}}} \right] \\ &= \frac{F}{RT} \left(-\frac{\partial \varphi_{\text{TS}}}{\partial \varphi_{\text{M}}} + \theta_{\text{BAH}^+_{\text{ad}}} \frac{\partial \varphi_{\text{BAH}^+_{\text{ad}}}}{\partial \varphi_{\text{M}}} \right) \end{aligned} \quad (\text{A18})$$

Due to the equilibrium of hydronium ions and gas hydrogen, the electrode potential of Pd can be written as,

$$\varphi_{\text{M}} = \varphi_{\text{SHE}} + \frac{RT}{F} \ln \frac{a_{\text{H}^+}}{\sqrt{P_{\text{H}_2}}} \quad (\text{A19})$$

In which φ_{SHE} is standard hydrogen electrode (SHE), which is often used as a reference and generally defined it as 0 V for convenience. It should be noted that φ_{M} is contact potential, and the electron work function of Pd is not considered here. With Equation A19, we can obtain,

$$\frac{\partial \varphi_M}{\partial \ln P_{\text{H}_2}} = - \frac{RT}{2F} \quad (\text{A20a})$$

$$\frac{\partial \varphi_M}{\partial \mu_{\text{H}_2}} = - \frac{1}{2F} \quad (\text{A20b})$$

$$-F = \frac{\partial \mu_{\text{H}_2}}{2 \partial \varphi_M} \quad (\text{A20c})$$

$$\frac{\partial \varphi_M}{\partial \ln a_{\text{H}^+}} = \frac{RT}{F} \quad (\text{A21a})$$

$$\frac{\partial \varphi_M}{\partial \mu_{\text{H}^+}} = \frac{1}{F} \quad (\text{A21b})$$

$$F = \frac{\partial \mu_{\text{H}^+}}{\partial \varphi_M} \quad (\text{A21c})$$

Substitute Equation A20c into Equation A16,

$$\frac{\partial \ln r}{\partial \ln P_{\text{H}_2}} = - \frac{1}{2} \theta_{\text{H}^+_{\text{ad}}} + \frac{\partial \varphi_{\text{TS}}}{2 \partial \varphi_M} - \theta_{\text{BAH}^+_{\text{ad}}} \frac{\partial \varphi_{\text{BAH}^+_{\text{ad}}}}{2 \partial \varphi_M} \quad (\text{A22})$$

Substitute Equation A21c into Equation A17,

$$\frac{\partial \ln r}{\partial \ln a_{\text{H}^+}} = 1 - \theta_{\text{BAH}^+_{\text{ad}}} - \frac{\partial \varphi_{\text{TS}}}{\partial \varphi_M} + \theta_{\text{BAH}^+_{\text{ad}}} \frac{\partial \varphi_{\text{BAH}^+_{\text{ad}}}}{\partial \varphi_M} \quad (\text{A23})$$

4.6 References

1. Corma A, Iborra S, Velty A. Chemical routes for the transformation of biomass into chemicals. *Chem Rev.* **107**, 2411-2502, (2007).
2. Gallezot P. Conversion of biomass to selected chemical products. *Chem Soc Rev.* **41**, 1538-1558, doi:10.1039/c1cs15147a (2012).
3. Wang M, Shi H, Camaioni DM, Lercher JA. Palladium-catalyzed hydrolytic cleavage of aromatic C–O bonds. *Angew Chemie - Int Ed.* **56**, 2110-2114, doi:10.1002/anie.201611076 (2017).
4. Mellmer MA, Sanpitakseree C, Demir B, et al. Solvent-enabled control of reactivity for liquid-phase reactions of biomass-derived compounds. *Nat Catal.* **1**, 199-207, doi:10.1038/s41929-018-0027-3 (2018).
5. Varghese JJ, Mushrif SH. Origins of complex solvent effects on chemical reactivity and computational tools to investigate them: A review. *React Chem Eng.* **4**, 165-206, doi:10.1039/c8re00226f (2019).
6. Takenouchi M, Kudoh S, Miyajima K, Mafuné F. Adsorption and desorption of hydrogen by gas-phase palladium clusters revealed by in situ thermal desorption spectroscopy. *J Phys Chem A.* **119**, 6766-6772, doi:10.1021/acs.jpca.5b03926 (2015).
7. Pang SH, Román AM, Medlin JW. Adsorption orientation-induced selectivity control of reactions of benzyl alcohol on Pd(111). *J Phys Chem C.* **116**, 13654-13660, doi:10.1021/jp303147c (2012).
8. Hensley AJR, Bray J, Shangguan J, Chin Y-HC, McEwen J-S. Catalytic consequences of hydrogen addition events and solvent-adsorbate interactions during guaiacol-H₂ reactions at the H₂O-Ru(0001) Interface. *J Catal.* **1**, doi:10.1016/j.jcat.2020.09.034 (2020).
9. Shangguan J, Hensley AJR, Gradiski M V., et al. The role of protons and hydrides in the catalytic hydrogenolysis of guaiacol at the ruthenium nanoparticle-water interface. *ACS Catal.* **10**, 12310-12332, doi:10.1021/acscatal.0c01963 (2020).
10. Akpa BS, D'Agostino C, Gladden LF, et al. Solvent effects in the hydrogenation of 2-butanone. *J Catal.*, **289**, 30-41, doi:10.1016/j.jcat.2012.01.011 (2012).
11. Strmcnik D, Kodama K, Van Der Vliet D, Greeley J, Stamenkovic VR, Marković NM.

- The role of non-covalent interactions in electrocatalytic fuel-cell reactions on platinum. *Nat Chem.* **1**, 466-472, doi:10.1038/nchem.330 (2009).
12. Zhao Z, Bababrik R, Xue W, et al. Solvent-mediated charge separation drives alternative hydrogenation path of furanics in liquid water. *Nat Catal.* **2**, 431-436, doi:10.1038/s41929-019-0257-z (2019).
 13. Sanyal U, Yuk SF, Koh K, et al. Hydrogen bonding enhances the electrochemical hydrogenation of benzaldehyde in the aqueous phase. *Angew Chemie.* **133**, 294-300, doi:10.1002/ange.202008178 (2021).
 14. Akhade SA, Singh N, Gutiérrez OY, et al. Electrocatalytic hydrogenation of biomass-derived organics: A review. *Chem Rev.* Published online 2020. doi:10.1021/acs.chemrev.0c00158 (2020).
 15. Singh N, Lee MS, Akhade SA, et al. Impact of pH on aqueous-phase phenol hydrogenation catalyzed by carbon-supported Pt and Rh. *ACS Catal.* **9**, 1120-1128, doi:10.1021/acscatal.8b04039 (2019).
 16. Ryu J, Surendranath Y. Tracking electrical fields at the Pt/H₂O interface during hydrogen catalysis. *J Am Chem Soc.* **141**, 15524-15531, doi:10.1021/jacs.9b05148 (2019).
 17. Ryu J, Wuttig A, Surendranath Y. Quantification of interfacial pH variation at molecular length scales using a concurrent non-faradaic reaction. *Angew Chemie - Int Ed.* **57**, 9300-9304, doi:10.1002/anie.201802756 (2018).
 18. Thakar N, Polder NF, Djanashvili K, Bekkum H Van, Kapteijn F, Moulijn JA. Deuteration study to elucidate hydrogenolysis of benzylic alcohols over supported palladium catalysts. **246**, 344-350, doi:10.1016/j.jcat.2006.12.016 (2007).
 19. Liu X, Lu G, Guo Y, Guo Y, Wang Y, Wang X. Catalytic transfer hydrogenolysis of 2-phenyl-2-propanol over palladium supported on activated carbon. **252**, 176-180. doi:10.1016/j.molcata.2006.02.055 (2006).
 20. Sawadjoon S, Lundstedt A, Samec JSM. Pd-catalyzed transfer hydrogenolysis of primary, secondary, and tertiary benzylic alcohols by formic acid: A mechanistic study. Published online 2013. doi:10.1021/cs300785r (2013).
 21. Ranade VS, Prins R. Hydrogenolysis of benzylic alcohols on rhodium catalysts. Published online 313-320 (2000).
 22. Zhu S, Gao X, Zhu Y, et al. Alkaline metals modified Pt-H₄SiW₁₂O₄₀/ZrO₂ catalysts for

- the selective hydrogenolysis of glycerol to 1,3-propanediol. *Appl Catal B Environ.* 140-141, doi:10.1016/j.apcatb.2013.03.041(2013).
23. Nakagawa Y, Tamura M, Tomishige K. Catalytic materials for the hydrogenolysis of glycerol to 1,3-propanediol. *J Mater Chem A.* **2**, 6688-6702, doi:10.1039/c3ta15384c (2014).
 24. Malyala R V., Rode C V., Arai M, Hegde SG, Chaudhari R V. Activity, selectivity and stability of Ni and bimetallic Ni-Pt supported on zeolite Y catalysts for hydrogenation of acetophenone and its substituted derivatives. *Appl Catal A Gen.* **193**, 71-86, doi:10.1016/S0926-860X(99)00442-1 (2000).
 25. Kwak B, Kim T, Lee S. Hydrogenolysis of α -methylbenzyl alcohol over bifunctional catalysts. **238**, 141-148, (2003).
 26. Lin HW, Yen CH, Tan CS. Aromatic hydrogenation of benzyl alcohol and its derivatives using compressed CO₂/water as the solvent. *Green Chem.* **14**, 682-687, doi:10.1039/c2gc15999f (2012).
 27. Kieboom APG, Kreuk JFDE, Bekkum HVAN. Substituent effects in the hydrogenolysis of benzyl alcohol over palladium. *J Catal.* **20**, 58-66, (1971).
 28. Ley S V., Stewart-Liddon AJP, Pears D, Perni RH, Treacher K. Hydrogenation of aromatic ketones, aldehydes, and epoxides with hydrogen and Pd(0)EnCat™ 30NP. *Beilstein J Org Chem.* **2**, 2-6, doi:10.1186/1860-5397-2-15 (2006).
 29. Singh N, Nguyen MT, Cantu DC, et al. Carbon-supported Pt during aqueous phenol hydrogenation with and without applied electrical potential: X-ray absorption and theoretical studies of structure and adsorbates. *J Catal.* **368**, 8-19, doi:10.1016/j.jcat.2018.09.021 (2018).
 30. Koh K, Sanyal U, Lee M, et al. Electrochemically Tunable Proton-Coupled Electron Transfer in Pd-Catalyzed Benzaldehyde Hydrogenation. *Angew Chemie.* **132**, 1517-1521, doi:10.1002/ange.201912241 (2020).
 31. Song Y, Sanyal U, Pangotra D, et al. Hydrogenation of benzaldehyde via electrocatalysis and thermal catalysis on carbon-supported metals. *J Catal.* **359**, 68-75, doi:10.1016/J.JCAT.2017.12.026 (2018).
 32. Wang M, Gutiérrez OY, Camaioni DM, Lercher JA. Palladium-catalyzed reductive insertion of alcohols into aryl ether bonds. *Angew Chemie - Int Ed.* **57**, 3747-3751,

doi:10.1002/anie.201709445 (2018).

33. Connolly JF, Flannery RJ, Aronowitz G. Electrochemical measurement of the available surface area of carbon-supported platinum. *J Electrochem Soc.* **113**, 577, doi:10.1149/1.2424030 (1966).

Chapter 5

Summary

The incentive of this dissertation is to figure out the intrinsic reasons behind the solvent effect on hydrodeoxygenation reaction on Pd/C, including benzaldehyde hydrogenation, cinnamaldehyde hydrogenation and benzyl alcohol hydrogenolysis, which all need H₂ activation on Pd for further reaction. The conversions were carried out under mild operating conditions, i.e., room temperature and ambient pressure in condensed phase. The apparent effects of solvents are present on the reaction rate, reaction orders as well as product selectivity. The reasons for these differences could be the change in the reaction mechanism, kinetic relevant step and energy barrier.

Protic solvents can contribute to the reaction via directly participating in the elementary steps to change the reaction mechanism, such as proton coupled electron transfer (PCET) and H transfer shuttle. Generally, detection of kinetic isotope effect (KIE) of H₂O versus D₂O (or normal solvent versus deuterated solvent) is an effective way to distinguish whether solvents involved in the reaction. A large kinetic isotope effect suggests the involvement of solvents in elementary steps, otherwise, an insignificant KIE hints the solvent effect via solvation of reactants. In benzaldehyde hydrogenation (Chapter 2), the rate difference is minimum in H₂O versus D₂O for both H₂ and D₂, excluding the reaction pathway of PCET. In contrast, a stronger isotope effect for the solvent (1.3~1.4) than the gas (1.0~1.1) was observed in benzyl alcohol hydrogenolysis (Chapter 4), indicating that the solvent is involved in the kinetic relevant step. In addition, another method is to detect if D involved in the product yielded in deuterated solvent-H₂, and if involved D is observed, reference samples of standard product in deuterated solvent will need to be analyzed to figure out whether the detected D is from the reaction process. In cinnamaldehyde hydrogenation (Chapter 3), the observation of D involvement in the product hydrocinnamaldehyde in C₂H₅OH-H₂ suggests the presence of H transfer in the hydrogenation process.

For substance with simple molecular structure, D labeling analysis of both reactant and products using mass spectra can help to distinguish H addition sequence. In benzaldehyde hydrogenation (Chapter 2), due to the asymmetry of the molecular, the H addition pathway could be the first H* is added to the O, forming a hydroxyl intermediate, before the second H* is being added to the C of the formyl group (hydroxyl pathway) or/and by adding H* first to the carbonyl carbon atom (carboxyl pathway). Because the 1st H addition is quasi-equilibrated, the formation rate of D-labeled benzaldehyde should be one order of magnitude larger than that benzyl alcohol if carboxyl pathway is dominated. With this method, we concluded that both reaction pathways coexist, while hydroxyl pathway is dominate.

Solvents may change the kinetic relevant step of reaction and the reaction orders reflect the relative abundance of sorbed species on catalyst surface. The determination of kinetic relevant step can be either by the reaction order with respect of H₂ or by the comparison of energy barrier of all elementary steps. In benzaldehyde hydrogenation (Chapter 2), the rate ratio of the forward and reverse reaction of 1st H addition confirmed the conclusion. Similarly, it was also concluded that the second H addition is slower in cinnamaldehyde hydrogenation (Chapter 3), for both C=C and C=O bond saturation due to the larger reaction order in H₂ (> 0.5). For benzyl alcohol hydrogenolysis (Chapter 4), the dehydration step is commonly accepted as a slow step which needs to overcome higher energy barrier compared to hydride addition step. The reaction orders in substrate and H₂ can help to confirm the relative coverage of H related species or substrate related species.

When the reaction mechanism and kinetic relevant steps are the same, then the solvent effect could be through solvation of adsorbed reactants as well as the transition state, which can change the binding energy and then the energy barrier. In benzaldehyde hydrogenation (Chapter 2), we found adsorbed benzaldehyde with the partly hydrogenated intermediate was influenced nearly identical by solvents, while the differences in the stabilization of binding of H* to the catalyst surface determine the reaction rates. Weaker hydrogen binding to the metal is positive for the rate of hydrogenation. For benzyl alcohol hydrogenolysis, hydronium ion participates in the reaction, on one hand contributes the concentration of transition state. On the other hand, hydronium ion changes the electric potential on Pd, and the chemical potential of ground state and transition state, thus to change the energy barrier.

Heterogeneous catalytic reactions in presence of solvent are more complex than that in gas phase. Solvents can compete for active sites and stabilize the sorbed species. Moreover, solvents can be directly involved in the elementary steps in some cases. The understanding of the above solvent effects enables us to manage the reactivity of hydrodeoxygenations and tuning reaction conditions for the targeted reaction.

Curriculum vitae

Guanhua Cheng was born on 4th February 1991 in Taian, Shandong, P. R. China. She started the study in Department of Materials Science and Engineering at Shandong University (Jinan, Shandong, China) and received her bachelor degree in July, 2013. She continued her study as a master student at Shandong University in the same year, and obtained her master degree after defending the thesis titled “Fabrication of Ni/Co-based electrode materials and their pseudocapacitive performances” under the supervision of Prof. Zhonghua Zhang in July 2016. In September 2010, she started the research as a Ph.D. student under the supervision of Prof. Dr. Johannes A. Lercher in Chair II of Chemical Technology at Technical University of Munich (Munich, Germany). The research focuses on the understanding of solvent effects on the hydrodeoxygenation (HDO) of biomass derived molecules. Some representative results of the work were summarized in the present thesis.

List of publications

1. Towards a quantitative understanding of solvent effects on Pd catalyzed benzaldehyde hydrogenation, Guanhua Cheng, Andreas Jentys, Oliver Y. Gutiérrez, Yue Liu, Ya-Huei (Cathy) Chin, and Johannes A. Lercher, *Nature Catalysis* (under review), 2021.
2. Understanding of the rate-enhancement with hydronium ions on benzyl alcohol hydrogenolysis over Pd/C, Guanhua Cheng, Andreas Jentys, Yue Liu, and Johannes A. Lercher, (under preparation).
3. Role of solvents on selective hydrogenation of cinnamaldehyde, Guanhua Cheng, Andreas Jentys, Erika Ember, Yue Liu, and Johannes A. Lercher, (under preparation).
4. Alkylation of lignin-derived aromatic oxygenates with cyclic alcohols on acidic zeolites, Yuanshuai Liu, Guanhua Cheng, EszterBaráth, HuiShi and Johannes A.Lercher, *Applied Catalysis B: Environmental*, 2021, 281, 119424–119434.
5. Rate enhancement of acid-catalyzed alcohol dehydration by supramolecular organic capsules, Wei Zhang, Guanhua Cheng, Gary L. Haller, Yue Liu and Johannes A. Lercher, *ACS Catalysis*, 2020, 10, 22, 13371–13376.
6. Electrochemically tunable proton-coupled electron transfer in Pd-catalyzed benzaldehyde hydrogenation, Katherine Koh, Udishnu Sanyal, Mal-Soon Lee, Guanhua Cheng, Miao Song, Vassiliki-Alexandra Glezakou, Yue Liu, Dongsheng Li, Roger Rousseau, Oliver Y. Gutiérrez, Abhijeet Karkamkar, Mirosław Derewinski and Johannes A. Lercher, *Angewandte Chemie*, 2020, 132, 1517-1521.
7. Impact of pH on aqueous-phase phenol hydrogenation catalyzed by carbon-supported Pt and Rh, Nirala Singh, Mal-Soon Lee, Sneha A. Akhade, Guanhua Cheng, Donald M. Camaioni, Oliver Y. Gutiérrez, Vassiliki-Alexandra Glezakou, Roger Rousseau, Johannes A. Lercher and Charles T. Campbell, *ACS Catalysis*, 2019, 9, 1120–1128.
8. O₂²⁻/O⁻ functionalized oxygen-deficient Co₃O₄ nanorods as high performance supercapacitor electrodes and electrocatalysts towards water splitting, Guanhua Cheng, Tianyi Kou, Jie Zhang, Conghui Si, Hui Gao and Zhonghua Zhang, *Nano Energy*, 2017, 38, 155–166.
9. Facile fabrication of cobalt oxalate nanostructures with superior specific capacitance and super-long cycling stability, Guanhua Cheng, Conghui Si, Jie Zhang, Yan Wang, Wanfeng Yang, Chaoqun Dong and Zhonghua Zhang, *Journal of Power Source*, 2016, 312, 184–191.

10. New-type nickel oxalate nanostructures for ultrahigh sensitive electrochemical biosensing of glucose, Chaoqun Dong, Xuejiao Yan, Conghui Si, Hui Gao, Wensheng Ma, Guanhua Cheng, Wanfeng Yang, Hua Zhong and Zhonghua Zhang, *Advance Materials interface*, 2016, 3, 1600197–1600204.
11. Free-standing CuO nanoflake arrays coated Cu foam for advanced lithium ion battery anodes, Wanfeng Yang, Jiawei Wang, Wensheng Ma, Conghui Dong, Guanhua Cheng and Zhonghua Zhang, *Journal of Power Sources*, 2016, 333, 88–98.
12. Nickel oxide nanopetal-decorated 3D nickel network with enhanced pseudocapacitive properties, Guanhua Cheng, Qingguo Bai, Conghui Si, Wanfeng Yang, Chaoqun Dong, Hao Wang, Yulai Gao and Zhonghua Zhang, *RSC Advances*, 2015, 5, 15042–15051.
13. Ultrathin mesoporous NiO nanosheet-anchored 3D nickel foam as an advanced electrode for supercapacitors, Guanhua Cheng, Wanfeng Yang, Chaoqun Dong, Tianyi Kou, Qingguo Bai, Hao Wang and Zhonghua Zhang, *Journal of Materials Chemistry A*, 2015, 3, 17469–17478.
14. Flexible and ultralong-life cuprous oxide microsphere-nanosheets with superior pseudocapacitive properties, Chaoqun Dong, Qingguo Bai, Guanhua Cheng, Bingge Zhao, Hao Wang, Yulai Gao and Zhonghua Zhang, *RSC Advances*, 2015, 5, 6207–6214.
15. Anodization driven synthesis of nickel oxalate nanostructures with excellent performance for asymmetric supercapacitors, Guanhua Cheng, Junling Xu, Chaoqun Dong, Wanfeng Yang, Tianyi Kou and Zhonghua Zhang, *Journal of Materials Chemistry A*, 2014, 2, 17307–17313.
16. NiO nanorod array anchored Ni foam as a binder-free anode for high-rate lithium ion batteries, Wanfeng Yang, Guanhua Cheng, Chaoqun Dong, Qingguo Bai, Xiaoting Chen, Zhangquan Peng and Zhonghua Zhang, *Journal of Materials Chemistry A*, 2014, 2, 20022–20029.
17. 3D binder-free Cu₂O@Cu nanoneedle arrays for high-performance asymmetric supercapacitors, Chaoqun Dong, Yan Wang, Junling. Xu, Guanhua Cheng, Wanfeng Yang, Tianyi Kou, Zhonghua Zhang and Yi Ding, *Journal of Materials Chemistry A*, 2014, 2, 18229–18235.

List of presentations

1. Significance of hydronium ions in Pd catalyzed benzyl alcohol dehydration (Poster), Guanhua Cheng, Erika Ember, Andreas Jentys, Yue Liu and Johannes A. Lercher, 54. Jahrestreffen Deutscher Katalytiker, 2021, Weimar, Germany (online conference).
2. Bifunctional metal and acid catalyzed benzyl alcohol dehydration (Poster), Guanhua Cheng, Erika Ember, Andreas Jentys, Yue Liu and Johannes A. Lercher, 53. Jahrestreffen Deutscher Katalytiker, 2020, Weimar, Germany (The conference was cancelled due to Coronavirus).
3. Role of solvents in Pd Catalyzed C=O Bond Hydrogenation (Talk), Guanhua Cheng, Erika Ember, Andreas Jentys, Yue Liu, Oliver Y. Gutiérrez, Ya-Huei (Cathy) Chin and Johannes A. Lercher, 14th European Conference on Catalysis, 2019, Aachen, Germany.
4. Mechanism of Pd Catalyzed C=O Bond Hydrogenation—Significance of Solvents (Poster), Guanhua Cheng, Erika Ember, Andreas Jentys, Yue Liu, Oliver Y. Gutiérrez, Ya-Huei (Cathy) Chin and Johannes A. Lercher, Nam 26 2019 North American Catalysis Society Meeting, 2019, Chicago, America.
5. Mechanistic Insight of Benzyl Aldehyde Hydrogenation Effects of Solvent on Hydrogenation Step (Poster), Guanhua Cheng, Erika Ember, Oliver Y. Gutiérrez, Andreas Jentys, Johannes A. Lercher, 52. Jahrestreffen Deutscher Katalytiker, 2019, Weimar, Germany.
6. Effect of pH and electrolyte composition on Pd/C catalyzed (electro-)catalytical hydrogenation of benzaldehyde (Poster), Guanhua Cheng, Erika Ember, Andreas Jentys, Oliver Y. Gutiérrez and Johannes A. Lercher, 51. Jahrestreffen Deutscher Katalytiker, 2018, Weimar, Germany.
7. Aqueous phase electrocatalytic hydrogenation of benzaldehyde: A mechanistic study (Poster), Yang Song, Udishnu Sanyal, Guanhua Cheng, Andreas Jentys, Oliver Y. Gutiérrez, and Johannes A. Lercher, 13rd European Conference on Catalysis, 2017, Florence, Italy.